

The structure and thermochemistry of K₂CO₃-MgCO₃ glass

WILDING, Martin, PHILLIPS, Brian, WILSON, Mark, SHARMA, Geetu, NAVROTSKY, Alexandra, BINGHAM, Paul <<http://orcid.org/0000-0001-6017-0798>>, BROOKER, Richard and PARISE, John

Available from Sheffield Hallam University Research Archive (SHURA) at:

<https://shura.shu.ac.uk/24953/>

This document is the Accepted Version [AM]

Citation:

WILDING, Martin, PHILLIPS, Brian, WILSON, Mark, SHARMA, Geetu, NAVROTSKY, Alexandra, BINGHAM, Paul, BROOKER, Richard and PARISE, John (2019). The structure and thermochemistry of K₂CO₃-MgCO₃ glass. *Journal of Materials Research*, 34 (19), 3377-3388. [Article]

Copyright and re-use policy

See <http://shura.shu.ac.uk/information.html>



The structure and thermochemistry of K_2CO_3 - $MgCO_3$ glass

Journal:	<i>Journal of Materials Research</i>
Manuscript ID	JMR-2019-0305.R2
Manuscript Type:	Article
Date Submitted by the Author:	31-Jul-2019
Complete List of Authors:	Wilding, Martin; Sheffield Hallam University, Materials and Engineering Research Institute; Phillips, Brian; Stony Brook University, Geosciences Wilson, Mark; University of Oxford, Chemistry Sharma, Geetu; University of California Davis, Thermochemistry Facility Navrotsky, Alexandra; University of California Davis, Peter A. Rock Thermochemistry Laboratory and NEAT ORU Bingham, Paul; Sheffield Hallam University, Materials and Engineering Research Institute Brooker, Richard; University of Bristol, Earth Sciences Parise, John; Stony Brook University, Geosciences
Key Words:	nuclear magnetic resonance (NMR), calorimetry, simulation

SCHOLARONE™
Manuscripts

THE STRUCTURE AND THERMOCHEMISTRY OF K_2CO_3 - $MgCO_3$ GLASS

Martin C. Wilding^{1,2i}, Brian L. Phillips², Mark Wilson³, Geetu Sharma⁴, Alexandra Navrotsky⁴,
Paul A. Bingham¹, Richard Brooker⁵, John B. Parise²

1. Materials and Engineering Research Institute, Sheffield Hallam University, Howard Street, Sheffield, S1 1WB, UK
2. Department of Geosciences, Stony Brook University, Stony Brook, NY11794, USA
3. Department of Chemistry, Physical and Theoretical Chemistry Laboratory, University of Oxford, South Parks Road, Oxford OX1 3QZ, UK
4. Peter A. Rock Thermochemistry Laboratory, University of California, Davis, One Shields Avenue, Davis, CA 95616, USA.
5. School of Earth Sciences, University of Bristol, Wills Memorial Building, Queens Road, Bristol, BS8 1RJ, UK.

ABSTRACT

Carbonates glasses can be formed routinely in the system K_2CO_3 - $MgCO_3$. The enthalpy of formation for one such $0.55K_2CO_3$ - $0.45MgCO_3$ glass was determined at 298 K to be 115.00 ± 1.21 kJ/mol by drop solution calorimetry in molten sodium molybdate ($3Na_2O \cdot MoO_3$) at 975 K. The corresponding heat of formation from oxides at 298 K is -261.12 ± 3.02 kJ/mol. This ternary glass is shown to be slightly metastable with respect to binary crystalline components (K_2CO_3 and $MgCO_3$) and may be further stabilized by entropy terms arising from cation disorder and carbonate group distortions. This high degree of disorder is confirmed by ^{13}C MAS NMR measurement of the average chemical shift tensor values, which show asymmetry of the carbonate anion significantly larger than previously reported values. Molecular dynamics simulations show that the structure of this carbonate glass reflects the strong interaction between the oxygen atoms in distorted carbonate anions and potassium cations.

INTRODUCTION

A variety of experimental and simulation techniques have been used to investigate the structure of glasses and glass-forming liquids. Such studies have aimed to make a connection between the atomic-scale glass or liquid structure and macroscopic properties such as viscosity, fragility and optical characteristics. Much of this research has concentrated on commercially important systems, such as silicates and borosilicates, whilst less conventional glass systems have received considerably less attention. One such class of glasses form over narrow compositional ranges in nitrate, sulphate and carbonate systems, where the process of vitrification itself remains poorly understood. Certain compositions in these dominantly ionic systems can form so-called fragile liquids, even though the glass-forming ability is generally assumed to be poor, due to a supercooled liquid structure that is temperature-dependent and is expected to change during the process of glass formation. The absence of covalent network structures may also play a role. [1].

In a series of related studies on the structure of molten salts that include nitrates, sulphates and carbonates, combined high energy X-ray diffraction experiments and molecular dynamics simulations indicate that the structure and dynamics of molten salt systems are influenced by the emergence of secondary length scales implying some linkage between the anionic groups [2-4]. In the case of carbonates, networks and other complex structures are formed from the molecular anion, the extent of which depends on temperature [2, 4]. Properties such as diffusion and, by extension, viscosity, are dependent on the length of these carbonate network chains. These studies have shown how the structures within carbonates and other molten salt liquids differ from those assumed from ionic liquid behavior. Significantly, it has been shown that the experimentally observed configurations for carbonates are best reproduced by simulations that allow molecular anions to be treated as flexible, rather than rigid structures with the carbon atom moving out of the planar trigonal geometry, allowing a second C-O bond length to emerge as the carbon atom forms a weak linkage to oxygens of other carbonate groups, i.e. a network. Unfortunately, the ionic melt systems studied so far are not glass-forming under practically-accessible cooling rates, so there is currently no direct link between the emergence of the secondary length scale and the formation of a glass forming mechanism. Whilst the rapid crystallization kinetics in most carbonate liquids limit the degree of supercooling of carbonate melts and largely prevent vitrification, there are a few

1
2
3 carbonate compositions that are known to form a glass[5] which can be used to evaluate the
4 development and extent of the proposed low-dimensional structures. In addition a biogenic form
5 of amorphous calcium carbonate (ACC) also provides a useful structural comparison [6]. In this
6 contribution we present combined thermochemical and NMR spectroscopic studies of one such
7 carbonate glass composition in the K_2CO_3 - $MgCO_3$ system, in order to determine which mechanism
8 might be responsible for its glass forming ability.
9

10
11
12
13
14 The formation of a glass in the system K_2CO_3 - $MgCO_3$ was reported by Eitel and Skalik as long
15 ago as 1929 [7], although this was a passing observation and has, with a few exceptions[8-10]
16 received little attention since. Glass in this system can be quenched successfully above a deep
17 eutectic region at a molar K_2CO_3 : $MgCO_3$ ratio of ~55:45 and at pressures of ~50 MPa [11, 12].The
18 elevated pressure is believed to prevent the carbonate from decomposing. Carbonates, along with
19 other ionic glass formers such as sulphates [13, 14] and nitrates [15], lack conventional network-
20 formers such as silicate tetrahedra, and there is considerable speculation about how these exotic
21 glasses form. In theory, the ionic nature of the carbonate anion should be dictated by the electronic
22 structure in which all the “bonding” oxygen orbitals are incorporated into C-O $p\pi$ and $s\sigma$ bonds
23 leaving none for covalent interactions. As such, they should not form the covalently-bonded
24 polymerized network usually associated with glass formation [16]. Spectroscopic studies of the
25 K_2CO_3 - $MgCO_3$ glass [8, 9, 17] indicate the presence of two structurally distinct populations of
26 carbonate anions. Genge *et al.* [8] suggest that the more symmetrical units form a flexible network
27 that comprises carbonate anions with bridging, strongly interacting metal cations (here Mg^{2+})
28 while non-bridging species (here K^+) modify the network and are associated with distorted
29 carbonate groups. It has also been suggested that glass formation in sulphate and nitrate systems
30 requires the presence of two different cations with different field strengths and different degrees
31 of polarizability [13-15]. Our proposed structure of K_2CO_3 - $MgCO_3$ glass is significantly more
32 complicated than simple ionic molten salt models would predict; and is also defined by the
33 flexibility of the molecular anion.
34
35
36
37
38
39
40
41
42
43
44
45
46
47
48

49
50 As has been demonstrated for alkali carbonate and nitrate liquids, molecular dynamics simulations
51 using the flexible anion approach provide a means of exploring parameter space, in the case of
52 Na_2CO_3 for example we are able to identify the development of complicated, low dimensional
53 structures that have temperature dependence. Since carbonate liquids are important agents of
54
55
56
57
58
59
60

1
2
3 geochemical transport and have a substantive role in deep Earth processes pressure is an important
4 state variable and in part motivates this study. High pressure and high temperature studies of
5 carbonate and indeed other liquids are challenging and it is common to use glasses to evaluate the
6 influence of pressure. Carbonate glass is therefore suitable for such an ambient temperature, high
7 pressure study and the $55\text{K}_2\text{CO}_3\text{-}45\text{MgCO}_3$ glass is the focus of a related ultra high-pressure study
8 using energy dispersive diffraction techniques and requires an understanding of the structure and
9 structure-dependent properties of the glass at ambient pressure. There are significant changes
10 within the glass structure with increasing pressure and, based on the success of the combined
11 HEXRD and MD modelling of carbonate liquids and other molten salts using a flexible anion
12 approach [2-4] we can identify the structural trends by simulating the liquid structures at different
13 densities. The trigonal geometry of the carbonate anion is imposed using harmonic springs that
14 act between O-O and C-O pairs. This flexibility is clearly important in determining the observed
15 ‘liquid’ structure and reproduces the pressure-dependent changes; and although the changes in the
16 diffraction pattern are dominated by K-K, K-O and O-O atom pairs these changes are themselves
17 indicative of associated changes in the underlying structure of the carbonate anions. The
18 relationship between the K^+ cations and the carbonate anions is characterized by structures that
19 result from the strong electrostatic interactions between the oxygen ions in the carbonates and K^+
20 cations, which result in preferential formation of close CO_3 pairs and the emergence of a second
21 C-O length-scale at 2.4 \AA with increasing pressure. This represents the development of CO_{3+1}
22 structure which is heading towards CO_4 but the flexible carbon forms a weaker, longer bond with
23 the oxygen of another group. The pressure induced linkage in $55\text{K}_2\text{CO}_3\text{-}45\text{MgCO}_3$ glass represents
24 the development of a carbonate ‘network’ similar to that observed in Na_2CO_3 melts at ambient
25 pressure and has profound implications for melt properties such as viscosity. The simulations
26 suggest relatively little change in the partial contributions from the Mg^{2+} cations in either
27 reciprocal or real space: the Mg-O partial functions remain effectively independent of pressure.
28 This is inconsistent with the model of Genge *et al.* (1995) [8] which has a modified polymerized
29 network with Mg^{2+} acting as a “bridging species” and K^+ ions act as a “modifier species”.

1
2
3 The formation of the glass in this system is not well understood, the underlying structural
4 information and accompanying simulation indicate that the flexibility of the carbonate anion is key
5 in controlling the glass-forming ability. In this study we examine further the energetic and
6 structural basis for glass formation in this system by determining the heat of formation of the glass
7 using solution calorimetry, accompanied by ^{13}C NMR and infrared spectroscopy studies that reveal
8 the local environment of carbon and the degree of distortion of the carbonate anion. These
9 experimental data are combined with the molecular dynamics simulations.

16 RESULTS AND DISCUSSION

19 INFRARED SPECTROSCOPY

21 Attenuated Total Reflectance (ATR) infrared spectroscopy data was collected on two glass
22 samples synthesized using the high pressure techniques. One sample was made using reagent grade
23 K_2CO_3 and magnesite as starting materials, the second sample was ^{13}C enriched made using
24 $\text{K}_2^{13}\text{CO}_3$ starting material (5 wt. % of the sample is ^{13}C). These spectra are shown in figure 1. The
25 use of ATR allows a better resolved and more complete absorbance spectra for the fundamental
26 internal vibrational mode of the carbonate groups, compared to that of Genge *et al.* [5], allowing
27 a better assignment of peaks. There are clearly two distinct ν_1 symmetric stretching and two ν_2
28 out-of-plane bending peaks. This strongly suggests there are two distinct carbonate groups present.
29 The degeneracy of the two ν_{3a} and ν_{3b} asymmetric stretch modes appears to be lifted to produce
30 doublets with the two carbonate types then producing 4 peaks.

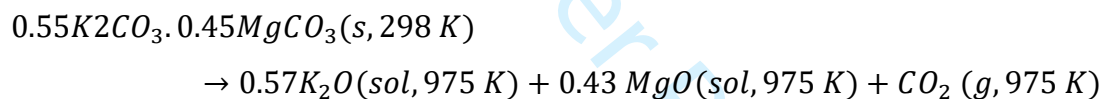
31
32
33
34
35
36
37
38
39
40 The lifting of degeneracy implies some distortion with the 3 oxygens of the carbonate groups
41 experiencing different environments for both the carbonates. The ν_4 in-plane-bend region is cut
42 off by the detector, but the Raman spectrum for this glass shows a complex peak envelope in the
43 680-720 cm^{-1} region.

44
45
46
47
48
49
50
51
52
53
54
55
56
57
58
59
60
The presence of water in the glass produced from the high pressure synthesis and deterioration of
the glass due to hydration is a persistent problem, the glasses are known to be hygroscopic and the
presence of O-H at high frequencies has been reported by Genge *et al.* In figure 1b the progressive
hydration of the glass is shown for both ^{12}C and ^{13}C -enriched samples. Note that for the ^{13}C sample
(for NMR) there is more water present, possibly because that starting materials may not have been
perfectly dry). Whilst water is undoubtedly present, there is no evidence that the water content

changes over the course of 24 hours. Over the course of several weeks the samples deteriorated, even when stored in a desiccator, and the appearance changes from that of the transparent pristine glass to an opaque white powder. However, we assume for the calorimetry, NMR and diffraction experiments that, although there is water introduced during the high pressure synthesis, the degree of hydration does not change over the course of measurement.

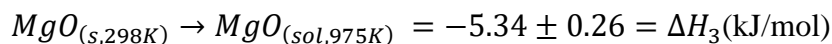
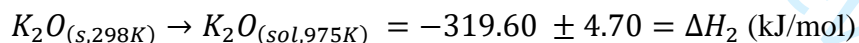
THERMOCHEMISTRY

The calorimetric data are summarized in Table 1. The average heat of solution for seven pellets of the $0.55\text{K}_2\text{CO}_3 \cdot 0.45\text{MgCO}_3$ glass is 115.00 ± 1.21 kJ/mol. To calculate the enthalpy of formation of the glass, not only is the heat of drop solution for the glass samples required but also the heat of solution of the component oxides. These are obtained from literature values and the following thermochemical cycle is used to calculate the enthalpy of formation of the $0.55\text{K}_2\text{CO}_3 \cdot 0.45\text{MgCO}_3$ glass. The measured heat of drop solution (kJ/mol) obtained from the calorimetry experiment is associated with the reaction:

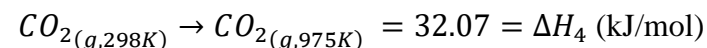


$$\Delta H_{drop\ solution, 975\text{ K}} = \Delta H_1 = 115.00 \pm 1.21\text{ (kJ/mol)}$$

The values for the heat of drop solution of K_2O and MgO [18, 19] are:



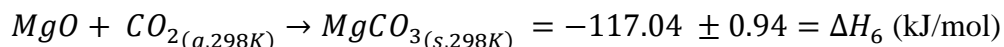
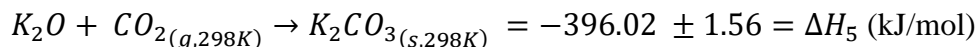
The value for CO_2 gas is obtained from tabulated heat capacity values[20],



So the enthalpy of formation of the $0.55\text{K}_2\text{CO}_3 \cdot 0.45\text{MgCO}_3$ glass from the oxides is calculated from

$$\Delta H_{f, 298\text{ K}} = -\Delta H_1 + (0.55\Delta H_2 + 0.45\Delta H_3 + \Delta H_4) = -261.12 \pm 3.02\text{ (kJ/mol)}$$

This value can be compared with the enthalpy of formation of the end-member carbonates determined from the following thermochemical cycle using literature values for the enthalpy of formation of carbonates [21-23]



$$\Delta H(f, 298K) = 0.55\Delta H_5 + 0.45\Delta H_6 = -270.06 \pm 1.81 \text{ (kJ/mol)}$$

These results indicate that the glass is only slightly metastable in enthalpy by $+9.36 \pm 1.95$ kJ/mol relative to the end members. This destabilization, which can be considered an effective vitrification enthalpy is rather small compared to typical heats of vitrification of other materials, although no data are available for potassium and magnesium carbonates, which are not glass-forming. This small enthalpy is consistent with the relative ease of glass formation in this composition and the absence of vitrification in the endmembers. The configurational entropy arising from the mixing of K^+ and Mg^{2+} ions in the glass may be sufficient to stabilize the glass under these synthesis conditions. For one mole of carbonate there are 1.55 moles of cations and, assuming random mixing, the configurational entropy is:

$$S_{conf} = -1.55 R(x \ln x + (1 - x) \ln(1 - x)) = 7.76 \text{ (J/molK)}$$

where x is the mole fraction of potassium ions equal to $1.10/1.55 = 0.71$. At the synthesis temperature of 1053 K, the $T\Delta S$ term (TS_{conf}) would be 8.2 kJ/mol which is enough to compensate the enthalpic instability obtained by calorimetry. Thus we conclude that the glass may indeed be stable in free energy compared to a mixture of the crystalline end-members. We note that the calculated configurational entropy represents a maximum value for random mixing, so the actual configurational entropy contribution may be somewhat smaller.

However the distortions of the carbonate polyhedra may also contribute to the enthalpy and entropy terms. The main point of the argument above is that the energetic destabilization of the ternary carbonate glass relative to binary crystalline carbonate end-members is very small and can be compensated by entropy terms arising from several types of disorder. Such thermodynamic behavior is not uncommon in ternary oxide systems showing strong acid-base interactions. For

example, a glass of diopside ($\text{CaMgSi}_2\text{O}_6$) composition is stable in both enthalpy and free energy relative to a mixture of crystalline CaO , MgO and 2SiO_2) but crystalline diopside is even more stable[24-26]). A crystalline ternary carbonate phase $\text{K}_2\text{Mg}(\text{CO}_3)_{\text{ternary}}$ and its hydrated forms have been reported in early studies [27-30] but there appear to be only limited thermodynamic data for such materials [31]. Thus we cannot make a direct comparison of the thermodynamics of the ternary glass and corresponding crystalline ternary carbonates.

It is apparent on the basis of the ATR and also the NMR measurements (see below) that some water is present in the glass sample. This water is structurally-bound and introduced during the synthesis. The heat of solution measurements could therefore be influenced by water. The influence of ~10 mole % water on the thermodynamic cycle outlined above, also determined from heat capacity measurements, would make the glass even less energetically stable and would increase the effective heat of vitrification term from +9.36 to $+30.87 \pm 1.95$ kJ/mol and would increase the magnitude of the $T\Delta S$ term.

Table 1: Enthalpy of drop solution of $0.55\text{K}_2\text{CO}_3\text{-}0.45\text{MgCO}_3$ glass at 975 K

Mass (mg)	$\Delta H_{\text{drop solution}}$ (kJ/mol)
6.11	115.36
4.28	115.32
6.15	111.05
4.15	116.38
5.01	115.52
4.15	114.87
5.63	116.53
Average	115.00
2 standard deviations of mean	1.84
Error %	1.21

NMR SPECTROSCOPY

The ^{13}C MAS-NMR spectra for the carbonate glass (Fig. 2a) show a broad, nearly symmetrical center band at 168.7 ppm, with a FWHM of 4.7 ppm. This chemical shift is typical for alkali and alkaline earth carbonates [32-34] and is slightly below values typically published for end member

1
2
3 crystalline K_2CO_3 at 170.7 ppm or $MgCO_3$ at 169.9 ppm, the 4.7 ppm FWHM being significantly greater
4 than either at 0.3 and 0.5 respectively [35, 36]. The large peak width indicates the presence of a
5 significant degree of disorder, consistent with an absence of any crystalline phases, and is greater
6 than that for additive-free amorphous calcium carbonate (ACC) [33, 34, 37]. This peak breadth
7 corresponds to a broad distribution of chemical shifts in the glass that spans the chemical shift
8 range for carbonate groups. The width is similar to distorted 'network carbonate' dissolved in
9 fully polymerised silicate glasses on the SiO_2 - $NaAlO_2$ join (4-6 ppm) (see Kohn *et al.* 1991;
10 Brooker *et al.* 1999 [38, 39]). The $55K_2CO_3$ - $45MgCO_3$ spectrum is otherwise consistent with that
11 expected from triangular carbonate anions, but it does not provide any further detail on the degree of
12 distortion of the carbonate anions anticipated from the molecular dynamics simulation of this composition.
13
14

15
16
17
18
19
20
21 More information on the distortion of the carbonate anions can potentially be extracted by
22 determining the anisotropy and asymmetry of the chemical shift tensor. In a conventional solid
23 state MAS-NMR experiment, the chemical shift tensor is intentionally averaged by rapid sample
24 rotation to yield the high resolution isotropic line-shape shown in Figure 2a. Slower rotation MAS
25 techniques yield a complex spinning sideband pattern (Fig. 2b), from which the principal axis
26 values of the chemical shift tensor $\delta_{xx} = 214 \pm 2$ ppm, $\delta_{yy} = 175 \pm 1$ ppm, $\delta_{zz} = 117 \pm 1$ ppm were
27 determined. The mean of the principal tensor values corresponds to the isotropic chemical shift
28 $\delta_{iso} = (\delta_{xx} + \delta_{yy} + \delta_{zz})/3$, the position of the peak in the MAS-NMR spectrum at high spinning rate
29 (Fig. 2a). From these principal values can be calculated the anisotropy $\Delta = |\delta_{zz} - \delta_{iso}| = 52 \pm 1$ ppm,
30 which provides a measure of the departure from cubic symmetry, and the asymmetry $\eta = (\delta_{yy} -$
31 $\delta_{xx})/(\delta_{zz} - \delta_{iso}) = 0.75 \pm 0.04$ as the departure from axial symmetry ($0 \leq \eta \leq 1$).
32
33
34
35
36
37
38
39
40

41
42 Owing to the hygroscopic nature of the starting materials, we used standard CP/MAS and REDOR
43 methods to ascertain whether hydration of the glass exhibited any direct effect on the ^{13}C chemical
44 shift tensor values. Observation of reasonably strong CP/MAS intensity (Fig. 2c) and a slow build-
45 up of REDOR dephasing, with a REDOR fraction asymptotically reaching 0.95 by about 20 ms
46 (Fig. S1; supporting information) indicate that essentially all carbonate groups occur in proximity
47 to H with mainly moderate to weak C-H dipolar coupling. However the spinning sideband patterns
48 obtained by CP/MAS, by REDOR difference at short dephasing time (1 ms; representing C
49 proximal to H), and with REDOR dephasing at long dephasing time (6 ms; representing C distal
50 to H) showed no systematic differences (Fig. 2c; Fig. S2, supporting information). The CSA
51
52
53
54
55
56
57
58
59
60

1
2
3 parameters obtained from these spectra are within uncertainty of the values given above from
4 spectra obtained by direct-excitation. This result indicates that although the glass contains H, the
5 average chemical shift tensor for the carbonate groups is unrelated to proximity to H. The ^{13}C -
6 detected ^1H NMR spectrum (Fig. S3; supporting information) is dominated by the signal from rigid
7 structural water, with a smaller peak for hydroxyl groups, and a minor signal for hydrogen
8 carbonate. The presence of minor hydrogen carbonate is also evident in the ^{13}C CP/MAS spectrum
9 as a small shoulder near 162 ppm (Fig. 2, inset).

16 A previous study of the CSA parameters for amorphous calcium carbonate has been used to
17 investigate the degree of distortion of the carbonate anion [6] and compared with crystalline
18 carbonates, although the amorphous calcium carbonate is never anhydrous and water may play a
19 role in controlling the degree of carbonate distortion. It was found that values for the asymmetry
20 parameter, η , show a strong relationship to the axial distortion of the carbonate group expressed
21 as the difference between the longest and shortest C-O bond lengths (σ). In contrast, very little
22 variation in the anisotropy is found for carbonate groups in crystalline phases and ACC, which fall
23 in the range 45-55 ppm. The anisotropy for $0.55\text{K}_2\text{CO}_3\cdot 0.45\text{MgCO}_3$ glass (52 ppm) falls well
24 within this range and is similar to that observed for ACC (49.3 ppm). These observations suggest
25 limited departure of the carbonate group from planar geometry. The value for the asymmetry
26 determined for the $0.55\text{K}_2\text{CO}_3\cdot 0.45\text{MgCO}_3$ glass (0.75) is significantly larger than any previously
27 reported, including those for hydromagnesite (0.55) and ACC (0.50) that are influenced by
28 significant hydrogen bonding interactions. Extrapolation of the relationship between η and σ
29 suggested by Sen *et al.*[6], yields a value of $\sigma \approx 0.054 \text{ \AA}$ for the $0.55\text{K}_2\text{CO}_3\cdot 0.45\text{MgCO}_3$ glass.
30 This significant value for σ inferred from the large observed η supports the simulation approach
31 we have used in allowing the anion to be flexible. We do note however, that this estimate arises
32 from an average CSA that represents the sum of what is likely to be a wide spread in the distribution
33 of values among carbonate anions in the glass as indicated by the large range of chemical shifts
34 represented by the breadth of the isotropic peak shape.

SIMULATION AND EDXED

AMBIENT PRESSURE

The structure of the ambient pressure glass has been studied as part of a broader investigation into the behavior of carbonate liquids at high pressure. Simulation of the ambient pressure liquid has been carried out using the flexible anion approach outlined above, which has successfully modelled the changes in the carbonate liquid structure with high pressure. Figure 3 shows the X-ray total structure factor obtained from EDXRD compared to that obtained from computer simulation. The figure also shows the X-ray weighted contributions from selected partial structure factors which sum to form the total scattering function. The agreement between the experimental and simulated total scattering functions is reasonable, both at low and high Q , the latter being dominated by the well-defined C-O and O-O nearest-neighbor length-scales arising from the carbonate anions. The agreement at intermediate Q is poor, with the oscillations over this Q -range arising from a complex superposition of all ten partial structure factors. As a result, the detailed structure in this Q -range is highly sensitive to subtle variations either in the structure factors or in the weightings used to re-combine them to form the total functions. For example, relatively small changes in the X-ray form factors[40] (which weight the partial structure factor contributions to the total scattering function) lead to large changes in $S(Q)$ in this intermediate Q -range. In the present work we make standard corrections in considering the presence of oxygen anions and apply standard tabulated form factors for carbon and the potassium and magnesium cations. It is possible that the highly correlated nature of the carbon and oxygen atoms (in forming the carbonate anions) requires a detailed re-evaluation of the appropriate form factors. In addition, our modelling focus has, to date, been on the liquid state (as part of a broader study of a range of molecular systems combined with high temperature levitation experiments). It is entirely possible that (even relatively small) changes in structure on vitrification may alter the balance of weightings of the partial structure factors and improve agreement with experiment. However, generating effective glass structures from simulation models is a well-known and significant problem in condensed matter simulation and will be the focus of future work.

1
2
3 The ambient pressure liquid structure is shown in a molecular dynamics snapshot in figure 4. The
4 figure illustrates the distortions of the carbonate anions away from the ideal trigonal planar
5 configuration (4a). Note that there is no evidence that the carbonates form chains or the other
6 complex structures as observed in simulation models for Na_2CO_3 . There is, however, clear
7 evidence that the additional C-O length scale is beginning to develop even at ambient pressure. As
8 a result the ambient pressure structure shows isolated, distorted carbonate anions with different C-
9 O bond lengths consistent with the in-plane distortion identified by the NMR measurements. The
10 flexibility of the carbonate anion, which allows the carbon atom to move out of the plane of the
11 three oxygen atoms, appears limited at ambient pressure, consistent with the NMR data that
12 suggests this deviation from the planar geometry is within the range of that for crystalline
13 carbonates.
14
15
16
17
18
19
20
21
22

23 The ambient pressure crystal structure of synthetic $\text{K}_2\text{Mg}(\text{CO}_3)_2$, determined by Hesse and Simons
24 [41] is shown for comparison in figure 4. The ambient structure is rhombohedral ($R\bar{3}m$) with
25 planar, CO_3 units arranged in the a-b plane. Magnesium octahedra are corner shared with the
26 carbonate and edge-shared with alternate KO_9 coordinate polyhedra. This structure contrasts with
27 that obtained from the simulation of the liquid, wherein the carbonate is more distorted and both
28 magnesium and potassium cations occur in irregular channels or percolation domains.
29
30
31
32
33

34 APPLICATION OF PRESSURE

35
36
37 In previous interpretations of this carbonate glass structure, magnesium is assumed to act as a
38 bridging species and to form a network with the carbonate anions. A motivation for that
39 interpretation was the combination of larger formal ion charge and smaller ionic radius which
40 make the magnesium cation significantly more polarising than the potassium cation. Although the
41 ambient pressure structure does show magnesium adopting this role, both magnesium and
42 potassium could be argued to adopt a bridging role, at the very least in the sense that they form
43 strong coulombic interactions with the carbonate anions. Although magnesium clearly has an
44 important role in stabilizing the glass, the greatest changes in response to the application of
45 pressure are observed in the relationship between the potassium and oxygen ions. To highlight
46 these changes, figure 5 shows the (unweighted) partial pair distribution functions for six selected
47 ion pairs. On application of pressure the Mg-O pair distribution function appears relatively
48 invariant with the nearest-neighbor length-scale shortening slightly (consistent with a simple
49
50
51
52
53
54
55
56
57
58
59
60

1
2
3 increase in density). The C-C, O-O and C-O pair distribution functions show significant changes
4 consistent with the greater emergence of the second C-O near-neighbor lengths-scale indicated
5 above. The most dramatic changes are observed in the K-O pair distribution function. At ambient
6 pressure the nearest-neighbor distribution is relatively broad and at relatively long range, indicative
7 of the potassium cation acting more as a network modifier than a network former. As the pressure
8 increases the nearest-neighbor length-scale shifts to significantly lower range (from $r_{\text{KO}} \sim 3.4 \text{ \AA}$ to
9 $\sim 2 \text{ \AA}$) indicative of the change in role of the potassium cation to acting as a network-former,
10 moderating the change in structure observed for the carbonate anions. More important, however,
11 is that these contributions reflect underlying changes in the carbonate anion, and it is the flexibility
12 of this anion that determines the response of this system to pressure [19]. The flexibility in the
13 anion results in the changes to the O-O and K-O contributions that result in the dramatic, pressure-
14 induced changes in the diffraction pattern which accompany the emergence of a second C-O length
15 scale. The complex relationship between the K^+ cations and the oxygen atoms in the carbonate
16 determines the high pressure response, while changes in the magnesium atom-pair contributions
17 are limited.

18
19
20
21
22
23
24
25
26
27
28
29
30 The simulated liquid structure can be compared with those of double carbonates [27] at elevated
31 pressures. The $\text{K}_2\text{Mg}(\text{CO}_3)_2$ crystal transforms from a rhombohedral ($R\bar{3}m$) structure into a
32 monoclinic polymorph with pressure [27, 30]: in this case the carbonate anion remains rigid with
33 limited change in the C-O distances, in contrast to the glass. The response to pressure of the
34 crystalline double carbonates reflects the anisotropy of compression along a - and c -axes since the
35 polyhedron of the larger cation is more compressible than that of magnesium. In the liquid it is the
36 distortion of the carbonate anion that influences the response to pressure and also the formation of
37 the glass. The structure of this glass is therefore more similar to those proposed for aqueous
38 calcium carbonate where there is strong interaction between H_2O molecules and the distorted
39 carbonate units in close proximity, stabilizing the structure against crystallization [5]. In the K-Mg
40 carbonate glass it appears that the magnesium cations form strong interactions with the carbonate
41 anions across the whole pressure range (consistent with the expected strong electrostatic
42 interactions) in a manner which can be considered network-forming. However, the role of the
43 potassium cations is more interesting as this appears to change from being largely network-
44 modifying at low pressure to network-forming at high pressure.

CONCLUSIONS

In this study we have determined the enthalpy of formation of a rare carbonate glass by high temperature oxide calorimetry. This completely glassy sample has an enthalpy of formation from the oxides of -261.12 ± 3.02 kJ/mol. The glass is energetically metastable with respect to a mixture of the crystalline endmembers by only $+9.36 \pm 1.95$ kJ/mol, and this small contribution to the free energy is balanced by the configurational entropy of K-Mg mixing, providing the ternary glass possible stability with respect to the binary crystalline end-members. Further entropic stabilization may arise from carbonate group distortions and disorder confirmed by analysis of the ^{13}C MAS NMR spectra, collected for a similarly prepared glass sample. The results show an asymmetry parameter (η), a measure of departure from axial symmetry, to be larger than for any alkali or alkaline earth carbonate, indicating that the carbonate anion is distorted, with an average difference in C-O bond length of about 0.06\AA . However, the anisotropy shows that the deviation from planar geometry falls within the range of crystalline carbonates. Molecular dynamics simulations for the equivalent liquids using the flexible anion approach also show distorted carbonate units with the carbon atom moving slightly out of plane but not forming the higher coordinate CO_{3+1} configurations proposed for high pressure versions of this glass. The ambient pressure glass sample has distorted carbonate anions that are isolated and do not form networks but show a complex relationship with the potassium cations. The interaction between the potassium cations and the oxygens from the carbonate define the glass structure at low pressure, and the same flexibility of the carbonate anion dictates the high pressure response. The ambient pressure glass is superficially similar in structure to amorphous hydrated calcium carbonate, where the structure is defined by distorted carbonate anions in close proximity to a hydrogen bonded network.

EXPERIMENTAL DETAILS

Glasses were prepared using a starting mixture of 55 mol % K_2CO_3 and 45 mol % MgCO_3 , which is the ratio at the eutectic (at ~ 730 K) on the binary join [11]. Reagent grade K_2CO_3 , or for ATR and NMR measurements, 98 % ^{13}C labelled $\text{K}_2^{13}\text{CO}_3$ (MSD isotopes), were dried at 673 K. The MgCO_3 was in the form of a natural, optically clear magnesite crystal from Brumado, Brazil (virtually water-free as confirmed by FTIR) which was ground into fine powder immediately prior to the experiment. The mixture was loaded into 3.8mm length Au capsules which were welded shut and placed into a Tuttle-type cold-seal bomb with a rapid quench rod extension[42].

1
2
3 Experiments were conducted at 1050 K, 0.1 GPa for ~10-15 hrs and then quenched ($>200^{\circ}\text{C}/\text{sec}$).
4 The resulting glass was removed from the Au capsule, mostly as a single solid slug, representing
5 the central part of the quenched melt.
6
7

8
9 IR spectra were collected using a ThermoNicolet i10 FTIR spectrometer fitted with a Ge-tipped
10 Attenuated Total Reflectance (ATR) head. 128 scans were collected at a resolution of 8cm^{-1} using
11 a MCT detector and a KBr beamsplitter in absorbance mode. The sample was polished using dry
12 alumina grit coated sheets (to a $1\mu\text{m}$ finish) and the collection area was approximately a $30\mu\text{m}$
13 square.
14
15
16
17

18
19 The enthalpy of drop solution of the carbonate glass was determined by high temperature oxide
20 melt solution calorimetry. These experiments use a custom-built, Tian-Calvet isoperibol
21 calorimeters at the Peter A. Rock Thermochemistry Laboratory at UC Davis and follow standard
22 practice reviewed in several recent publications [18, 43, 44]. In these experiments, a series of small
23 pellets of the carbonate glass (~5 mg) are dropped from room temperature into a molten oxide
24 solvent. In this case the solvent was sodium molybdate ($3\text{Na}_2\text{O}\cdot 4\text{MoO}_3$) contained in a large
25 platinum crucible which is contained in a silica glass crucible and outer silica glass liner. For these
26 experiments the entire glass assembly is flushed with oxygen at 43 mL/min. Oxygen is bubbled,
27 at 4.5 mL/min, through the solvent using a platinum-tipped silica tube; this not only mixes the
28 solvent to ensure complete dissolution of the sample and evolve the CO_2 but can also be used to
29 control the oxidation state.
30
31
32
33
34
35
36
37

38 The individual pellets are dropped from room temperature into the solvent at 975 K with the heat
39 flow resulting from the drop measured as a change in voltage in the calorimeter thermopile. Each
40 measurement comprises a 10 minute collection of the initial calorimeter baseline and the return to
41 the sample baseline following the drop solution measurement. The overall reaction times were 28-
42 30 minutes. The integral of the voltage change is converted to the reaction enthalpy by using a
43 calibration factor determined by dropping pellets of known heat contents ($\alpha\text{-Al}_2\text{O}_3$).
44
45
46
47
48
49

50 Solid-state NMR spectra were acquired at Stony Brook University with a 400 MHz (9.4 T) Varian
51 Inova spectrometer operating at 100.56 MHz and a 500 MHz Varian Infinity plus at 125.68 MHz.
52 A set of small pellets of the ^{13}C -labelled $0.55\text{K}_2\text{CO}_3\cdot 0.45\text{MgCO}_3$ glass was loaded directly into a
53 3.2 mm rotor assembly and sealed with an air-tight press-fit cap. The direct-excitation ^{13}C MAS-
54
55
56
57
58
59
60

1
2
3 NMR (Magic Angle Spinning) spectra were acquired with standard single-pulse methods with
4 $4.5\mu\text{s}$ 80° pulses and a 30 s relaxation delay at spinning rates that varied from 1.5 to 10.3 kHz.
5 The T_1 spin-lattice relaxation time was estimated to be 10 s by bracketing the null point in a series
6 of inversion-recovery experiments. Additional abbreviated acquisition spectra at a longer (50 s)
7 relaxation delay were acquired before and after each spectrum but showed no evidence of spectral
8 changes that could indicate onset of crystallization during the NMR experiments. The average ^{13}C
9 chemical shift tensor values were estimated from analysis of the spinning sideband intensities for
10 a spectrum acquired at a 1.5 kHz spinning rate according to the method of Herzfeld and Berger[45]
11 as implemented in the “HBA” software [46]. To assess potential hydration of the glass, additional
12 spectra were acquired by $^1\text{H}\rightarrow^{13}\text{C}$ cross-polarization MAS (CP-MAS) methods at contact times
13 ranging from 0.2 to 10 ms and spinning rates of 1.5 and 8.0 kHz and by $^{13}\text{C}[^1\text{H}]$ rotational echo
14 double resonance (REDOR) methods. A two-dimensional $^{13}\text{C}[^1\text{H}]$ CP heteronuclear correlation
15 spectrum was acquired at a spinning rate of 8.0 kHz and contact time of 2 ms, as 64 hypercomplex
16 points in t_1 at a $10\mu\text{s}$ interval ($100\text{ kHz } ^1\text{H}$ spectral width). Linear prediction methods were used
17 to complete the signal decay in t_1 to mitigate truncation artifacts. From these data, ^{13}C -detected
18 ^1H NMR spectra were obtained as a 1-dimensional cross-sections extracted at the ^{13}C peak
19 position. The chemical shifts were referenced to those of tetramethylsilane via secondary
20 referencing to adamantane (38.6 ppm for the methylene ^{13}C , 2.0 ppm for ^1H).
21
22
23
24
25
26
27
28
29
30
31
32
33
34

35 In previous work molecular dynamics simulations have been performed on carbonate liquids using
36 a potential developed by Tissen and Janssen, of the Born-Huggins-Mayer form [47]. The trigonal
37 geometry of the carbonate anion is imposed by employing harmonic springs that act between C-O
38 and O-O pairs. In later studies [3, 4] we developed an approach that allows both flexibility of the
39 molecular anion and fluctuation of the internal charge distribution [48-51]. In the simulations
40 carried out here we fix the charge distribution on the anion). The simulations have been carried
41 out at a fixed temperature (of $T=1800\text{ K}$) and constant volume. $F^x(Q)$ was generated by combining
42 the partial (Ashcroft-Langreth) structure factors (of which there are ten for the four component
43 system). These were calculated directly from the Fourier components of the ion densities, $S_{\alpha,\beta} =$
44 $\langle A_\alpha^*(Q)A_\beta(Q) \rangle$ where $A_\alpha(Q) = \frac{1}{\sqrt{N_\alpha}} \sum_{j=1}^{N_\alpha} \exp(i\mathbf{Q}\cdot\mathbf{r}^j)$. Total X-ray structure factors were
45 constructed from weighted sums of these partial structure factors using X-ray form factors taken
46 from standard sources [52].
47
48
49
50
51
52
53
54
55
56
57
58
59
60

The energy dispersive X-ray diffraction data were collected at HPCAT, Sector 16 at the Advanced Photon Source (APS), Argonne National Laboratory. The total X-ray structure factor was obtained using the multi-angle energy dispersive technique which uses a focused, white X-ray beam with 7 x 7_μm size. Scattering data was collected on a Ge solid state detector (Canberra) at 2 theta angles of 3.14°, 4.14°, 5.14°, 7.14°, 9.14°, 12.15°, 16.15°, 22.15°, 28.14° and 31.32°. This detector was calibrated using gold peaks at ambient pressure conditions. The total exposure for each pressure point was obtained by normalizing each detector pattern to the white X-ray beam with further corrections using the optimisation techniques described by Shen *et al.*[53] and Kono *et al.*[54]. The energy dispersive patterns for each detector were rescaled and merged to form a Faber- Ziman type total structure factor. In this study we eliminated the data from the 3.14° detector bank since these clearly showed crystalline peaks from the sample assembly. The scattering intensity in the 31.32° detector bank was very low and these latter data are also eliminated from the subsequent normalization. The individual segments were smoothed by an error weighted spline and scaled to the energy of the primary X-ray beam in the highest angle segment.

ACKNOWLEDGEMENTS

M.C.W and P.A.B. would like to acknowledge funding support from EPSRC under grant EP/R036225/1. M.W. is grateful for support from the EPSRC Centre for Doctoral Training, Theory and Modeling in Chemical Sciences, under grant EP/L015722/1. R.A.B was funded by the NERC Thematic Grant consortium NE/M000419/1. The diffraction study was performed at HPCAT (Sector 16) of the Advanced Photon Source (APS). The Advanced Photon Source is a US DOE Office of Science User facility, operated for the DOE Office of Science by Argonne National Laboratory under contract DE-AC02-06CH11357. Calorimetry at UC Davis was supported by the U.S. Department of Energy, Office of Science, Office of Basic Energy Sciences, Chemical Sciences, Geosciences, and Biosciences Division under Award DE-FG02ER1474).

REFERENCES

1. Angell, C.A., *Formation of glasses from liquids and biopolymers*. Science, 1995. **267**(5206): p. 1924-1935.
2. Wilding, M.C., et al., *Low-Dimensional Network Formation in Molten Sodium Carbonate*. Scientific Reports, 2016. **6**.
3. Wilding, M.C., et al., *The structure of liquid alkali nitrates and nitrites*. Physical Chemistry Chemical Physics, 2017. **19**(32): p. 21625-21638.

4. Wilson, M., et al., *Structure and Liquid Fragility in Sodium Carbonate*. Journal of Physical Chemistry A, 2018. **122**(4): p. 1071-1076.
5. Genge, M.J., A.P. Jones, and G.D. Price, *An Infrared and Raman Study of Carbonate Glasses-Implications for carbonatite magmas*. Geochimica et Cosmochimica Acta, 1995. **59**(5): p. 927-937.
6. Sen, S., et al., *Hydrogen bonding induced distortion of CO₃ units and kinetic stabilization of amorphous calcium carbonate: results from 2D C-13 NMR spectroscopy*. Physical Chemistry Chemical Physics, 2016. **18**(30): p. 20330-20337.
7. Eitel, W. and W. Skalijs, *Double Carbonates of Alkalis and Alkaline Earths*. Zeitschrift für Anorganische und Allgemeine Chemie, 1929. **183**: p. 263-286.
8. Genge, M.J., A.P. Jones, and G.D. Price, *An Infrared and Raman Study of Carbonate Glasses-Implications for the structure of Carbonatite Magmas*. Geochimica et Cosmochimica Acta, 1995. **59**(5): p. 927-937.
9. Genge, M.J., G.D. Price, and A.P. Jones, *Molecular Dynamics Simulations of CaCO₃ melts to Mantle Pressures and Temperatures - Implications for Carbonatite Magmas*. Earth and Planetary Science Letters, 1995. **131**(3-4): p. 225-238.
10. Dobson, D.P., et al., *In-situ measurement of viscosity and density of carbonate melts at high pressure*. Earth and Planetary Science Letters, 1996. **143**(1-4): p. 207-215.
11. Ragone, S.E., et al., *The System Potassium Carbonate-Magnesium Carbonate*. The Journal of Physical Chemistry, 1966. **70**: p. 3360-3361.
12. Datta, R.K., et al., *Glass Formation in Carbonate Systems*. Journal of The American Ceramic Society, 1964. **47**: p. 153.
13. Forland, T. and W.A. Weyl, *Formation of a Sulfate Glass*. Journal of the American Ceramic Society, 1950. **33**(6): p. 186-187.
14. MacFarlane, D.R., *Attempted Glass Formation in Pure KHSO₄*. Communications of the American Ceramic Society, 1984: p. C-28.
15. van Uitert, L.G. and W.H. Grodkiewicz, *Nitrate Glasses*. Materials Research Bulletin, 1971. **6**: p. 283-292.
16. Jones, A.P., M. Genge, and L. Carmody, *Carbonate Melts and Carbonatites*, in *Carbon in Earth*, R.M. Hazen, A.P. Jones, and J.A. Baross, Editors. 2013. p. 289-322.
17. Sharma, S.K. and B. Simons, *Raman Study of K₂CO₃-MgCO₃ glasses*. Carnegie Institute of Washington Yearbook, 1980. **79**: p. 322-326.
18. Navrotsky, A., *Progress and New Directions in Calorimetry: A 2014 Perspective*. Journal of the American Ceramic Society, 2014. **97**(11): p. 3349-3359.
19. Sahu, S.K., L.A. Boatner, and A. Navrotsky, *Formation and Dehydration Enthalpy of Potassium Hexaniobate*. Journal of the American Ceramic Society, 2017. **100**(1): p. 304-311.
20. Shivaramaiah, R. and A. Navrotsky, *Energetics of Order-Disorder in Layered Magnesium Aluminum Double Hydroxides with Inter layer Carbonate*. Inorganic Chemistry, 2015. **54**(7): p. 3253-3259.
21. Chai, L.A. and A. Navrotsky, *Thermochemistry of Carbonate-Pyroxene Equilibria*. Contributions to Mineralogy and Petrology, 1993. **114**(2): p. 139-147.
22. Kiseleva, I., et al., *Thermochemistry of natural potassium sodium calcium leonhardite and its cation-exchanged forms*. American Mineralogist, 1996. **81**(5-6): p. 668-675.
23. Navrotsky, A., et al., *Thermochemistry of double carbonates in the K₂CO₃-CaCO₃ system*. American Mineralogist, 1997. **82**(5-6): p. 546-548.

24. Tarina, I., A. Navrotsky, and H. Gan, *Direct Calorimetric Measurement of Enthalpies in Diopside-Anorthite-Wollastonite Melts at 1773K*. *Geochimica Et Cosmochimica Acta*, 1994. **58**(17): p. 3665-3673.
25. Navrotsky, A., P. Maniar, and R. Oestrike, *Energetics of Glasses in the System Diopside-Anorthite-Forsterite*. *Contributions to Mineralogy and Petrology*, 1990. **105**(1): p. 81-86.
26. Hon, R., et al., *Enthalpies of Mixing of Glasses in the System Albite-Anorthite-Diopside*. *Transactions-American Geophysical Union*, 1977. **58**(12): p. 1243-1243.
27. Golubkova, A., M. Merlini, and M.W. Schmidt, *Crystal structure, high-pressure, and high-temperature behavior of carbonates in the $K_2Mg(CO_3)_2$ - $Na_2Mg(CO_3)_2$ join*. *American Mineralogist*, 2015. **100**(11-12): p. 2458-2467.
28. Shatskiy, A., et al., *Phase relations on the K_2CO_3 - $CaCO_3$ - $MgCO_3$ join at 6 GPa and 900-1400 degrees C: Implications for incipient melting in carbonated mantle domains*. *American Mineralogist*, 2016. **101**(1-2): p. 437-447.
29. Shatskiy, A., et al., *Phase relationships in the system K_2CO_3 - $CaCO_3$ at 6 GPa and 900-1450 degrees C*. *American Mineralogist*, 2015. **100**(1): p. 223-232.
30. Shatskiy, A., et al., *The system K_2CO_3 - $MgCO_3$ at 6 GPa and 900-1450 degrees C*. *American Mineralogist*, 2013. **98**(8-9): p. 1593-1603.
31. Alekseev, A.I., et al., *Thermodynamic Values of Binary Carbonate Salts $K_2CO_3.MgCO_3.nH_2O$* . *Journal of Applied Chemistry of the USSR*, 1984. **57**(6): p. 1168-1172.
32. Papenguth, H.W., et al., *C-13 MAS NMR-Spectroscopy of Inorganic and Biogenic Carbonates*. *American Mineralogist*, 1989. **74**(9-10): p. 1152-1158.
33. Michel, F.M., et al., *Structural characteristics of synthetic amorphous calcium carbonate*. *Chemistry of Materials*, 2008. **20**(14): p. 4720-4728.
34. Michel, F.M., et al., *Structural characteristics of synthetic amorphous calcium carbonate*. *Geochimica Et Cosmochimica Acta*, 2008. **72**(12): p. A626-A626.
35. Sevelsted, T.F., D. Herfort, and J. Skibsted, *C-13 chemical shift anisotropies for carbonate ions in cement minerals and the use of C-13, Al-27 and Si-29 MAS NMR in studies of Portland cement including limestone additions*. *Cement and Concrete Research*, 2013. **52**: p. 100-111.
36. Moore, J.K., et al., *Quantitative Identification of Metastable Magnesium Carbonate Minerals by Solid-State C-13 NMR Spectroscopy (vol 49, pg 657, 2015)*. *Environmental Science & Technology*, 2015. **49**(3): p. 1986-1986.
37. Nebel, H., et al., *On the structure of amorphous calcium carbonate - A detailed study by solid-state NMR spectroscopy*. *Inorganic Chemistry*, 2008. **47**(17): p. 7874-7879.
38. Kohn, S.C., R.A. Brooker, and R. Dupree, *C-13 MAS NMR - A method for Studying CO_2 speciation in Glasses*. *Geochimica Et Cosmochimica Acta*, 1991. **55**(12): p. 3879-3884.
39. Brooker, R.A., et al., *Solubility, speciation and dissolution mechanisms for CO_2 in melts on the $NaAlO_2$ - SiO_2 join*. *Geochimica Et Cosmochimica Acta*, 1999. **63**(21): p. 3549-3565.
40. Su, Z.W. and P. Coppens, *Relativistic X-ray elastic scattering factors for neutral atoms $Z=1$ -54 from multiconfiguration Dirac-Fock wavefunctions in the 0-12 angstrom(-1) sin theta/lambda range, and six-Gaussian analytical expressions in the 0-6 angstrom(-1) range (vol A53, pg 749, 1997)*. *Acta Crystallographica Section A*, 1998. **54**: p. 357-357.
41. Hesse, K.F. and B. Simons, *Crystal Structure of Synthetic $K_2Mg(CO_3)_2$* . *Zeitschrift Fur Kristallographie*, 1982. **161**(3-4): p. 289-292.

- 1
2
3 42. Ihinger, P.D., *An Experimental Study of the Interaction of Water with Granitic Melt*. 1991, California Institute of Technology.
- 4
5 43. Navrotsky, A., *High temperature reaction calorimetry applied to metastable and*
6 *nanophase materials*. Journal of Thermal Analysis and Calorimetry, 1999. **57**(3): p. 653-
7 658.
- 8
9 44. Navrotsky, A., *High-temperature oxide melt calorimetry of oxides and nitrides*. Journal of
10 Chemical Thermodynamics, 2001. **33**(8): p. 859-871.
- 11 45. Herzfeld, J. and A.E. Berger, *Sideband Intensities in NMR-Spectra of Samples Spinning at*
12 *the Magic Angle*. Journal of Chemical Physics, 1980. **73**(12): p. 6021-6030.
- 13 46. Eichele, K., *HBA*. 2015, Universitaet Tuebingen.
- 14 47. Tissen, J., G.J.M. Janssen, and J.P. Vandereerden, *Molecular Dynamics Simulation fo*
15 *Binary Mixtures of Molten Alkali Carboantes*. Molecular Physics, 1994. **82**(1): p. 101-111.
- 16 48. Costa, M.F. and M.C.C. Ribeiro, *Molecular dynamics of molten Li₂CO₃-K₂CO₃ (vol 138,*
17 *pg 61, 2008)*. Journal of Molecular Liquids, 2008. **142**(1-3): p. 161-161.
- 18 49. Ribeiro, M.C.C., *First sharp diffraction peak in the fragile liquid Ca_{0.4}K_{0.6}(NO₃)(1.4)*.
19 Physical Review B, 2000. **61**(5): p. 3297-3302.
- 20 50. Ribeiro, M.C.C., *Ionic dynamics in the glass-forming liquid Ca_{0.4}K_{0.6}(NO₃)(1.4): A*
21 *molecular dynamics study with a polarizable model*. Physical Review B, 2001. **63**(9).
- 22 51. Ribeiro, M.C.C., *Molecular dynamics study on the glass transition in*
23 *Ca_{0.4}K_{0.6}(NO₃)(1.4)*. Journal of Physical Chemistry B, 2003. **107**(35): p. 9520-9527.
- 24 52. Cromer, D.T. and J.B. Mann, *X-ray Scattering Functions Compuited from Numerical*
25 *Hartree-Fock Functions*. Acta Crystallographica Section a-Crystal Physics Diffraction
26 Theoretical and General Crystallography, 1968. **A 24**: p. 321-&.
- 27 53. Shen, G.Y., et al., *Structural investigation of amorphous materials at high pressures using*
28 *the diamond anvil cell*. Review of Scientific Instruments, 2003. **74**(6): p. 3021-3026.
- 29 54. Kono, Y., et al., *Ultralow viscosity of carbonate melts at high pressures*. Nature
30 Communications, 2014. **5**.
- 31
32
33
34
35
36
37
38
39
40
41
42
43
44
45
46
47
48
49
50
51
52
53
54
55
56
57
58
59
60

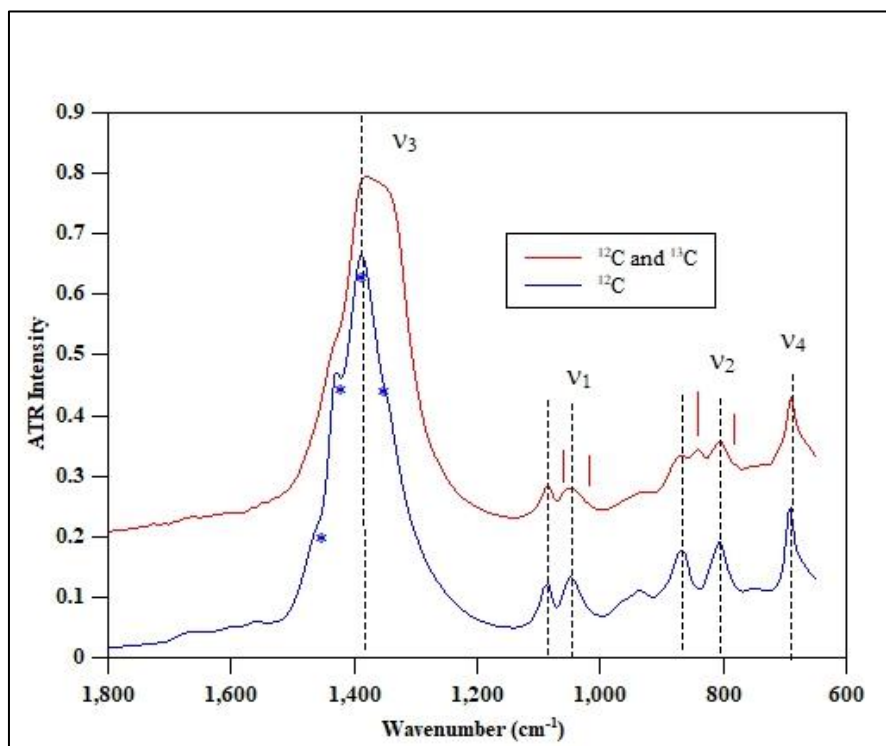


Figure 1a. FTIR absorbance spectra taken using micro-ATR. The ^{12}C sample has two peaks assigned to ν_1 symmetric stretching at 1049 and 1088 cm^{-1} and two peaks assigned to ν_2 out-of-plane bending at 806 and 870 cm^{-1} . Only one ν_4 in-plane bend peak is seen at 691 cm^{-1} , but the detector response may have cut off a second peak at lower wavenumber. The ν_3 asymmetric stretch is more complex, but can be fitted with 4 peaks representing two doublets. ν_3 are approximately at 1340 , 1377 , 1395 and 1431 cm^{-1} . In the upper spectra, the approximate magnitude of the isotopic shift related to ^{13}C is indicated by vertical ticks. The ^{13}C peaks are marked with an asterisk.

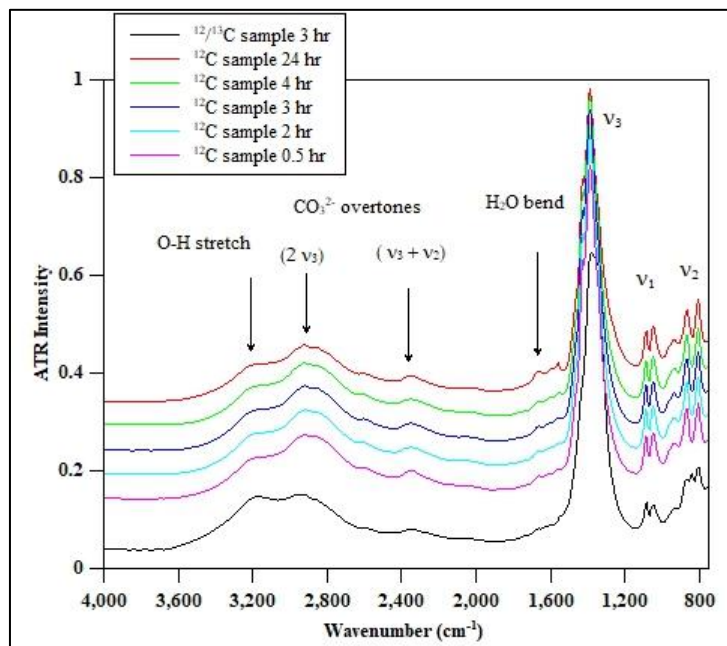


Fig 1b shows the glasses do not change their water content in the first 24 hrs. However it should be noted that they eventually turn to a white powder within 3-4 weeks. The peak at 3200 cm⁻¹ is assumed to represent O-H stretching, but is a lower frequency than observed in silicate glasses.

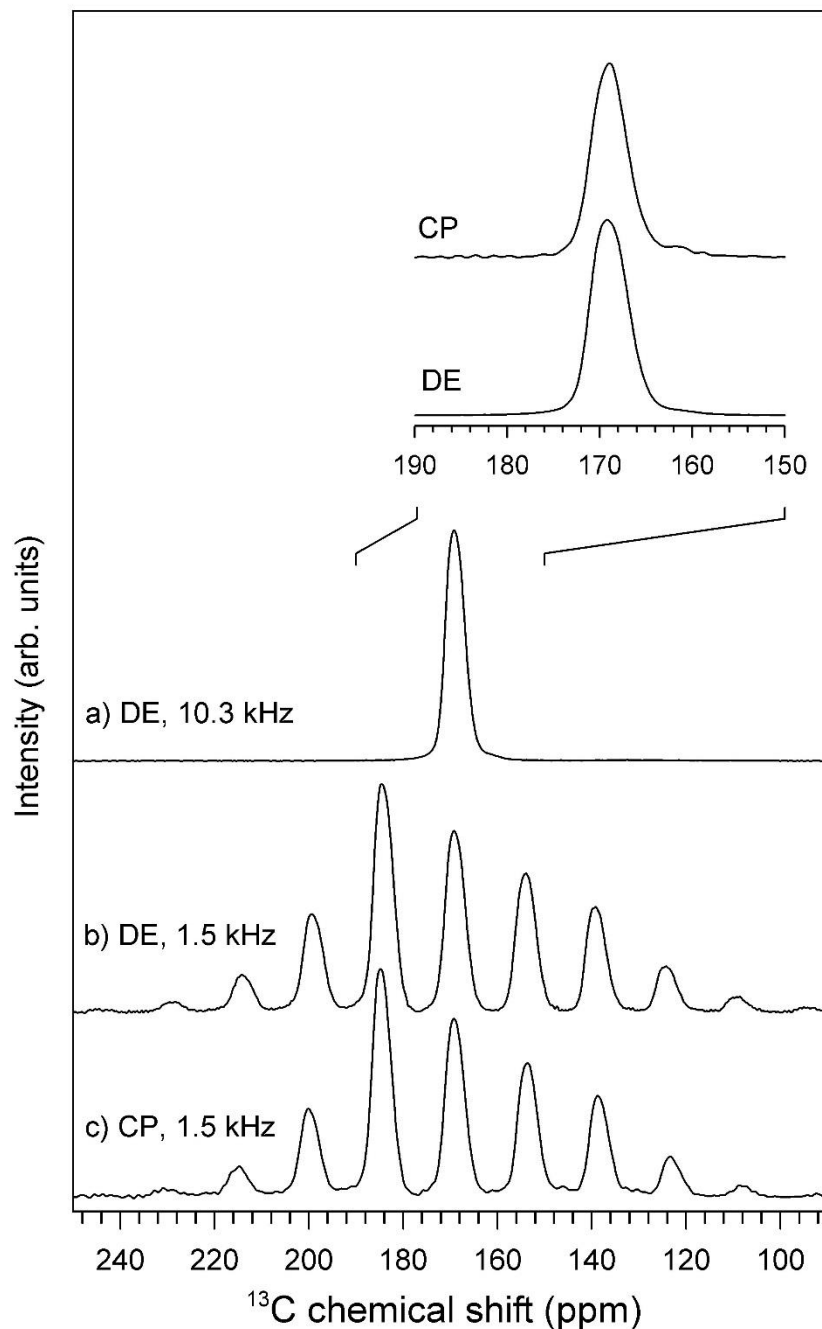


Figure 2. ^{13}C MAS-NMR spectra of ^{13}C -labelled $0.55\text{K}_2\text{CO}_3 \cdot 0.45\text{MgCO}_3$ glass acquired at 100.56 MHz (9.4 T) and spinning rates of (a) 10.3 kHz and (b-c) 1.5 kHz. Spectra in (a-b) were taken by direct ^{13}C excitation (DE) with 4.5 μs pulses separated by a 30 s relaxation delay for (a) 800 and (b) 280 acquisitions, and in (c) by standard $^1\text{H} \rightarrow ^{13}\text{C}$ cross-polarization (CP) with a 2 ms contact time, 2 s relaxation delay, for 800 scans. Inset shows center bands at expanded scale.

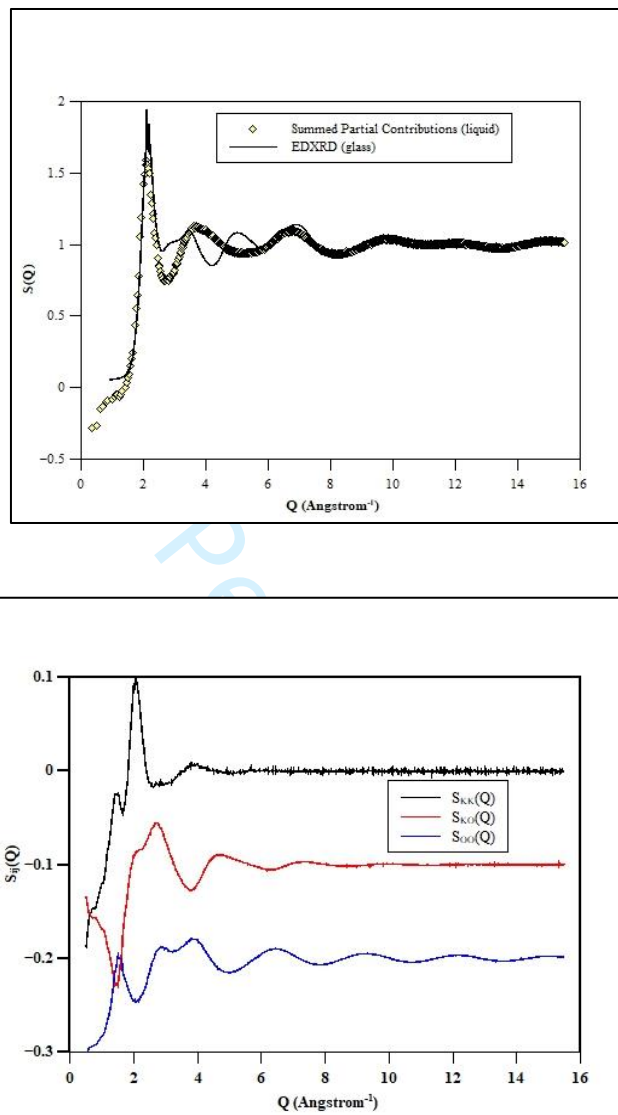


Figure 3. Energy dispersive (collected at sector 16 APS) for 55% K_2CO_3 -45% $MgCO_3$ glass compared with the summed partial contributions for the simulated liquids of the same composition (top) the lower panel shows the individual partial contributions with X-ray weighting (Ashcroft-Langreth) for K-K, K-O and O-O which dominate the X-ray scattering pattern. There is considerable mismatch between the experiment and simulation. This could result from difference between the fully relaxed liquid and the vitreous form of this carbonate.

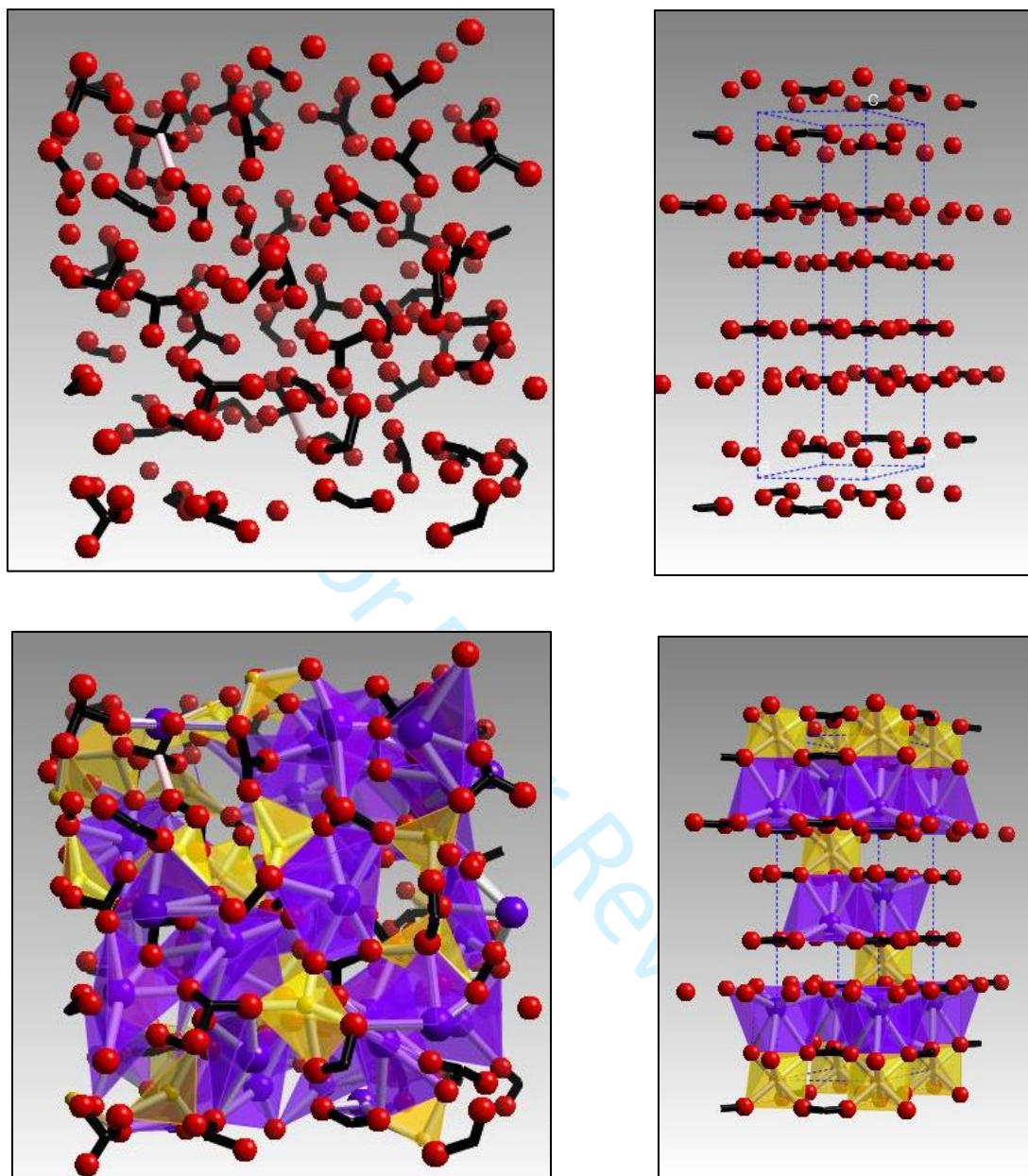


Figure 4: Molecular dynamics snapshots of the 55% K_2CO_3 -45% MgCO_3 liquid at 1800K showing the distribution of the carbonate anions. C-O bonds are shown in black (a) with some longer C-O bond lengths (shown in grey) and formation of the CO_{3+1} configuration apparent even at ambient pressure. This is compared with the rhombohedral crystal structure of $\text{K}_2\text{Mg}(\text{CO}_3)_2$ [41](b) with the unit cell illustrated, the rigid, triangular carbonate anions form planes perpendicular to the c-axis. In the lower figure potassium and magnesium atoms are also shown (c) the structure is dominated by the strong interaction between the large, blue potassium cations and the distorted carbonate. The coordination polyhedral of potassium and magnesium are shown for the ambient pressure crystal structure.

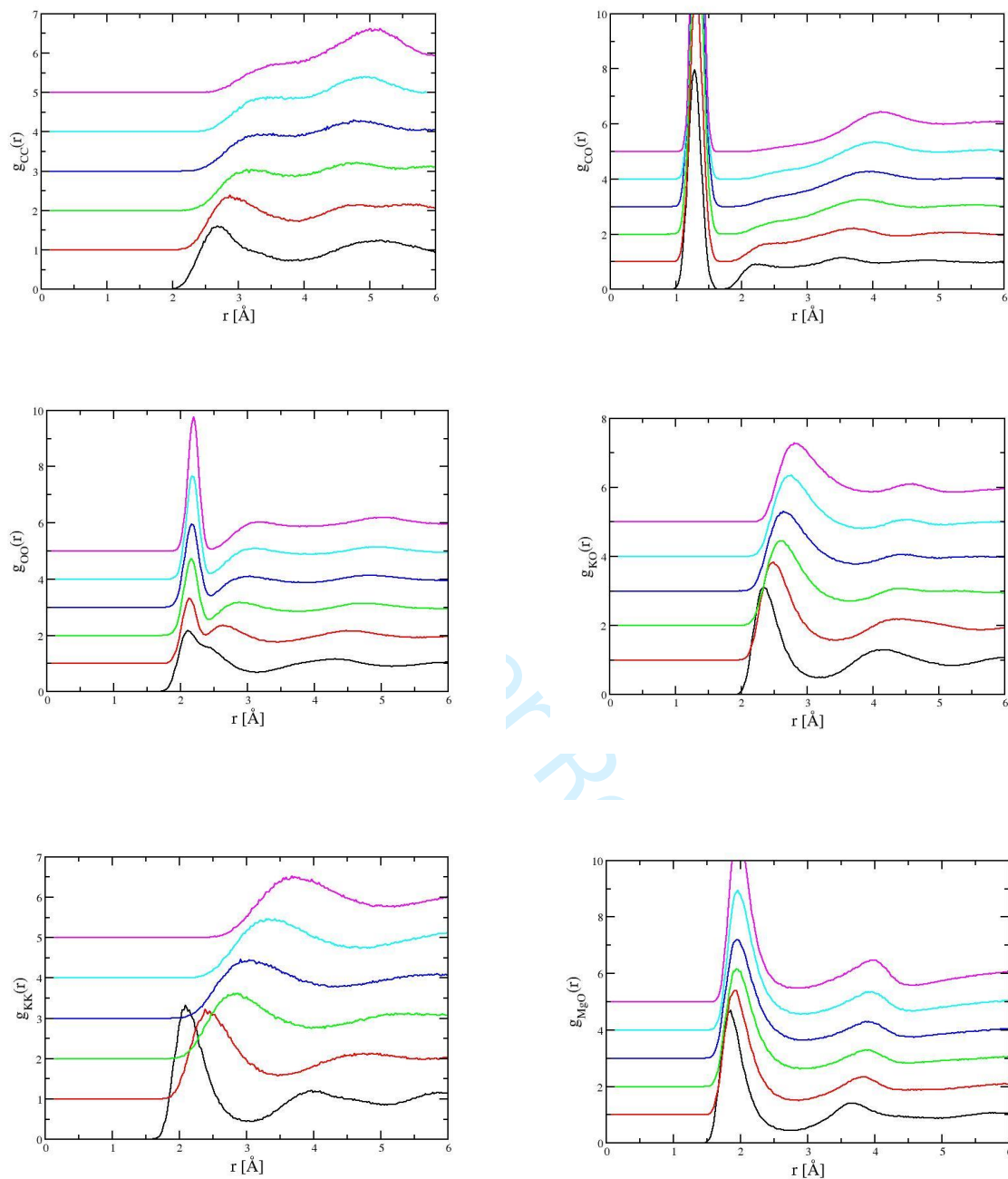


Figure 5. Six of the partial radial distribution functions to illustrate the response of the K_2CO_3 - $MgCO_3$ liquids to pressure. The curves are generated by the simulations at six different densities (pressures) with the lowest densities the topmost curves. The changes in O-O, K-K and K-O partial contribution represent the changes in the potassium sub-density and strong interaction between the oxygen atoms in the carbonate anion and the potassium cations. This results in the emergence of the second C-O length scale seen at high pressure in the C-O and C-C partial contributions. The Mg-O partial contribution changes little with pressure.

SUPPORTING INFORMATION

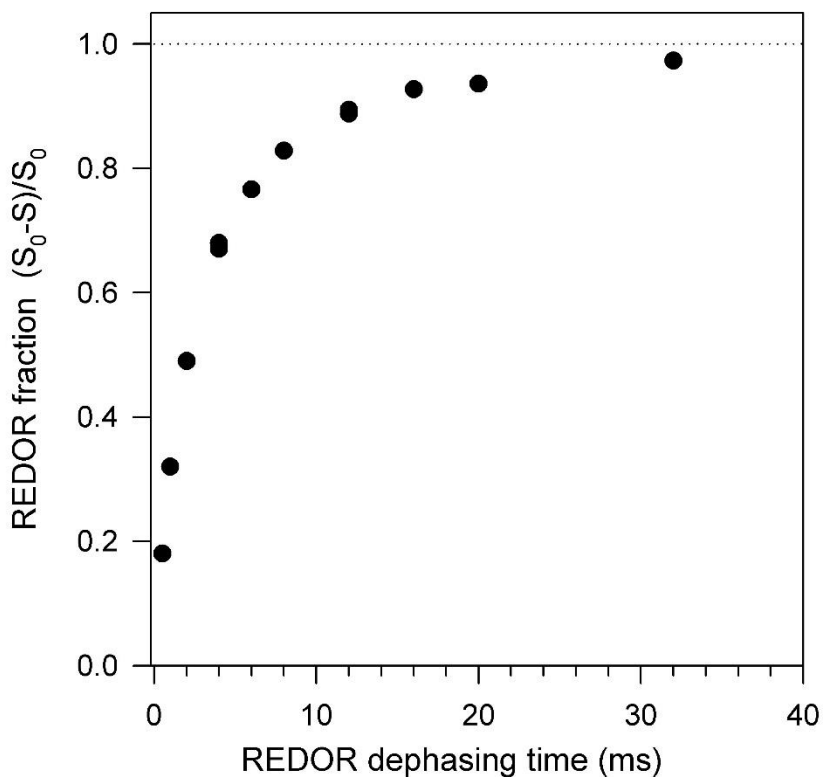


Figure S1. $^{13}\text{C}\{^1\text{H}\}$ rotational echo double resonance (REDOR) dephasing for the ^{13}C -labelled $0.55\text{K}_2\text{CO}_3 \cdot 0.45\text{MgCO}_3$ glass obtained from the intensities of the spin echo (S_0) and dephased (S) spectra. The data were acquired at 125.68 MHz (11.7 T) and a spinning rate of 8.0 kHz. The ^{13}C spin echoes were obtained by direct excitation pulses of 4 and 8 μs ($90^\circ/180^\circ$). ^1H dephasing employed 10 μs 180° pulses every one-half rotor period.

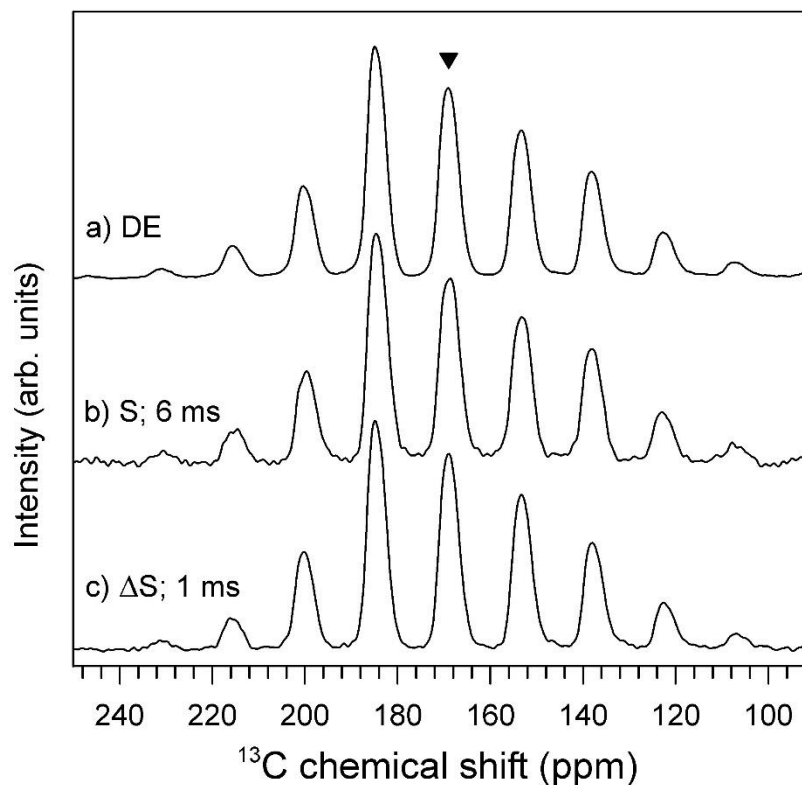


Figure S2. Comparison of ^{13}C MAS-NMR and $^{13}\text{C}\{^1\text{H}\}$ rotational echo double resonance (REDOR) spectra of ^{13}C -labelled $0.55\text{K}_2\text{CO}_3 \cdot 0.45\text{MgCO}_3$ glass acquired at 125.68 MHz (11.7 T) and spinning rate of 1.95 kHz. (a) acquired by direct ^{13}C excitation (DE) with 4 μs pulses separated by a 30 s relaxation delay; (b) REDOR dephased spectrum (S) at 77% dephasing (6 ms), emphasizing ^{13}C weakly coupled to ^1H ; (c) REDOR difference spectrum ($\Delta S = S_0 - S$) at 30% dephasing (1 ms), emphasizing ^{13}C more strongly coupled to ^1H . Center band is denoted by triangle symbol; all other peaks are spinning sidebands. Analysis of these spinning sideband intensities for all three spectra yields chemical shift tensor values that are within uncertainty.

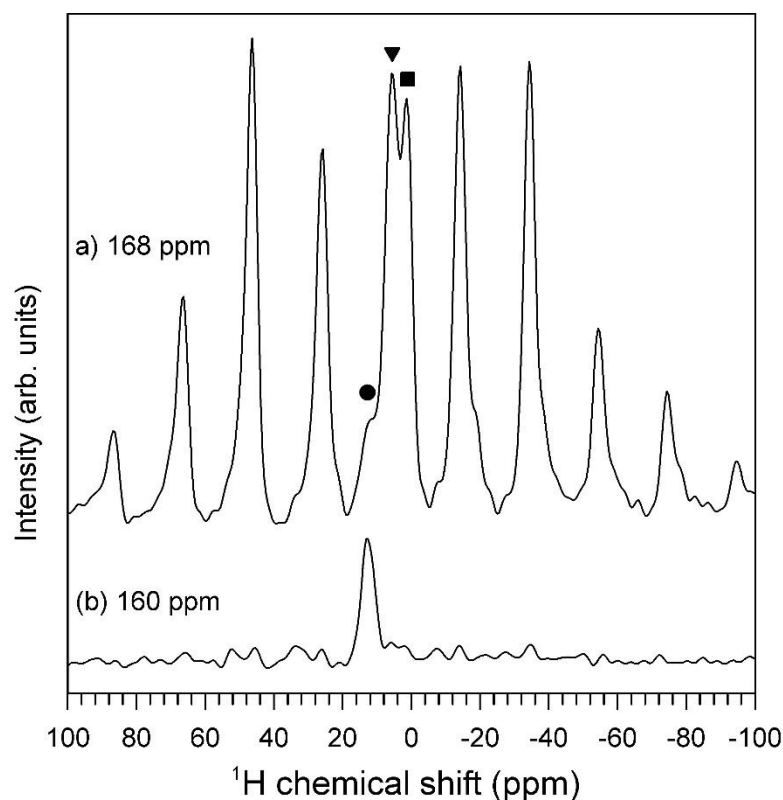


Figure S3. ^{13}C -detected ^1H MAS-NMR spectra of ^{13}C -labelled $0.55\text{K}_2\text{CO}_3 \cdot 0.45\text{MgCO}_3$ glass acquired at 399.97 MHz (9.4 T) and a spinning rate of 8.0 kHz. Spectra correspond to 1-dimensional cross-sections from 2-dimensional CP-heteronuclear correlation data, taken at ^{13}C chemical shifts corresponding to the main carbonate peak (a), and a minor hydrogen carbonate signal (b). The CP contact time was 2 ms. Center bands are denoted by symbols, including hydrogen carbonate (●; 12.5 ppm), rigid structural water (▼; 5.5 ppm), and hydroxyl (■; 1.1 ppm). All other peaks are spinning sidebands arising dominantly from the structural water.

1
2
3
4
5
6
7
8
9
10
11
12
13
14
15
16
17
18
19
20
21
22
23
24
25
26
27
28
29
30
31
32
33
34
35
36
37
38
39
40
41
42
43
44
45
46
47
48
49
50
51
52
53
54
55
56
57
58
59
60

ⁱ Currently at University of Manchester at Harwell, Diamond Light Source, Harwell Campus, Didcot, Oxfordshire, OX11 0DE

For Peer Review

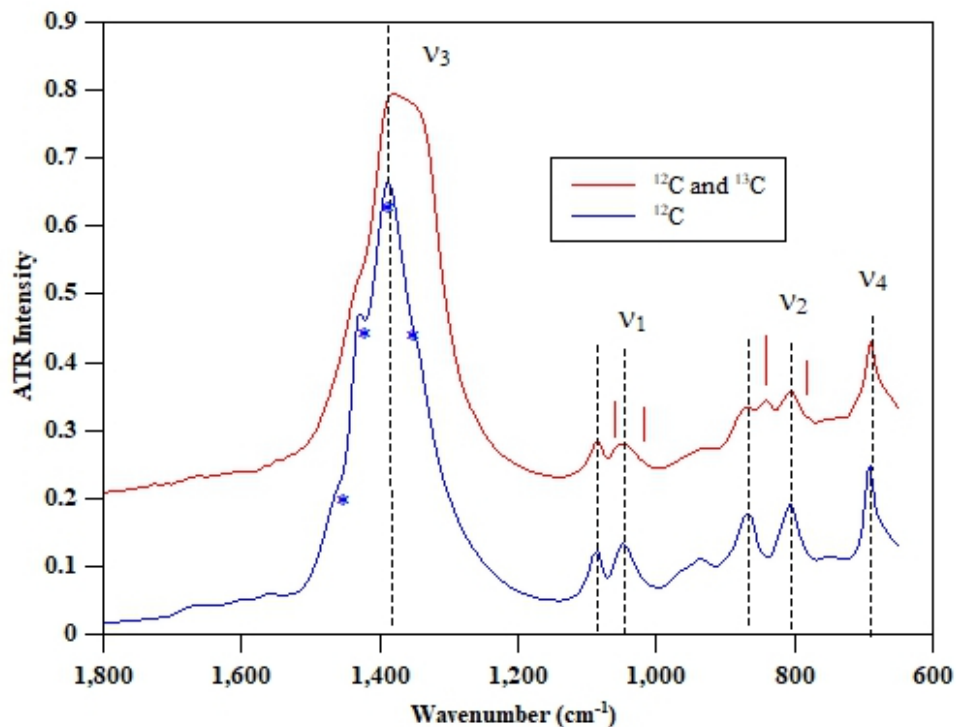


Figure 1a. FTIR absorbance spectra taken using micro-ATR. The ^{12}C sample has two peaks assigned to $\square 1$ symmetric stretching at 1049 and 1088 cm^{-1} and two peaks assigned to $\square 2$ out-of-plane bending at 806 and 870 cm^{-1} . Only one $\square 4$ in-plane bend peak is seen at 691 cm^{-1} , but the detector response may have cut off a second peak at lower wavenumber. The $\square 3$ asymmetric stretch is more complex, but can be fitted with 4 peaks representing two doublets. $\square\square 3$ are approximately at 1340 , 1377 , 1395 and 1431 cm^{-1} . In the upper spectra, the approximate magnitude of the isotopic shift related to ^{13}C is indicated by vertical ticks. The ^{13}C peaks are marked with an asterisk.

136x113mm (96 x 96 DPI)

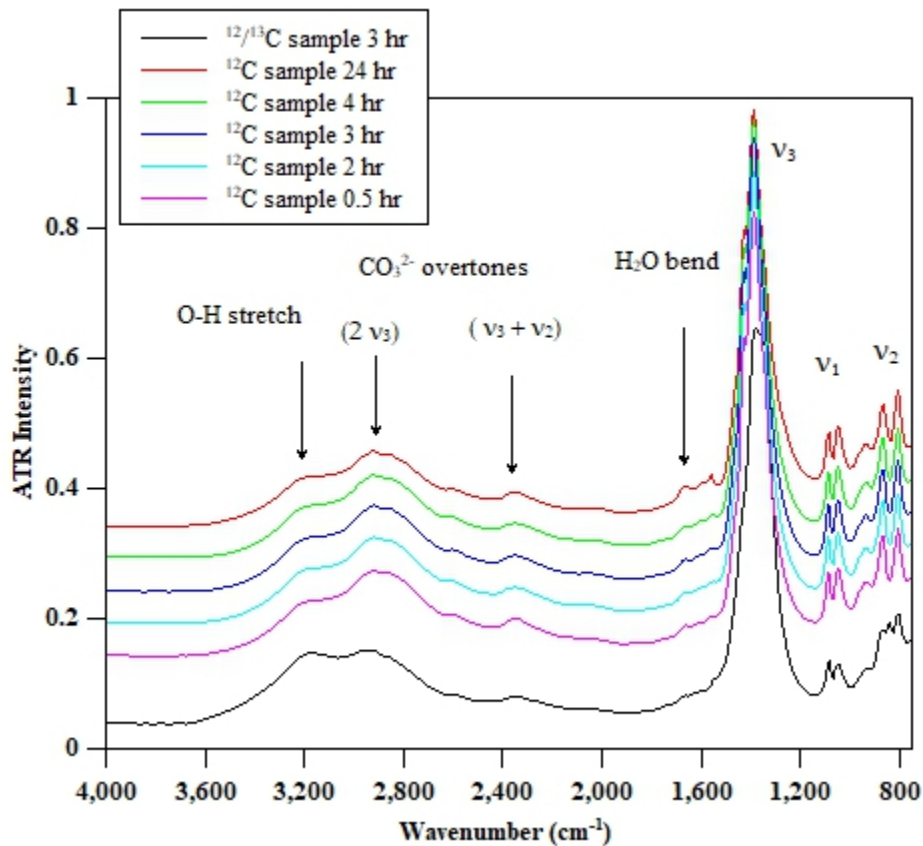


Fig 1b shows the glasses do not change their water content in the first 24 hrs. However it should be noted that they eventually turn to a white powder within 3-4 weeks. The peak at 3200 cm^{-1} is assumed to represent O-H stretching, but is a lower frequency than observed in silicate glasses.

128x112mm (96 x 96 DPI)

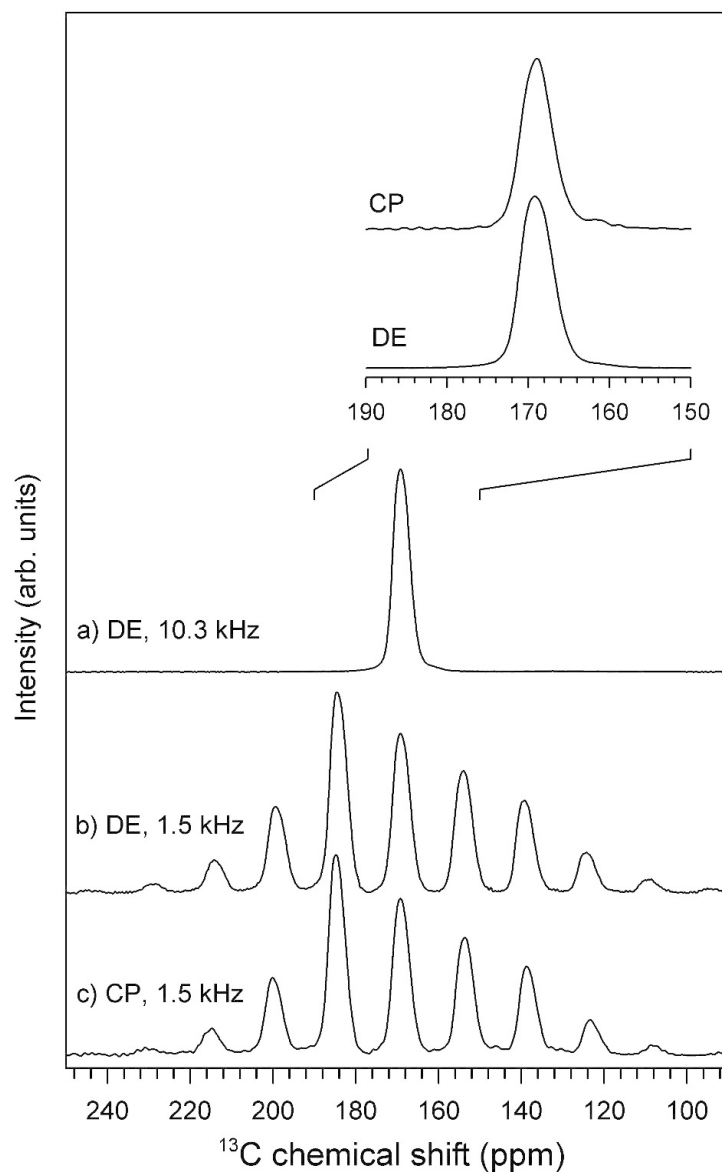


Figure 2. ^{13}C MAS-NMR spectra of ^{13}C -labelled $0.55\text{K}_2\text{CO}_3 \cdot 0.45\text{MgCO}_3$ glass acquired at 100.56 MHz (9.4 T) and spinning rates of (a) 10.3 kHz and (b-c) 1.5 kHz. Spectra in (a-b) were taken by direct ^{13}C excitation (DE) with 4.5 μs pulses separated by a 30 s relaxation delay for (a) 800 and (b) 280 acquisitions, and in (c) by standard $1\text{H} \rightarrow ^{13}\text{C}$ cross-polarization (CP) with a 2 ms contact time, 2 s relaxation delay, for 800 scans. Inset shows center bands at expanded scale.

113x180mm (220 x 220 DPI)

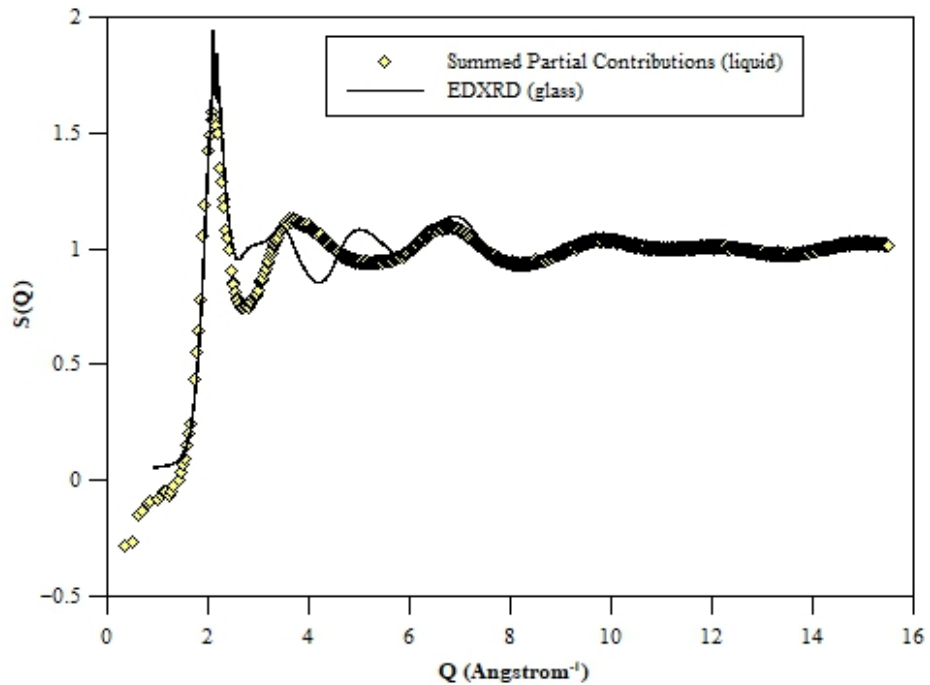


Figure 3. Energy dispersive (collected at sector 16 APS) for 55% K_2CO_3 -45% $MgCO_3$ glass compared with the summed partial contributions for the simulated liquids of the same composition (top) the lower panel shows the individual partial contributions with X-ray weighting (Ashcroft-Langreth) for K-K, K-O and O-O which dominate the X-ray scattering pattern. There is considerable mismatch between the experiment and simulation. This could result from difference between the fully relaxed liquid and the vitreous form of this carbonate.

136x113mm (96 x 96 DPI)

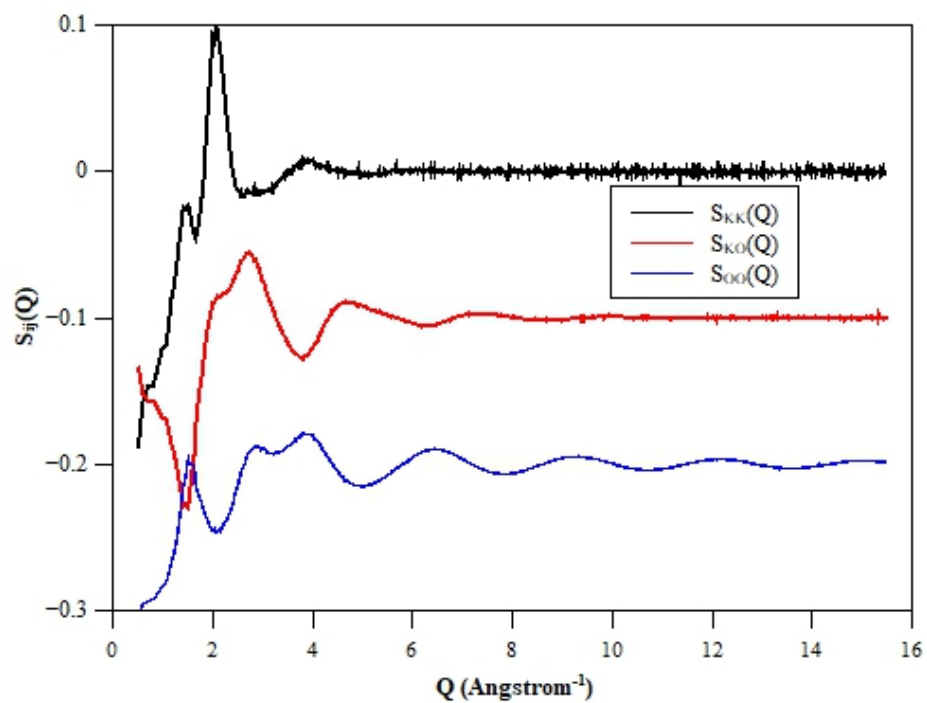
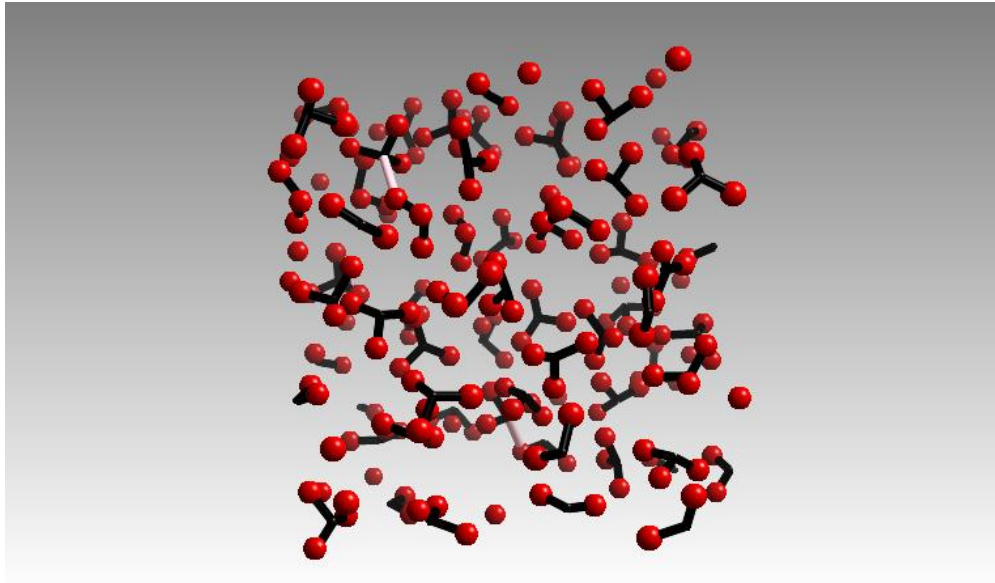


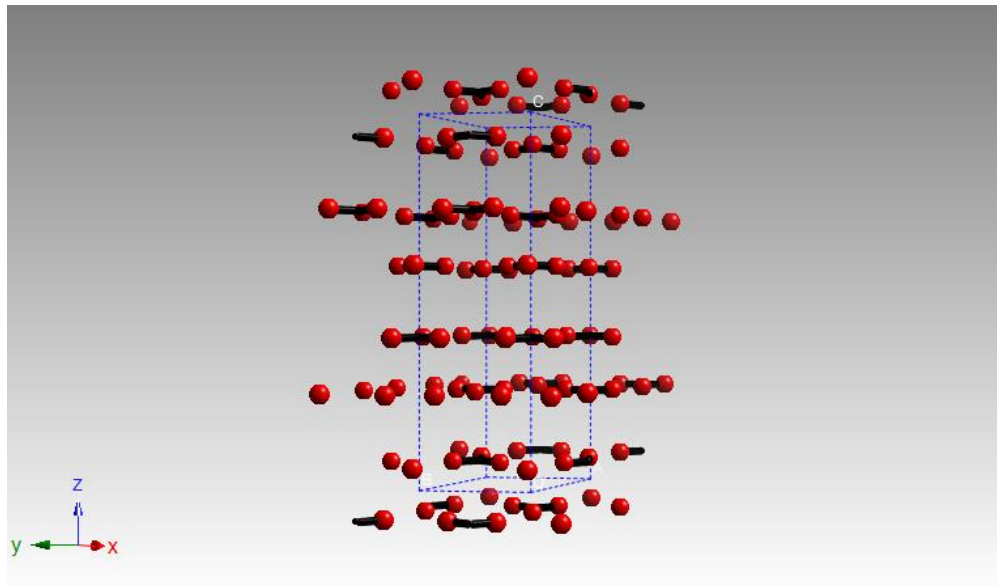
Figure 3. Energy dispersive (collected at sector 16 APS) for 55% K_2CO_3 -45% $MgCO_3$ glass compared with the summed partial contributions for the simulated liquids of the same composition (top) the lower panel shows the individual partial contributions with X-ray weighting (Ashcroft-Langreth) fo K-K, K-O and O-O which dominate the X-ray scattering pattern. There is considerable mismatch between the experiment and simulation. This could result from difference between the fully relaxed liquid and the vitreous form of this carbonate.

139x113mm (96 x 96 DPI)



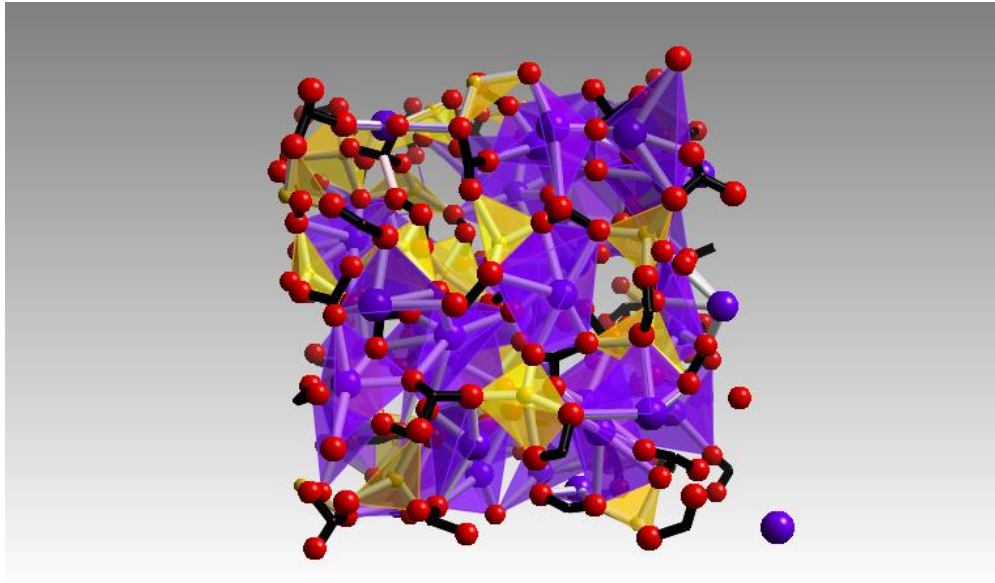
Molecular dynamics snapshots of the 55% K_2CO_3 -45% $MgCO_3$ liquid at 1800K showing the distribution of the carbonate anions. C-O bonds are shown in black (a) with some longer C-O bond lengths (shown in grey) and formation of the CO_{3+1} configuration apparent even at ambient pressure. This is compared with the rhombohedral crystal structure of $K_2Mg(CO_3)_2$ [41](b) with the unit cell illustrated, the rigid, triangular carbonate anions form planes perpendicular to the c-axis. In the lower figure potassium and magnesium atoms are also shown (c) the structure is dominated by the strong interaction between the large, blue potassium cations and the distorted carbonate. The coordination polyhedral of potassium and magnesium are shown for the ambient pressure crystal structure.

202x119mm (96 x 96 DPI)



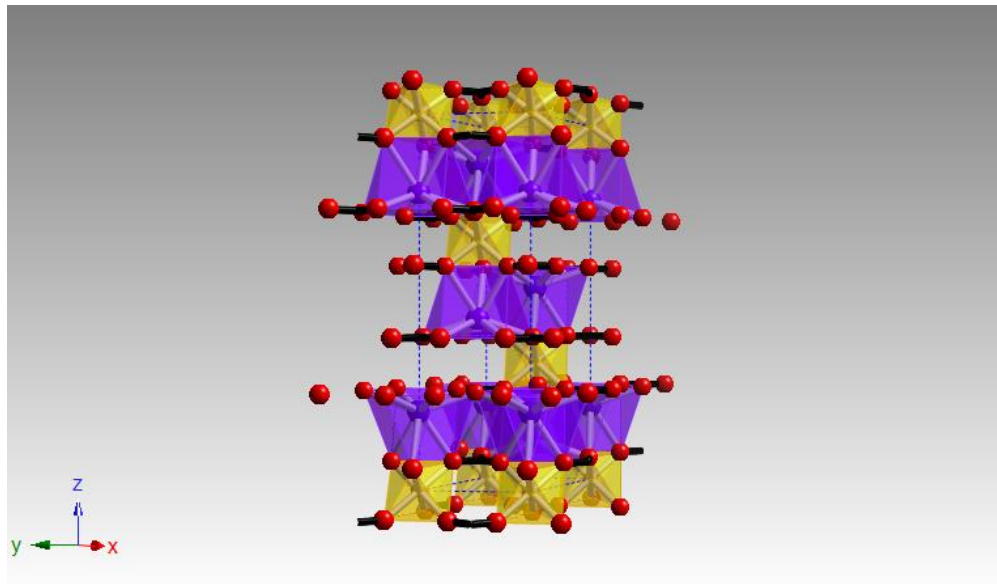
Molecular dynamics snapshots of the 55% K_2CO_3 -45% $MgCO_3$ liquid at 1800K showing the distribution of the carbonate anions. C-O bonds are shown in black (a) with some longer C-O bond lengths (shown in grey) and formation of the CO_{3+1} configuration apparent even at ambient pressure. This is compared with the rhombohedral crystal structure of $K_2Mg(CO_3)_2$ [41](b) with the unit cell illustrated, the rigid, triangular carbonate anions form planes perpendicular to the c-axis. In the lower figure potassium and magnesium atoms are also shown (c) the structure is dominated by the strong interaction between the large, blue potassium cations and the distorted carbonate. The coordination polyhedral of potassium and magnesium are shown for the ambient pressure crystal structure.

202x119mm (96 x 96 DPI)



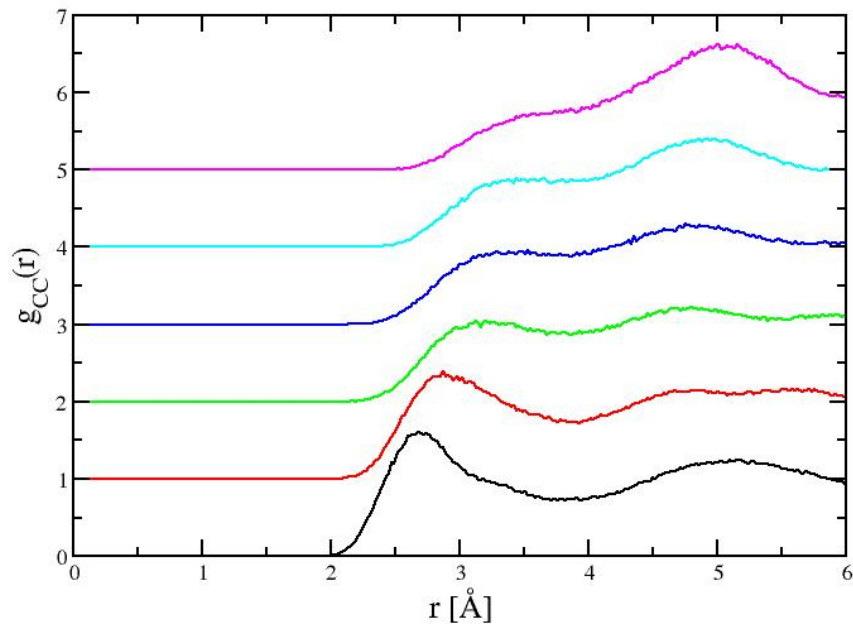
Molecular dynamics snapshots of the 55% K_2CO_3 -45% $MgCO_3$ liquid at 1800K showing the distribution of the carbonate anions. C-O bonds are shown in black (a) with some longer C-O bond lengths (shown in grey) and formation of the CO_{3+1} configuration apparent even at ambient pressure. This is compared with the rhombohedral crystal structure of $K_2Mg(CO_3)_2$ [41](b) with the unit cell illustrated, the rigid, triangular carbonate anions form planes perpendicular to the c-axis. In the lower figure potassium and magnesium atoms are also shown (c) the structure is dominated by the strong interaction between the large, blue potassium cations and the distorted carbonate. The coordination polyhedral of potassium and magnesium are shown for the ambient pressure crystal structure.

202x119mm (96 x 96 DPI)



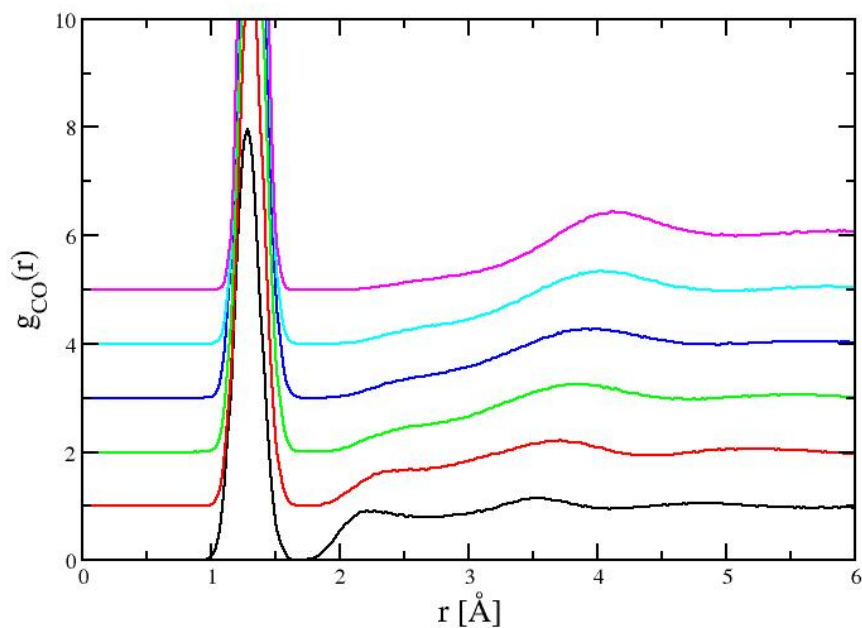
Molecular dynamics snapshots of the 55% K_2CO_3 -45% MgCO_3 liquid at 1800K showing the distribution of the carbonate anions. C-O bonds are shown in black (a) with some longer C-O bond lengths (shown in grey) and formation of the CO_{3+1} configuration apparent even at ambient pressure. This is compared with the rhombohedral crystal structure of $\text{K}_2\text{Mg}(\text{CO}_3)_2$ [41](b) with the unit cell illustrated, the rigid, triangular carbonate anions form planes perpendicular to the c-axis. In the lower figure potassium and magnesium atoms are also shown (c) the structure is dominated by the strong interaction between the large, blue potassium cations and the distorted carbonate. The coordination polyhedral of potassium and magnesium are shown for the ambient pressure crystal structure.

202x119mm (96 x 96 DPI)



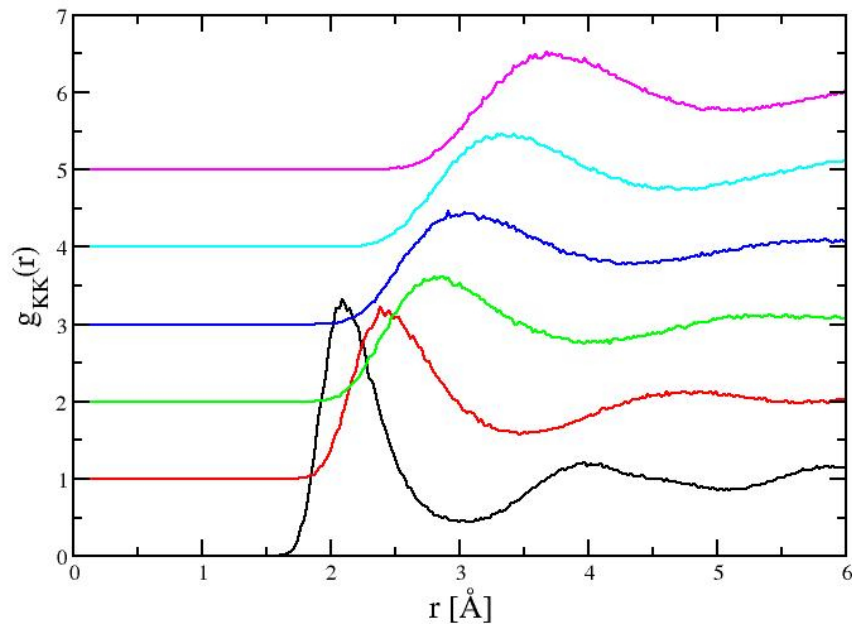
Six of the partial radial distribution functions to illustrate the response of the $\text{K}_2\text{CO}_3\text{-MgCO}_3$ liquids to pressure. The curves are generated by the simulations at six different densities (pressures) with the lowest densities the topmost curves. The changes in O-O, K-K and K-O partial contribution represent the changes in the potassium sub-density and strong interaction between the oxygen atoms in the carbonate anion and the potassium cations. This results in the emergence of the second C-O length scale seen at high pressure in the C-O and C-C partial contributions. The Mg-O partial contribution changes little with pressure.

279x215mm (72 x 72 DPI)



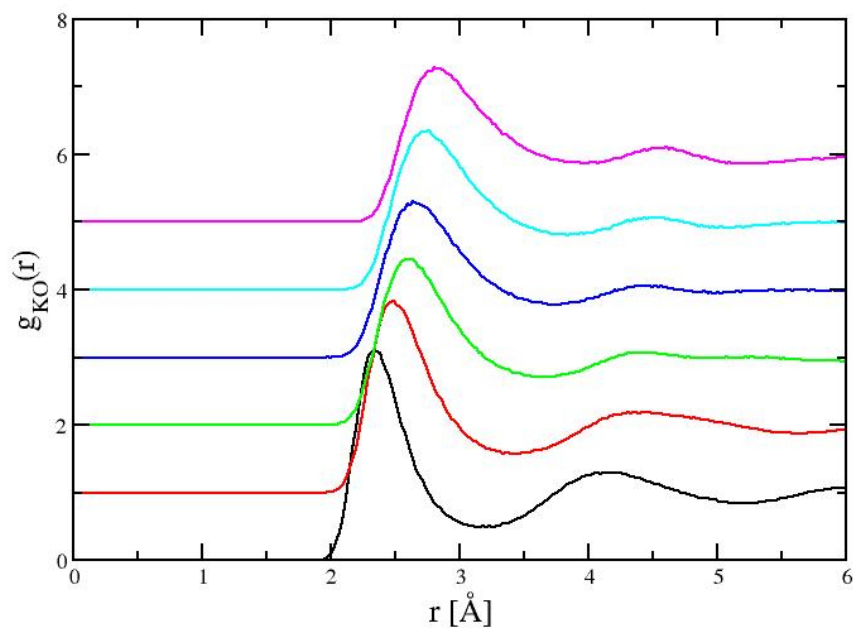
Six of the partial radial distribution functions to illustrate the response of the $\text{K}_2\text{CO}_3\text{-MgCO}_3$ liquids to pressure. The curves are generated by the simulations at six different densities (pressures) with the lowest densities the topmost curves. The changes in O-O, K-K and K-O partial contribution represent the changes in the potassium sub-density and strong interaction between the oxygen atoms in the carbonate anion and the potassium cations. This results in the emergence of the second C-O length scale seen at high pressure in the C-O and C-C partial contributions. The Mg-O partial contribution changes little with pressure.

279x215mm (72 x 72 DPI)



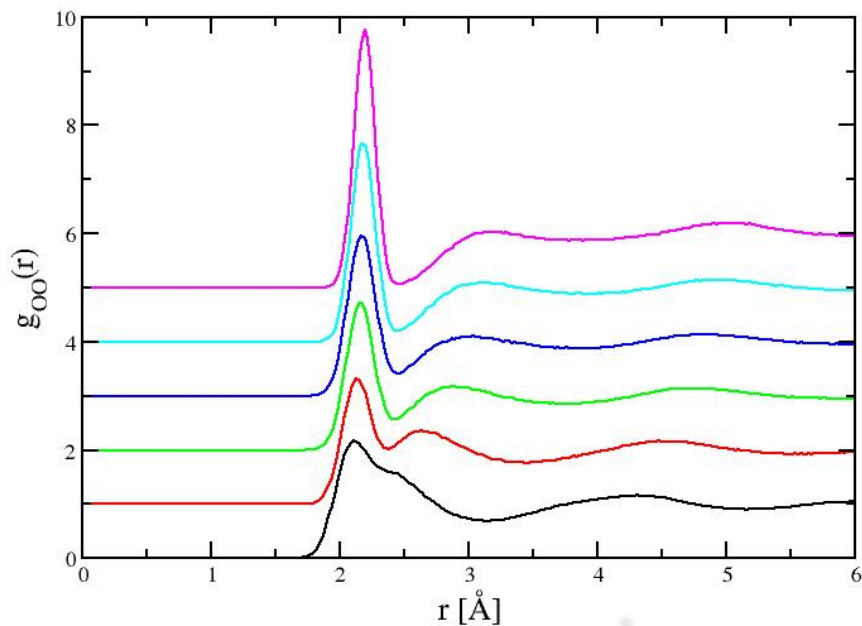
Six of the partial radial distribution functions to illustrate the response of the $\text{K}_2\text{CO}_3\text{-MgCO}_3$ liquids to pressure. The curves are generated by the simulations at six different densities (pressures) with the lowest densities the topmost curves. The changes in O-O, K-K and K-O partial contribution represent the changes in the potassium sub-density and strong interaction between the oxygen atoms in the carbonate anion and the potassium cations. This results in the emergence of the second C-O length scale seen at high pressure in the C-O and C-C partial contributions. The Mg-O partial contribution changes little with pressure.

279x215mm (72 x 72 DPI)



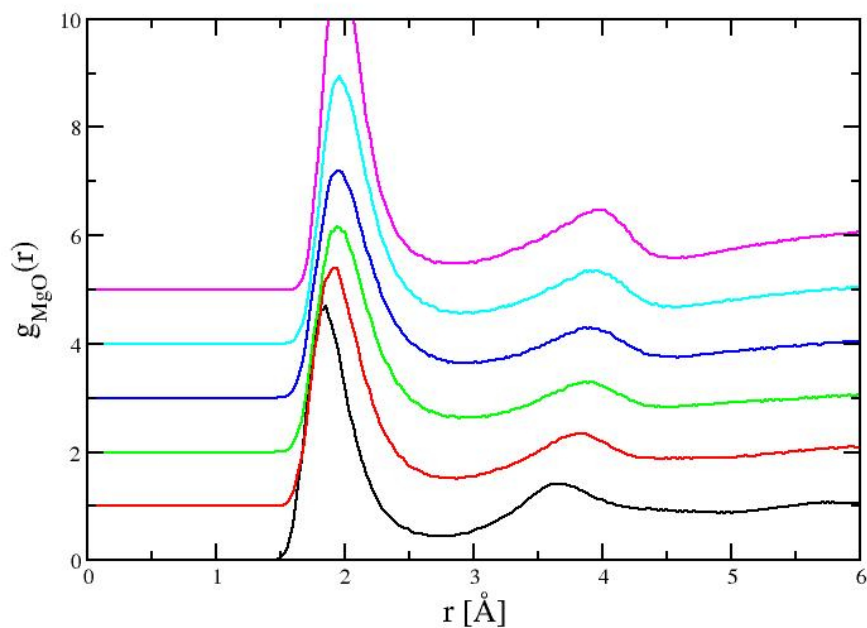
Six of the partial radial distribution functions to illustrate the response of the $\text{K}_2\text{CO}_3\text{-MgCO}_3$ liquids to pressure. The curves are generated by the simulations at six different densities (pressures) with the lowest densities the topmost curves. The changes in O-O, K-K and K-O partial contribution represent the changes in the potassium sub-density and strong interaction between the oxygen atoms in the carbonate anion and the potassium cations. This results in the emergence of the second C-O length scale seen at high pressure in the C-O and C-C partial contributions. The Mg-O partial contribution changes little with pressure.

279x215mm (72 x 72 DPI)



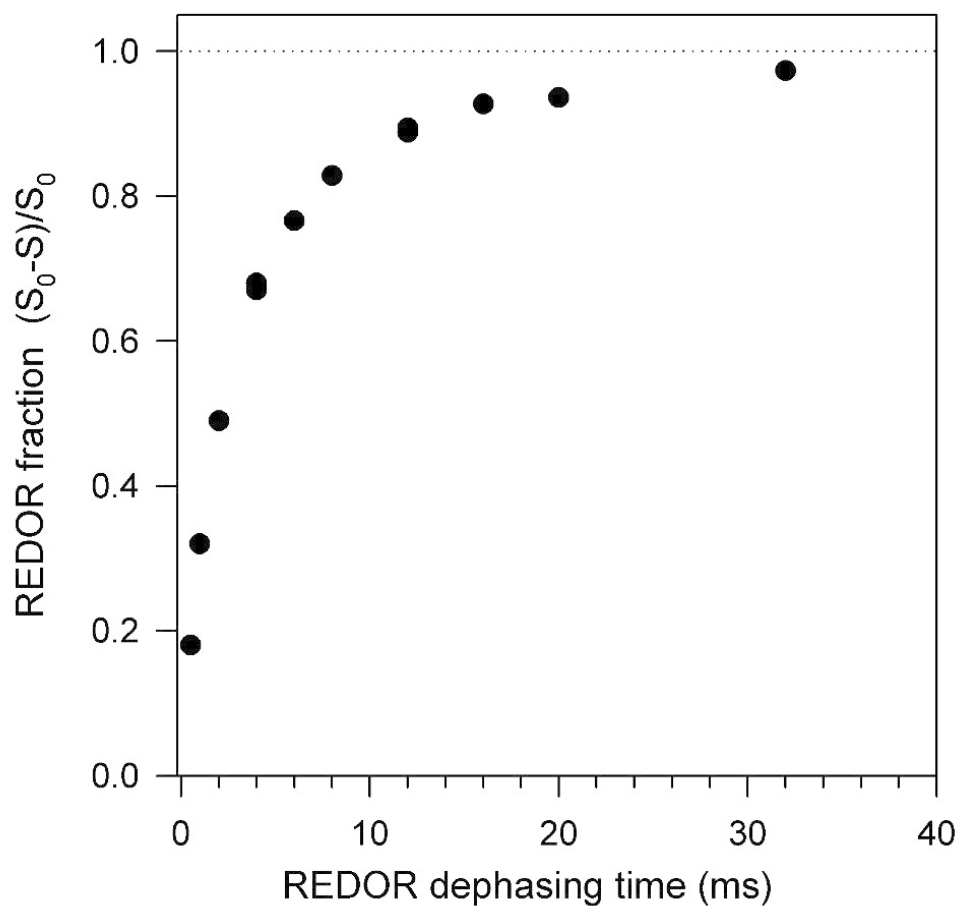
Six of the partial radial distribution functions to illustrate the response of the $\text{K}_2\text{CO}_3\text{-MgCO}_3$ liquids to pressure. The curves are generated by the simulations at six different densities (pressures) with the lowest densities the topmost curves. The changes in O-O, K-K and K-O partial contribution represent the changes in the potassium sub-density and strong interaction between the oxygen atoms in the carbonate anion and the potassium cations. This results in the emergence of the second C-O length scale seen at high pressure in the C-O and C-C partial contributions. The Mg-O partial contribution changes little with pressure.

279x215mm (72 x 72 DPI)



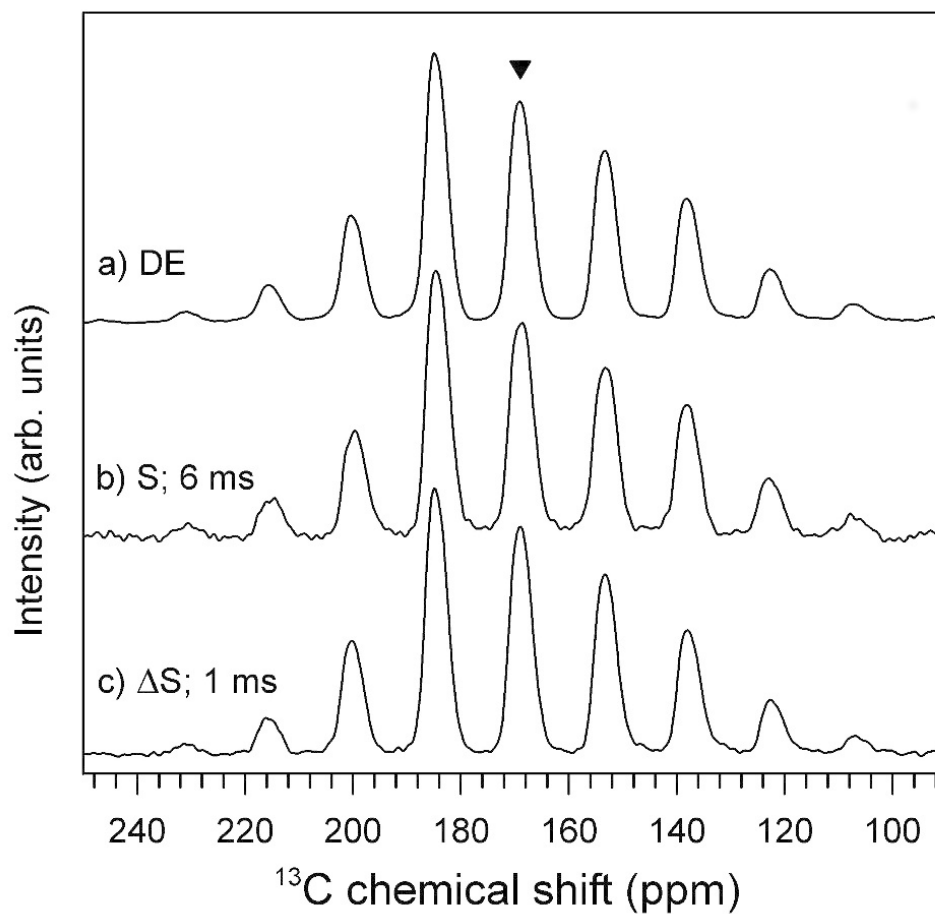
Six of the partial radial distribution functions to illustrate the response of the K_2CO_3 - $MgCO_3$ liquids to pressure. The curves are generated by the simulations at six different densities (pressures) with the lowest densities the topmost curves. The changes in O-O, K-K and K-O partial contribution represent the changes in the potassium sub-density and strong interaction between the oxygen atoms in the carbonate anion and the potassium cations. This results in the emergence of the second C-O length scale seen at high pressure in the C-O and C-C partial contributions. The Mg-O partial contribution changes little with pressure.

279x215mm (72 x 72 DPI)



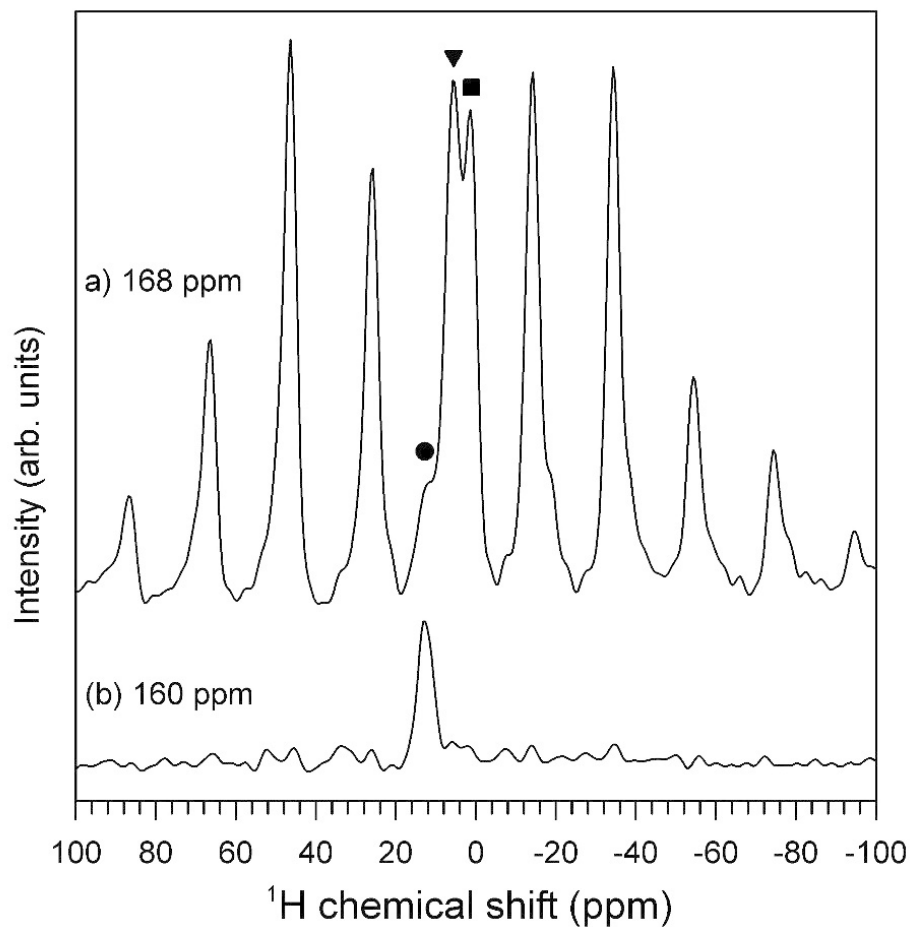
$^{13}\text{C}\{^1\text{H}\}$ rotational echo double resonance (REDOR) dephasing for the ^{13}C -labelled $0.55\text{K}_2\text{CO}_3 \cdot 0.45\text{MgCO}_3$ glass obtained from the intensities of the spin echo (S_0) and dephased (S) spectra. The data were acquired at 125.68 MHz (11.7 T) and a spinning rate of 8.0 kHz. The ^{13}C spin echoes were obtained by direct excitation pulses of 4 and 8 μs ($90^\circ/180^\circ$). ^1H dephasing employed 10 μs 180° pulses every one-half rotor period.

113x109mm (220 x 220 DPI)



Comparison of ^{13}C MAS-NMR and $^{13}\text{C}\{^1\text{H}\}$ rotational echo double resonance (REDOR) spectra of ^{13}C -labelled $0.55\text{K}_2\text{CO}_3 \cdot 0.45\text{MgCO}_3$ glass acquired at 125.68 MHz (11.7 T) and spinning rate of 1.95 kHz. (a) acquired by direct ^{13}C excitation (DE) with 4 μs pulses separated by a 30 s relaxation delay; (b) REDOR dephased spectrum (S) at 77% dephasing (6 ms), emphasizing ^{13}C weakly coupled to ^1H ; (c) REDOR difference spectrum ($\Delta S = S_0 - S$) at 30% dephasing (1 ms), emphasizing ^{13}C more strongly coupled to ^1H . Center band is denoted by triangle symbol; all other peaks are spinning sidebands. Analysis of these spinning sideband intensities for all three spectra yields chemical shift tensor values that are within uncertainty.

113x108mm (220 x 220 DPI)



^{13}C -detected ^1H MAS-NMR spectra of ^{13}C -labelled $0.55\text{K}_2\text{CO}_3 \cdot 0.45\text{MgCO}_3$ glass acquired at 399.97 MHz (9.4 T) and a spinning rate of 8.0 kHz. Spectra correspond to 1-dimensional cross-sections from 2-dimensional CP-heteronuclear correlation data, taken at ^{13}C chemical shifts corresponding to the main carbonate peak (a), and a minor hydrogen carbonate signal (b). The CP contact time was 2 ms. Center bands are denoted by symbols, including hydrogen carbonate (●; 12.5 ppm), rigid structural water (▼; 5.5 ppm), and hydroxyl (■; 1.1 ppm). All other peaks are spinning sidebands arising dominantly from the structural water.

113x107mm (220 x 220 DPI)

THE STRUCTURE AND THERMOCHEMISTRY OF K_2CO_3 - $MgCO_3$ GLASS

Martin C. Wilding^{1,2i}, Brian L. Phillips², Mark Wilson³, Geetu Sharma⁴, Alexandra Navrotsky⁴,
Paul A. Bingham¹, Richard Brooker⁵, John B. Parise²

1. Materials and Engineering Research Institute, Sheffield Hallam University, Howard Street,
Sheffield, S1 1WB, UK

2. Department of Geosciences, Stony Brook University, Stony Brook, NY11794, USA

3. Department of Chemistry, Physical and Theoretical Chemistry Laboratory, University of
Oxford, South Parks Road, Oxford OX1 3QZ, UK

4. Peter A. Rock Thermochemistry Laboratory, University of California, Davis, One Shields
Avenue, Davis, CA 95616, USA.

5. School of Earth Sciences, University of Bristol, Wills Memorial Building, Queens Road,
Bristol, BS8 1RJ, UK.

ABSTRACT

Carbonates glasses can be formed routinely in the system K_2CO_3 - $MgCO_3$. The enthalpy of formation for one such $0.55K_2CO_3$ - $0.45MgCO_3$ glass was determined at 298 K to be 115.00 ± 1.21 kJ/mol by drop solution calorimetry in molten sodium molybdate ($3Na_2O \cdot MoO_3$) at 975 K. The

1
2
3 corresponding heat of formation from oxides at 298 K is -261.12 ± 3.02 kJ/mol. This ternary glass
4
5 is shown to be slightly metastable with respect to binary crystalline components (K_2CO_3 and
6
7 $MgCO_3$) and may be further stabilized by entropy terms arising from cation disorder and carbonate
8
9 group distortions. This high degree of disorder is confirmed by ^{13}C MAS NMR measurement of
10
11 the average chemical shift tensor values, which show asymmetry of the carbonate anion
12
13 significantly larger than previously reported values. Molecular dynamics simulations show that
14
15 the structure of this carbonate glass reflects the strong interaction between the oxygen atoms in
16
17 distorted carbonate anions and potassium cations.
18
19
20
21
22
23
24
25
26
27
28
29
30
31
32
33
34
35
36
37
38
39
40
41
42
43
44
45
46
47
48
49
50
51
52
53
54
55
56
57
58
59
60

INTRODUCTION

A variety of experimental and simulation techniques have been used to investigate the structure of glasses and glass-forming liquids. Such studies have aimed to make a connection between the atomic-scale glass or liquid structure and macroscopic properties such as viscosity, fragility and optical characteristics. Much of this research has concentrated on commercially important systems, such as silicates and borosilicates, whilst less conventional glass systems have received considerably less attention. One such class of glasses form over narrow compositional ranges in nitrate, sulphate and carbonate systems, where the process of vitrification itself remains poorly understood. Certain compositions in these dominantly ionic systems can form so-called fragile liquids, even though the glass-forming ability is generally assumed to be poor, due to a supercooled liquid structure that is temperature-dependent and is expected to change during the process of glass formation. The absence of covalent network structures may also play a role. [1].

In a series of related studies on the structure of molten salts that include nitrates, sulphates and carbonates, combined high energy X-ray diffraction experiments and molecular dynamics simulations indicate that the structure and dynamics of molten salt systems are influenced by the emergence of secondary length scales implying some linkage between the anionic groups [2-4]. In the case of carbonates, networks and other complex structures are formed from the molecular anion, the extent of which depends on temperature [2, 4]. Properties such as diffusion and, by extension, viscosity, are dependent on the length of these carbonate network chains. These studies have shown how the structures within carbonates and other molten salt liquids differ from those assumed from ionic liquid behavior. Significantly, it has been shown that the experimentally observed configurations for carbonates are best reproduced by simulations that allow molecular anions to be treated as flexible, rather than rigid structures with the carbon atom moving out of the

1
2
3 planar trigonal geometry, allowing a second C-O bond length to emerge as the carbon atom forms
4 a weak linkage to oxygens of other carbonate groups, i.e. a network. Unfortunately, the ionic melt
5 systems studied so far are not glass-forming under practically-accessible cooling rates, so there is
6 currently no direct link between the emergence of the secondary length scale and the formation of
7 a glass forming mechanism. Whilst the rapid crystallization kinetics in most carbonate liquids limit
8 the degree of supercooling of carbonate melts and largely prevent vitrification, there are a few
9 carbonate compositions that are known to form a glass[5] which can be used to evaluate the
10 development and extent of the proposed low-dimensional structures. In addition a biogenic form
11 of amorphous calcium carbonate (ACC) also provides a useful structural comparison [6]. In this
12 contribution we present combined thermochemical and NMR spectroscopic studies of one such
13 carbonate glass composition in the K_2CO_3 - $MgCO_3$ system, in order to determine which mechanism
14 might be responsible for its glass forming ability.
15
16
17
18
19
20
21
22
23
24
25
26
27
28
29
30

31 The formation of a glass in the system K_2CO_3 - $MgCO_3$ was reported by Eitel and Skaliks as long
32 ago as 1929 [7], although this was a passing observation and has, with a few exceptions[8-10]
33 received little attention since. Glass in this system can be quenched successfully above a deep
34 eutectic region at a molar K_2CO_3 : $MgCO_3$ ratio of ~55:45 and at pressures of ~50 MPa [11, 12]. The
35 elevated pressure is believed to prevent the carbonate from decomposing. Carbonates, along with
36 other ionic glass formers such as sulphates [13, 14] and nitrates [15], lack conventional network-
37 formers such as silicate tetrahedra, and there is considerable speculation about how these exotic
38 glasses form. In theory, the ionic nature of the carbonate anion should be dictated by the electronic
39 structure in which all the “bonding” oxygen orbitals are incorporated into C-O $p\pi$ and $s\sigma$ bonds
40 leaving none for covalent interactions. As such, they should not form the covalently-bonded
41 polymerized network usually associated with glass formation [16]. Spectroscopic studies of the
42
43
44
45
46
47
48
49
50
51
52
53
54
55
56
57
58
59
60

1
2
3 K_2CO_3 - $MgCO_3$ glass [8, 9, 17] indicate the presence of two structurally distinct populations of
4 carbonate anions. Genge *et al.* [8] suggest that the more symmetrical units form a flexible network
5 that comprises carbonate anions with bridging, strongly interacting metal cations (here Mg^{2+})
6 while non-bridging species (here K^+) modify the network and are associated with distorted
7 carbonate groups. It has also been suggested that glass formation in sulphate and nitrate systems
8 requires the presence of two different cations with different field strengths and different degrees
9 of polarizability [13-15]. Our proposed structure of K_2CO_3 - $MgCO_3$ glass is significantly more
10 complicated than simple ionic molten salt models would predict; and is also defined by the
11 flexibility of the molecular anion.
12
13
14
15
16
17
18
19
20
21
22
23

24
25 As has been demonstrated for alkali carbonate and nitrate liquids, molecular dynamics simulations
26 using the flexible anion approach provide a means of exploring parameter space, in the case of
27 Na_2CO_3 for example we are able to identify the development of complicated, low dimensional
28 structures that have temperature dependence. Since carbonate liquids are important agents of
29 geochemical transport and have a substantive role in deep Earth processes pressure is an important
30 state variable and in part motivates this study. High pressure and high temperature studies of
31 carbonate and indeed other liquids are challenging and it is common to use glasses to evaluate the
32 influence of pressure. Carbonate glass is therefore suitable for such an ambient temperature, high
33 pressure study and the 55 K_2CO_3 -45 $MgCO_3$ glass is the focus of a related ultra high-pressure study
34 using energy dispersive diffraction techniques and requires an understanding of the structure and
35 structure-dependent properties of the glass at ambient pressure. There are significant changes
36 within the glass structure with increasing pressure and, based on the success of the combined
37 HEXRD and MD modelling of carbonate liquids and other molten salts using a flexible anion
38 approach [2-4] we can identify the structural trends by simulating the liquid structures at different
39
40
41
42
43
44
45
46
47
48
49
50
51
52
53
54
55
56
57
58
59
60

1
2
3 densities. The trigonal geometry of the carbonate anion is imposed using harmonic springs that
4 act between O-O and C-O pairs. This flexibility is clearly important in determining the observed
5
6
7
8 ‘liquid’ structure and reproduces the pressure-dependent changes; and although the changes in the
9
10
11
12
13
14
15
16
17
18
19
20
21
22
23
24
25
26
27
28
29
30
31
32
33
34
35
36
37
38
39
40
41
42
43
44
45
46
47
48
49
50
51
52
53
54
55
56
57
58
59
60

densities. The trigonal geometry of the carbonate anion is imposed using harmonic springs that act between O-O and C-O pairs. This flexibility is clearly important in determining the observed ‘liquid’ structure and reproduces the pressure-dependent changes; and although the changes in the diffraction pattern are dominated by K-K, K-O and O-O atom pairs these changes are themselves indicative of associated changes in the underlying structure of the carbonate anions. The relationship between the K^+ cations and the carbonate anions is characterized by structures that result from the strong electrostatic interactions between the oxygen ions in the carbonates and K^+ cations, which result in preferential formation of close CO_3 pairs and the emergence of a second C-O length-scale at 2.4 Å with increasing pressure. This represents the development of CO_{3+1} structure which is heading towards CO_4 but the flexible carbon forms a weaker, longer bond with the oxygen of another group. The pressure induced linkage in $55K_2CO_3$ - $45MgCO_3$ glass represents the development of a carbonate ‘network’ similar to that observed in Na_2CO_3 melts at ambient pressure and has profound implications for melt properties such as viscosity. The simulations suggest relatively little change in the partial contributions from the Mg^{2+} cations in either reciprocal or real space: the Mg-O partial functions remain effectively independent of pressure. This is inconsistent with the model of Genge *et al.* (1995) [8] which has a modified polymerized network with Mg^{2+} acting as a “bridging species” and K^+ ions act as a “modifier species”.

The formation of the glass in this system is not well understood, the underlying structural information and accompanying simulation indicate that the flexibility of the carbonate anion is key

1
2
3 in controlling the glass-forming ability. In this study we examine further the energetic and
4 structural basis for glass formation in this system by determining the heat of formation of the glass
5 using solution calorimetry, accompanied by ^{13}C NMR and infrared spectroscopy studies that reveal
6 the local environment of carbon and the degree of distortion of the carbonate anion. These
7 experimental data are combined with the molecular dynamics simulations.
8
9
10
11
12
13

14 15 **RESULTS AND DISCUSSION**

16 17 **INFRARED SPECTROSCOPY**

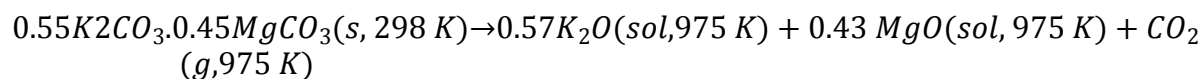
18
19 Attenuated Total Reflectance (ATR) infrared spectroscopy data was collected on two glass
20 samples synthesized using the high pressure techniques. One sample was made using reagent grade
21 K_2CO_3 and magnesite as starting materials, the second sample was ^{13}C enriched made using
22 $\text{K}_2^{13}\text{CO}_3$ starting material (5 wt. % of the sample is ^{13}C). These spectra are shown in figure 1. The
23 use of ATR allows a better resolved and more complete absorbance spectra for the fundamental
24 internal vibrational mode of the carbonate groups, compared to that of Genge *et al.* [5], allowing
25 a better assignment of peaks. There are clearly two distinct ν_1 symmetric stretching and two ν_2
26 out-of-plane bending peaks. This strongly suggests there are two distinct carbonate groups present.
27 The degeneracy of the two ν_{3a} and ν_{3b} asymmetric stretch modes appears to be lifted to produce
28 doublets with the two carbonate types then producing 4 peaks.
29
30
31
32
33
34
35
36
37
38
39
40
41
42
43
44
45

46 The lifting of degeneracy implies some distortion with the 3 oxygens of the carbonate groups
47 experiencing different environments for both the carbonates. The ν_4 in-plane-bend region is cut
48 off by the detector, but the Raman spectrum for this glass shows a complex peak envelope in the
49 680-720 cm^{-1} region.
50
51
52
53
54
55
56
57
58
59
60

The presence of water in the glass produced from the high pressure synthesis and deterioration of the glass due to hydration is a persistent problem, the glasses are known to be hygroscopic and the presence of O-H at high frequencies has been reported by Genge *et al.* In figure 1b the progressive hydration of the glass is shown for both ^{12}C and ^{13}C -enriched samples. Note that for the ^{13}C sample (for NMR) there is more water present, possibly because that starting materials may not have been perfectly dry). Whilst water is undoubtedly present, there is no evidence that the water content changes over the course of 24 hours. Over the course of several weeks the samples deteriorated, even when stored in a desiccator, and the appearance changes from that of the transparent pristine glass to an opaque white powder. However, we assume for the calorimetry, NMR and diffraction experiments that, although there is water introduced during the high pressure synthesis, the degree of hydration does not change over the course of measurement.

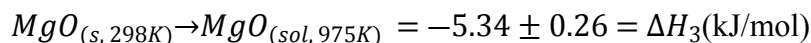
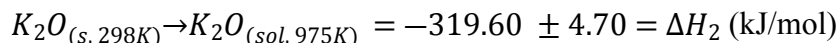
THERMOCHEMISTRY

The calorimetric data are summarized in Table 1. The average heat of solution for seven pellets of the $0.55\text{K}_2\text{CO}_3\cdot 0.45\text{MgCO}_3$ glass is 115.00 ± 1.21 kJ/mol. To calculate the enthalpy of formation of the glass, not only is the heat of drop solution for the glass samples required but also the heat of solution of the component oxides. These are obtained from literature values and the following thermochemical cycle is used to calculate the enthalpy of formation of the $0.55\text{K}_2\text{CO}_3\cdot 0.45\text{MgCO}_3$ glass. The measured heat of drop solution (kJ/mol) obtained from the calorimetry experiment is associated with the reaction:

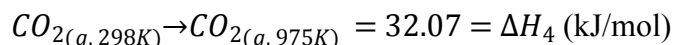


$$\Delta H_{drop\ solution, 975\text{K}} = \Delta H_1 = 115.00 \pm 1.21\text{ (kJ/mol)}$$

The values for the heat of drop solution of K_2O and MgO [18, 19] are:



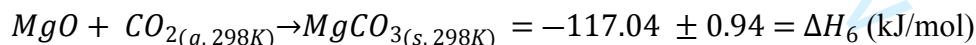
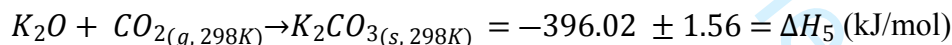
The value for CO_2 gas is obtained from tabulated heat capacity values[20],



So the enthalpy of formation of the $0.55K_2CO_3 \cdot 0.45MgCO_3$ glass from the oxides is calculated from

$$\Delta H_{f, 298K} = -\Delta H_1 + (0.55\Delta H_2 + 0.45\Delta H_3 + \Delta H_4) = -261.12 \pm 3.02 \text{ (kJ/mol)}$$

This value can be compared with the enthalpy of formation of the end-member carbonates determined from the following thermochemical cycle using literature values for the enthalpy of formation of carbonates [21-23]



$$\Delta H(f, 298K) = 0.55\Delta H_5 + 0.45\Delta H_6 = -270.06 \pm 1.81 \text{ (kJ/mol)}$$

These results indicate that the glass is only slightly metastable in enthalpy by $+9.36 \pm 1.95$ kJ/mol relative to the end members. This destabilization, which can be considered an effective vitrification enthalpy is rather small compared to typical heats of vitrification of other materials, although no data are available for potassium and magnesium carbonates, which are not glass-forming. This small enthalpy is consistent with the relative ease of glass formation in this composition and the

1
2
3 absence of vitrification in the endmembers. The configurational entropy arising from the mixing
4 of K^+ and Mg^{2+} ions in the glass may be sufficient to stabilize the glass under these synthesis
5 conditions. For one mole of carbonate there are 1.55 moles of cations and, assuming random
6 mixing, the configurational entropy is:
7
8
9
10
11

$$S_{conf} = -1.55 R(x \ln x + (1 - x) \ln (1 - x)) = 7.76 \text{ (J/molK)}$$

12
13
14
15
16 where x is the mole fraction of potassium ions equal to $1.10/1.55 = 0.71$. At the synthesis
17 temperature of 1053 K, the $T\Delta S$ term (TS_{conf}) would be 8.2 kJ/mol which is enough to compensate
18 the enthalpic instability obtained by calorimetry. Thus we conclude that the glass may indeed be
19 stable in free energy compared to a mixture of the crystalline end-members. We note that the
20 calculated configurational entropy represents a maximum value for random mixing, so the actual
21 configurational entropy contribution may be somewhat smaller.
22
23
24
25
26
27
28
29
30

31 However the distortions of the carbonate polyhedra may also contribute to the enthalpy and
32 entropy terms. The main point of the argument above is that the energetic destabilization of the
33 ternary carbonate glass relative to binary crystalline carbonate end-members is very small and can
34 be compensated by entropy terms arising from several types of disorder. Such thermodynamic
35 behavior is not uncommon in ternary oxide systems showing strong acid-base interactions. For
36 example, a glass of diopside ($CaMgSi_2O_6$) composition is stable in both enthalpy and free energy
37 relative to a mixture of crystalline CaO , MgO and $2SiO_2$) but crystalline diopside is even more
38 stable[24-26]). A crystalline ternary carbonate phase $K_2Mg(CO_3)_{ternary}$ and its hydrated forms
39 have been reported in early studies [27-30] but there appear to be only limited thermodynamic
40 data for such materials [31]. Thus we cannot make a direct comparison of the thermodynamics of
41 the ternary glass and corresponding crystalline ternary carbonates.
42
43
44
45
46
47
48
49
50
51
52
53
54
55
56
57
58
59
60

It is apparent on the basis of the ATR and also the NMR measurements (see below) that some water is present in the glass sample. This water is structurally-bound and introduced during the synthesis. The heat of solution measurements could therefore be influenced by water. The influence of ~10 mole % water on the thermodynamic cycle outlined above, also determined from heat capacity measurements, would make the glass even less energetically stable and would increase the effective heat of vitrification term from +9.36 to $+30.87 \pm 1.95$ kJ/mol and would increase the magnitude of the TΔS term.

Table 1: Enthalpy of drop solution of 0.55K₂CO₃-0.45MgCO₃ glass at 975 K

Mass (mg)	$\Delta H_{\text{drop solution}}$ (kJ/mol)
6.11	115.36
4.28	115.32
6.15	111.05
4.15	116.38
5.01	115.52
4.15	114.87
5.63	116.53
Average	115.00
2 standard deviations of mean	1.84
Error %	1.21

NMR SPECTROSCOPY

The ¹³C MAS-NMR spectra for the carbonate glass (Fig. 2a) show a broad, nearly symmetrical center band at 168.7 ppm, with a FWHM of 4.7 ppm. This chemical shift is typical for alkali and

1
2
3 alkaline earth carbonates [32-34] and is slightly below values typically published for end member
4 crystalline K_2CO_3 at 170.7 ppm or $MgCO_3$ at 169.9 ppm, the 4.7 ppm FWHM being significantly greater
5 than either at 0.3 and 0.5 respectively [35, 36]. The large peak width indicates the presence of a
6 significant degree of disorder, consistent with an absence of any crystalline phases, and is greater
7 than that for additive-free amorphous calcium carbonate (ACC) [33, 34, 37]. This peak breadth
8 corresponds to a broad distribution of chemical shifts in the glass that spans the chemical shift
9 range for carbonate groups. The width is similar to distorted 'network carbonate' dissolved in
10 fully polymerised silicate glasses on the SiO_2 - $NaAlO_2$ join (4-6 ppm) (see Kohn *et al.* 1991;
11 Brooker *et al.* 1999 [38, 39]). The $55K_2CO_3$ - $45MgCO_3$ spectrum is otherwise consistent with that
12 expected from triangular carbonate anions, but it does not provide any further detail on the degree of
13 distortion of the carbonate anions anticipated from the molecular dynamics simulation of this composition.
14
15 More information on the distortion of the carbonate anions can potentially be extracted by
16 determining the anisotropy and asymmetry of the chemical shift tensor. In a conventional solid
17 state MAS-NMR experiment, the chemical shift tensor is intentionally averaged by rapid sample
18 rotation to yield the high resolution isotropic line-shape shown in Figure 2a. Slower rotation MAS
19 techniques yield a complex spinning sideband pattern (Fig. 2b), from which the principal axis
20 values of the chemical shift tensor $\delta_{xx} = 214 \pm 2$ ppm, $\delta_{yy} = 175 \pm 1$ ppm, $\delta_{zz} = 117 \pm 1$ ppm were
21 determined. The mean of the principal tensor values corresponds to the isotropic chemical shift
22 $\delta_{iso} = (\delta_{xx} + \delta_{yy} + \delta_{zz})/3$, the position of the peak in the MAS-NMR spectrum at high spinning rate
23 (Fig. 2a). From these principal values can be calculated the anisotropy $\Delta = |\delta_{zz} - \delta_{iso}| = 52 \pm 1$ ppm,
24 which provides a measure of the departure from cubic symmetry, and the asymmetry $\eta = (\delta_{yy} -$
25 $\delta_{xx})/(\delta_{zz} - \delta_{iso}) = 0.75 \pm 0.04$ as the departure from axial symmetry ($0 \leq \eta \leq 1$).
26
27
28
29
30
31
32
33
34
35
36
37
38
39
40
41
42
43
44
45
46
47
48
49
50
51
52
53
54
55
56
57
58
59
60

Owing to the hygroscopic nature of the starting materials, we used standard CP/MAS and REDOR methods to ascertain whether hydration of the glass exhibited any direct effect on the ^{13}C chemical shift tensor values. Observation of reasonably strong CP/MAS intensity (Fig. 2c) and a slow build-up of REDOR dephasing, with a REDOR fraction asymptotically reaching 0.95 by about 20 ms (Fig. S1; supporting information) indicate that essentially all carbonate groups occur in proximity to H with mainly moderate to weak C-H dipolar coupling. However the spinning sideband patterns obtained by CP/MAS, by REDOR difference at short dephasing time (1 ms; representing C proximal to H), and with REDOR dephasing at long dephasing time (6 ms; representing C distal to H) showed no systematic differences (Fig. 2c; Fig. S2, supporting information). The CSA parameters obtained from these spectra are within uncertainty of the values given above from spectra obtained by direct-excitation. This result indicates that although the glass contains H, the average chemical shift tensor for the carbonate groups is unrelated to proximity to H. The ^{13}C -detected ^1H NMR spectrum (Fig. S3; supporting information) is dominated by the signal from rigid structural water, with a smaller peak for hydroxyl groups, and a minor signal for hydrogen carbonate. The presence of minor hydrogen carbonate is also evident in the ^{13}C CP/MAS spectrum as a small shoulder near 162 ppm (Fig. 2, inset).

A previous study of the CSA parameters for amorphous calcium carbonate has been used to investigate the degree of distortion of the carbonate anion [6] and compared with crystalline carbonates, although the amorphous calcium carbonate is never anhydrous and water may play a role in controlling the degree of carbonate distortion. It was found that values for the asymmetry parameter, η , show a strong relationship to the axial distortion of the carbonate group expressed as the difference between the longest and shortest C-O bond lengths (σ). In contrast, very little variation in the anisotropy is found for carbonate groups in crystalline phases and ACC, which fall

1
2
3 in the range 45-55 ppm. The anisotropy for $0.55\text{K}_2\text{CO}_3\cdot 0.45\text{MgCO}_3$ glass (52 ppm) falls well
4
5 within this range and is similar to that observed for ACC (49.3 ppm). These observations suggest
6
7 limited departure of the carbonate group from planar geometry. The value for the asymmetry
8
9 determined for the $0.55\text{K}_2\text{CO}_3\cdot 0.45\text{MgCO}_3$ glass (0.75) is significantly larger than any previously
10
11 reported, including those for hydromagnesite (0.55) and ACC (0.50) that are influenced by
12
13 significant hydrogen bonding interactions. Extrapolation of the relationship between η and σ
14
15 suggested by Sen *et al.*[6], yields a value of $\sigma \approx 0.054 \text{ \AA}$ for the $0.55\text{K}_2\text{CO}_3\cdot 0.45\text{MgCO}_3$ glass.
16
17 This significant value for σ inferred from the large observed η supports the simulation approach
18
19 we have used in allowing the anion to be flexible. We do note however, that this estimate arises
20
21 from an average CSA that represents the sum of what is likely to be a wide spread in the distribution
22
23 of values among carbonate anions in the glass as indicated by the large range of chemical shifts
24
25 represented by the breadth of the isotropic peak shape.
26
27
28
29
30
31
32
33
34
35
36
37
38
39
40
41
42
43
44
45
46
47
48
49
50
51
52
53
54
55
56
57
58
59
60

SIMULATION AND EDXED

AMBIENT PRESSURE

The structure of the ambient pressure glass has been studied as part of a broader investigation into the behavior of carbonate liquids at high pressure. Simulation of the ambient pressure liquid has been carried out using the flexible anion approach outlined above, which has successfully modelled the changes in the carbonate liquid structure with high pressure. Figure 3 shows the X-ray total structure factor obtained from EDXRD compared to that obtained from computer simulation. The figure also shows the X-ray weighted contributions from selected partial structure factors which sum to form the total scattering function. The agreement between the experimental and simulated total scattering functions is reasonable, both at low and high Q , the latter being dominated by the well-defined C-O and O-O nearest-neighbor length-scales arising from the carbonate anions. The agreement at intermediate Q is poor, with the oscillations over this Q -range arising from a complex superposition of all ten partial structure factors. As a result, the detailed structure in this Q -range is highly sensitive to subtle variations either in the structure factors or in the weightings used to re-combine them to form the total functions. For example, relatively small changes in the X-ray form factors^[40] (which weight the partial structure factor contributions to the total scattering function) lead to large changes in $S(Q)$ in this intermediate Q -range. In the present work we make standard corrections in considering the presence of oxygen anions and apply standard tabulated form factors for carbon and the potassium and magnesium cations. It is possible that the highly correlated nature of the carbon and oxygen atoms (in forming the carbonate anions) requires a detailed re-evaluation of the appropriate form factors. In addition, our modelling focus

1
2
3 has, to date, been on the liquid state (as part of a broader study of a range of molecular systems
4 combined with high temperature levitation experiments). It is entirely possible that (even relatively
5 small) changes in structure on vitrification may alter the balance of weightings of the partial
6 structure factors and improve agreement with experiment. However, generating effective glass
7 structures from simulation models is a well-known and significant problem in condensed matter
8 simulation and will be the focus of future work.
9
10
11
12
13
14
15
16
17

18 The ambient pressure liquid structure is shown in a molecular dynamics snapshot in figure 4. The
19 figure illustrates the distortions of the carbonate anions away from the ideal trigonal planar
20 configuration (4a). Note that there is no evidence that the carbonates form chains or the other
21 complex structures as observed in simulation models for Na_2CO_3 . There is, however, clear
22 evidence that the additional C-O length scale is beginning to develop even at ambient pressure. As
23 a result the ambient pressure structure shows isolated, distorted carbonate anions with different C-
24 O bond lengths consistent with the in-plane distortion identified by the NMR measurements. The
25 flexibility of the carbonate anion, which allows the carbon atom to move out of the plane of the
26 three oxygen atoms, appears limited at ambient pressure, consistent with the NMR data that
27 suggests this deviation from the planar geometry is within the range of that for crystalline
28 carbonates.
29
30
31
32
33
34
35
36
37
38
39
40
41
42
43

44 The ambient pressure crystal structure of synthetic $\text{K}_2\text{Mg}(\text{CO}_3)_2$, determined by Hesse and Simons
45 [41] is shown for comparison in figure 4. The ambient structure is rhombohedral ($R\bar{3}m$) with
46 planar, CO_3 units arranged in the a-b plane. Magnesium octahedra are corner shared with the
47 carbonate and edge-shared with alternate KO_9 coordinate polyhedra. This structure contrasts with
48 that obtained from the simulation of the liquid, wherein the carbonate is more distorted and both
49 magnesium and potassium cations occur in irregular channels or percolation domains.
50
51
52
53
54
55
56
57
58
59
60

APPLICATION OF PRESSURE

In previous interpretations of this carbonate glass structure, magnesium is assumed to act as a bridging species and to form a network with the carbonate anions. A motivation for that interpretation was the combination of larger formal ion charge and smaller ionic radius which make the magnesium cation significantly more polarising than the potassium cation. Although the ambient pressure structure does show magnesium adopting this role, both magnesium and potassium could be argued to adopt a bridging role, at the very least in the sense that they form strong coulombic interactions with the carbonate anions. Although magnesium clearly has an important role in stabilizing the glass, the greatest changes in response to the application of pressure are observed in the relationship between the potassium and oxygen ions. To highlight these changes, figure 5 shows the (unweighted) partial pair distribution functions for six selected ion pairs. On application of pressure the Mg-O pair distribution function appears relatively invariant with the nearest-neighbor length-scale shortening slightly (consistent with a simple increase in density). The C-C, O-O and C-O pair distribution functions show significant changes consistent with the greater emergence of the second C-O near-neighbor lengths-scale indicated above. The most dramatic changes are observed in the K-O pair distribution function. At ambient pressure the nearest-neighbor distribution is relatively broad and at relatively long range, indicative of the potassium cation acting more as a network modifier than a network former. As the pressure increases the nearest-neighbor length-scale shifts to significantly lower range (from $r_{KO} \sim 3.4 \text{ \AA}$ to $\sim 2 \text{ \AA}$) indicative of the change in role of the potassium cation to acting as a network-former, moderating the change in structure observed for the carbonate anions. More important, however, is that these contributions reflect underlying changes in the carbonate anion, and it is the flexibility of this anion that determines the response of this system to pressure [19]. The flexibility in the

1
2
3 anion results in the changes to the O-O and K-O contributions that result in the dramatic, pressure-
4 induced changes in the diffraction pattern which accompany the emergence of a second C-O length
5 scale. The complex relationship between the K^+ cations and the oxygen atoms in the carbonate
6 determines the high pressure response, while changes in the magnesium atom-pair contributions
7 are limited.
8
9

10
11
12 The simulated liquid structure can be compared with those of double carbonates [27] at elevated
13 pressures. The $K_2Mg(CO_3)_2$ crystal transforms from a rhombohedral ($R\bar{3}m$) structure into a
14 monoclinic polymorph with pressure [27, 30]: in this case the carbonate anion remains rigid with
15 limited change in the C-O distances, in contrast to the glass. The response to pressure of the
16 crystalline double carbonates reflects the anisotropy of compression along a - and c -axes since the
17 polyhedron of the larger cation is more compressible than that of magnesium. In the liquid it is the
18 distortion of the carbonate anion that influences the response to pressure and also the formation of
19 the glass. The structure of this glass is therefore more similar to those proposed for aqueous
20 calcium carbonate where there is strong interaction between H_2O molecules and the distorted
21 carbonate units in close proximity, stabilizing the structure against crystallization [5]. In the K-Mg
22 carbonate glass it appears that the magnesium cations form strong interactions with the carbonate
23 anions across the whole pressure range (consistent with the expected strong electrostatic
24 interactions) in a manner which can be considered network-forming. However, the role of the
25 potassium cations is more interesting as this appears to change from being largely network-
26 modifying at low pressure to network-forming at high pressure.
27
28
29
30
31
32
33
34
35
36
37
38
39
40
41
42
43
44
45
46
47
48
49
50
51
52
53
54
55
56
57
58
59
60

CONCLUSIONS

In this study we have determined the enthalpy of formation of a rare carbonate glass by high temperature oxide calorimetry. This completely glassy sample has an enthalpy of formation from the oxides of -261.12 ± 3.02 kJ/mol. The glass is energetically metastable with respect to a mixture of the crystalline endmembers by only $+9.36 \pm 1.95$ kJ/mol, and this small contribution to the free energy is balanced by the configurational entropy of K-Mg mixing, providing the ternary glass possible stability with respect to the binary crystalline end-members. Further entropic stabilization may arise from carbonate group distortions and disorder confirmed by analysis of the ^{13}C MAS NMR spectra, collected for a similarly prepared glass sample. The results show an asymmetry parameter (η), a measure of departure from axial symmetry, to be larger than for any alkali or alkaline earth carbonate, indicating that the carbonate anion is distorted, with an average difference in C-O bond length of about 0.06\AA . However, the anisotropy shows that the deviation from planar geometry falls within the range of crystalline carbonates. Molecular dynamics simulations for the equivalent liquids using the flexible anion approach also show distorted carbonate units with the carbon atom moving slightly out of plane but not forming the higher coordinate CO_{3+1} configurations proposed for high pressure versions of this glass. The ambient pressure glass sample has distorted carbonate anions that are isolated and do not form networks but show a complex relationship with the potassium cations. The interaction between the potassium cations and the oxygens from the carbonate define the glass structure at low pressure, and the same flexibility of the carbonate anion dictates the high pressure response. The ambient pressure glass is superficially similar in structure to amorphous hydrated calcium carbonate, where the structure is defined by distorted carbonate anions in close proximity to a hydrogen bonded network.

EXPERIMENTAL DETAILS

1
2
3 Glasses were prepared using a starting mixture of 55 mol % K_2CO_3 and 45 mol % $MgCO_3$, which
4 is the ratio at the eutectic (at ~ 730 K) on the binary join [11]. Reagent grade K_2CO_3 , or for ATR
5 and NMR measurements, 98 % ^{13}C labelled $K_2^{13}CO_3$ (MSD isotopes), were dried at 673 K. The
6
7
8
9
10 $MgCO_3$ was in the form of a natural, optically clear magnesite crystal from Brumado, Brazil
11 (virtually water-free as confirmed by FTIR) which was ground into fine powder immediately prior
12 to the experiment. The mixture was loaded into 3.8mm length Au capsules which were welded
13
14
15 shut and placed into a Tuttle-type cold-seal bomb with a rapid quench rod extension[42].
16
17
18 Experiments were conducted at 1050 K, 0.1 GPa for ~ 10 -15 hrs and then quenched ($>200^\circ C/sec$).
19
20
21 The resulting glass was removed from the Au capsule, mostly as a single solid slug, representing
22
23
24 the central part of the quenched melt.
25

26
27 IR spectra were collected using a ThermoNicolet i10 FTIR spectrometer fitted with a Ge-tipped
28
29
30 Attenuated Total Reflectance (ATR) head. 128 scans were collected at a resolution of $8cm^{-1}$ using
31
32
33 a MCT detector and a KBr beamsplitter in absorbance mode. The sample was polished using dry
34
35
36 alumina grit coated sheets (to a $1\mu m$ finish) and the collection area was approximately a $30\mu m$
37
38
39 square.
40

41
42 The enthalpy of drop solution of the carbonate glass was determined by high temperature oxide
43
44
45 melt solution calorimetry. These experiments use a custom-built, Tian-Calvet isoperibol
46
47
48 calorimeters at the Peter A. Rock Thermochemistry Laboratory at UC Davis and follow standard
49
50
51 practice reviewed in several recent publications [18, 43, 44]. In these experiments, a series of small
52
53
54 pellets of the carbonate glass (~ 5 mg) are dropped from room temperature into a molten oxide
55
56
57 solvent. In this case the solvent was sodium molybdate ($3Na_2O-4MoO_3$) contained in a large
58
59
60 platinum crucible which is contained in a silica glass crucible and outer silica glass liner. For these
experiments the entire glass assembly is flushed with oxygen at 43 mL/min. Oxygen is bubbled,

1
2
3 at 4.5 mL/min, though the solvent using a platinum-tipped silica tube; this not only mixes the
4 solvent to ensure complete dissolution of the sample and evolve the CO₂ but can also be used to
5 control the oxidation state.
6
7

8
9
10 The individual pellets are dropped from room temperature into the solvent at 975 K with the heat
11 flow resulting from the drop measured as a change in voltage in the calorimeter thermopile. Each
12 measurement comprises a 10 minute collection of the initial calorimeter baseline and the return to
13 the sample baseline following the drop solution measurement. The overall reaction times were 28-
14 30 minutes. The integral of the voltage change is converted to the reaction enthalpy by using a
15 calibration factor determined by dropping pellets of known heat contents (α -Al₂O₃).
16
17
18
19
20
21
22
23
24
25

26 Solid-state NMR spectra were acquired at Stony Brook University with a 400 MHz (9.4 T) Varian
27 Inova spectrometer operating at 100.56 MHz and a 500 MHz Varian Infinity plus at 125.68 MHz.
28 A set of small pellets of the ¹³C-labelled 0.55K₂CO₃:0.45MgCO₃ glass was loaded directly into a
29 3.2 mm rotor assembly and sealed with an air-tight press-fit cap. The direct-excitation ¹³C MAS-
30 NMR (Magic Angle Spinning) spectra were acquired with standard single-pulse methods with
31 4.5 μ s 80° pulses and a 30 s relaxation delay at spinning rates that varied from 1.5 to 10.3 kHz.
32
33
34
35
36
37
38
39
40 The T₁ spin-lattice relaxation time was estimated to be 10 s by bracketing the null point in a series
41 of inversion-recovery experiments. Additional abbreviated acquisition spectra at a longer (50 s)
42 relaxation delay were acquired before and after each spectrum but showed no evidence of spectral
43 changes that could indicate onset of crystallization during the NMR experiments. The average ¹³C
44 chemical shift tensor values were estimated from analysis of the spinning sideband intensities for
45 a spectrum acquired at a 1.5 kHz spinning rate according to the method of Herzfeld and Berger[45]
46
47
48
49
50
51
52
53
54 as implemented in the “HBA” software [46]. To assess potential hydration of the glass, additional
55
56
57
58
59
60

1
2
3 spectra were acquired by $^1\text{H} \rightarrow ^{13}\text{C}$ cross-polarization MAS (CP-MAS) methods at contact times
4 ranging from 0.2 to 10 ms and spinning rates of 1.5 and 8.0 kHz and by $^{13}\text{C}[^1\text{H}]$ rotational echo
5 double resonance (REDOR) methods. A two-dimensional $^{13}\text{C}[^1\text{H}]$ CP heteronuclear correlation
6 spectrum was acquired at a spinning rate of 8.0 kHz and contact time of 2 ms, as 64 hypercomplex
7 points in t_1 at a $10 \mu\text{s}$ interval (100 kHz ^1H spectral width). Linear prediction methods were used
8 to complete the signal decay in t_1 to mitigate truncation artifacts. From these data, ^{13}C -detected
9 ^1H NMR spectra were obtained as a 1-dimensional cross-sections extracted at the ^{13}C peak
10 position. The chemical shifts were referenced to those of tetramethylsilane via secondary
11 referencing to adamantane (38.6 ppm for the methylene ^{13}C , 2.0 ppm for ^1H).
12
13
14
15
16
17
18
19
20
21
22
23
24

25 In previous work molecular dynamics simulations have been performed on carbonate liquids using
26 a potential developed by Tissen and Janssen, of the Born-Huggins-Mayer form [47]. The trigonal
27 geometry of the carbonate anion is imposed by employing harmonic springs that act between C-O
28 and O-O pairs. In later studies [3, 4] we developed an approach that allows both flexibility of the
29 molecular anion and fluctuation of the internal charge distribution [48-51]. In the simulations
30 carried out here we fix the charge distribution on the anion). The simulations have been carried
31 out at a fixed temperature (of $T=1800 \text{ K}$) and constant volume. $F^x(Q)$ was generated by combining
32 the partial (Ashcroft-Langreth) structure factors (of which there are ten for the four component
33 system). These were calculated directly from the Fourier components of the ion densities, $S_{\alpha,\beta} =$
34 $\langle A_{\alpha}^*(Q)A_{\beta}(Q) \rangle$ where $A_{\alpha}(Q) = \frac{1}{\sqrt{N_{\alpha}}} \sum_{j=1}^{N_{\alpha}} \exp(i\mathbf{Q}\cdot\mathbf{r}^j)$. Total X-ray structure factors were
35 constructed from weighted sums of these partial structure factors using X-ray form factors taken
36 from standard sources [52].
37
38
39
40
41
42
43
44
45
46
47
48
49
50
51
52
53
54
55
56
57
58
59
60

1
2
3 The energy dispersive X-ray diffraction data were collected at HPCAT, Sector 16 at the Advanced
4 Photon Source (APS), Argonne National Laboratory. The total X-ray structure factor was obtained
5 using the multi-angle energy dispersive technique which uses a focused, white X-ray beam with 7
6 x 7_μm size. Scattering data was collected on a Ge solid state detector (Canberra) at 2 theta angles
7 of 3.14°, 4.14°, 5.14°, 7.14°, 9.14°, 12.15°, 16.15°, 22.15°, 28.14° and 31.32°. This detector was
8 calibrated using gold peaks at ambient pressure conditions. The total exposure for each pressure
9 point was obtained by normalizing each detector pattern to the white X-ray beam with further
10 corrections using the optimisation techniques described by Shen *et al.*[53] and Kono *et al.*[54].
11 The energy dispersive patterns for each detector were rescaled and merged to form a Faber- Ziman
12 type total structure factor. In this study we eliminated the data from the 3.14° detector bank since
13 these clearly showed crystalline peaks from the sample assembly. The scattering intensity in the
14 31.32° detector bank was very low and these latter data are also eliminated from the subsequent
15 normalization. The individual segments were smoothed by an error weighted spline and scaled to
16 the energy of the primary X-ray beam in the highest angle segment.
17
18
19
20
21
22
23
24
25
26
27
28
29
30
31
32
33
34
35

36 ACKNOWLEDGEMENTS

37
38
39 M.C.W and P.A.B. would like to acknowledge funding support from EPSRC under grant
40 EP/R036225/1. M.W. is grateful for support from the EPSRC Centre for Doctoral Training, Theory
41 and Modeling in Chemical Sciences, under grant EP/L015722/1. R.A.B was funded by the NERC
42 Thematic Grant consortium NE/M000419/1. The diffraction study was performed at HPCAT
43 (Sector 16) of the Advanced Photon Source (APS). The Advanced Photon Source is a US DOE
44 Office of Science User facility, operated for the DOE Office of Science by Argonne National
45 Laboratory under contract DE-AC02-06CH11357. Calorimetry at UC Davis was supported by the
46
47
48
49
50
51
52
53
54
55
56
57
58
59
60

1
2
3 U.S. Department of Energy, Office of Science, Office of Basic Energy Sciences, Chemical
4 Sciences, Geosciences, and Biosciences Division under Award DE-FG02ER1474).

5
6
7
8
9 **REFERENCES**

- 10
11
12
13
14 1. Angell, C.A., *Formation of glasses from liquids and biopolymers*. Science, 1995.
15 **267**(5206): p. 1924-1935.
16
17
18 2. Wilding, M.C., et al., *Low-Dimensional Network Formation in Molten Sodium Carbonate*.
19 Scientific Reports, 2016. **6**.
20
21
22 3. Wilding, M.C., et al., *The structure of liquid alkali nitrates and nitrites*. Physical Chemistry
23 Chemical Physics, 2017. **19**(32): p. 21625-21638.
24
25
26 4. Wilson, M., et al., *Structure and Liquid Fragility in Sodium Carbonate*. Journal of Physical
27 Chemistry A, 2018. **122**(4): p. 1071-1076.
28
29
30 5. Genge, M.J., A.P. Jones, and G.D. Price, *An Infrared and Raman Study of Carbonate*
31 *Glasses-Implications for carbonatite magmas*. Geochimica et Cosmochimica Acta, 1995.
32 **59**(5): p. 927-937.
33
34
35 6. Sen, S., et al., *Hydrogen bonding induced distortion of CO₃ units and kinetic stabilization*
36 *of amorphous calcium carbonate: results from 2D C-13 NMR spectroscopy*. Physical
37 Chemistry Chemical Physics, 2016. **18**(30): p. 20330-20337.
38
39
40 7. Eitel, W. and W. Skalijs, *Double Carbonates of Alkalis and Alkaline Earths*. Zeitschrift
41 für Anorganische und Allgemeine Chemie, 1929. **183**: p. 263-286.
42
43
44 8. Genge, M.J., A.P. Jones, and G.D. Price, *An Infrared and Raman Study of Carbonate*
45 *Glasses-Implications for the structure of Carbonatite Magmas*. Geochimica et
46 Cosmochimica Acta, 1995. **59**(5): p. 927-937.
47
48
49
50
51
52
53
54
55
56
57
58
59
60

- 1
2
3 9. Genge, M.J., G.D. Price, and A.P. Jones, *Molecular Dynamics Simulations of CaCO₃ melts*
4 *to Mantle Pressures and Temperatures - Implications for Carbonatite Magmas*. Earth and
5 Planetary Science Letters, 1995. **131**(3-4): p. 225-238.
6
7
- 8
9
10 10. Dobson, D.P., et al., *In-situ measurement of viscosity and density of carbonate melts at*
11 *high pressure*. Earth and Planetary Science Letters, 1996. **143**(1-4): p. 207-215.
12
13
- 14
15 11. Ragone, S.E., et al., *The System Potassium Carbonate-Magnesium Carbonate*. The Journal
16 of Physical Chemistry, 1966. **70**: p. 3360-3361.
17
18
- 19
20 12. Datta, R.K., et al., *Glass Formation in Carbonate Systems*. Journal of The American
21 Ceramic Society, 1964. **47**: p. 153.
22
23
- 24
25 13. Forland, T. and W.A. Weyl, *Formation of a Sulfate Glass*. Journal of the American
26 Ceramic Society, 1950. **33**(6): p. 186-187.
27
28
- 29
30 14. MacFarlane, D.R., *Attempted Glass Formation in Pure KHSO₄*. Communications of the
31 American Ceramic Society, 1984: p. C-28.
32
33
- 34
35 15. van Uitert, L.G. and W.H. Grodkiewicz, *Nitrate Glasses*. Materials Research Bulletin,
36 1971. **6**: p. 283-292.
37
38
- 39
40 16. Jones, A.P., M. Genge, and L. Carmody, *Carbonate Melts and Carbonatites*, in *Carbon in*
41 *Earth*, R.M. Hazen, A.P. Jones, and J.A. Baross, Editors. 2013. p. 289-322.
42
43
- 44
45 17. Sharma, S.K. and B. Simons, *Raman Study of K₂CO₃-MgCO₃ glasses*. Carnegie Institute
46 of Washington Yearbook, 1980. **79**: p. 322-326.
47
48
- 49
50 18. Navrotsky, A., *Progress and New Directions in Calorimetry: A 2014 Perspective*. Journal
51 of the American Ceramic Society, 2014. **97**(11): p. 3349-3359.
52
53
54
55
56
57
58
59
60

- 1
2
3 19. Sahu, S.K., L.A. Boatner, and A. Navrotsky, *Formation and Dehydration Enthalpy of*
4 *Potassium Hexaniobate*. Journal of the American Ceramic Society, 2017. **100**(1): p. 304-
5 311.
6
7
8
9
10 20. Shivaramaiah, R. and A. Navrotsky, *Energetics of Order-Disorder in Layered Magnesium*
11 *Aluminum Double Hydroxides with Inter layer Carbonate*. Inorganic Chemistry, 2015.
12 **54**(7): p. 3253-3259.
13
14
15
16
17 21. Chai, L.A. and A. Navrotsky, *Thermochemistry of Carbonate-Pyroxene Equilibria*.
18 *Contributions to Mineralogy and Petrology*, 1993. **114**(2): p. 139-147.
19
20
21 22. Kiseleva, I., et al., *Thermochemistry of natural potassium sodium calcium leonhardite and*
22 *its cation-exchanged forms*. American Mineralogist, 1996. **81**(5-6): p. 668-675.
23
24
25
26 23. Navrotsky, A., et al., *Thermochemistry of double carbonates in the K₂CO₃-CaCO₃ system*.
27 *American Mineralogist*, 1997. **82**(5-6): p. 546-548.
28
29
30
31 24. Tarina, I., A. Navrotsky, and H. Gan, *Direct Calorimetric Measurement of Enthalpies in*
32 *Diopside-Anorthite-Wollastonite Melts at 1773K*. *Geochimica Et Cosmochimica Acta*,
33 1994. **58**(17): p. 3665-3673.
34
35
36
37 25. Navrotsky, A., P. Maniar, and R. Oestrike, *Energetics of Glasses in the System Diopside-*
38 *Anorthite-Forsterite*. *Contributions to Mineralogy and Petrology*, 1990. **105**(1): p. 81-86.
39
40
41
42 26. Hon, R., et al., *Enthalpies of Mixing of Glasses in the System Albite-Anorthite-Diopside*.
43 *Transactions-American Geophysical Union*, 1977. **58**(12): p. 1243-1243.
44
45
46
47 27. Golubkova, A., M. Merlini, and M.W. Schmidt, *Crystal structure, high-pressure, and high-*
48 *temperature behavior of carbonates in the K₂Mg(CO₃)₂-Na₂Mg(CO₃)₂ join*. *American*
49 *Mineralogist*, 2015. **100**(11-12): p. 2458-2467.
50
51
52
53
54
55
56
57
58
59
60

- 1
2
3 28. Shatskiy, A., et al., *Phase relations on the K_2CO_3 - $CaCO_3$ - $MgCO_3$ join at 6 GPa and 900-*
4 *1400 degrees C: Implications for incipient melting in carbonated mantle domains.*
5
6 *American Mineralogist*, 2016. **101**(1-2): p. 437-447.
7
8
9
10 29. Shatskiy, A., et al., *Phase relationships in the system K_2CO_3 - $CaCO_3$ at 6 GPa and 900-*
11 *1450 degrees C.* *American Mineralogist*, 2015. **100**(1): p. 223-232.
12
13
14 30. Shatskiy, A., et al., *The system K_2CO_3 - $MgCO_3$ at 6 GPa and 900-1450 degrees C.*
15 *American Mineralogist*, 2013. **98**(8-9): p. 1593-1603.
16
17
18 31. Alekseev, A.I., et al., *Thermodynamic Values of Binary Carbonate Salts*
19 *K_2CO_3 . $MgCO_3$. nH_2O .* *Journal of Applied Chemistry of the USSR*, 1984. **57**(6): p. 1168-
20 1172.
21
22
23
24
25 32. Papenguth, H.W., et al., *C-13 MAS NMR-Spectroscopy of Inorganic and Biogenic*
26 *Carbonates.* *American Mineralogist*, 1989. **74**(9-10): p. 1152-1158.
27
28
29 33. Michel, F.M., et al., *Structural characteristics of synthetic amorphous calcium carbonate.*
30 *Chemistry of Materials*, 2008. **20**(14): p. 4720-4728.
31
32
33 34. Michel, F.M., et al., *Structural characteristics of synthetic amorphous calcium carbonate.*
34 *Geochimica Et Cosmochimica Acta*, 2008. **72**(12): p. A626-A626.
35
36
37 35. Sevelsted, T.F., D. Herfort, and J. Skibsted, *C-13 chemical shift anisotropies for carbonate*
38 *ions in cement minerals and the use of C-13, Al-27 and Si-29 MAS NMR in studies of*
39 *Portland cement including limestone additions.* *Cement and Concrete Research*, 2013. **52**:
40 p. 100-111.
41
42
43
44
45
46
47
48 49 36. Moore, J.K., et al., *Quantitative Identification of Metastable Magnesium Carbonate*
50 *Minerals by Solid-State C-13 NMR Spectroscopy (vol 49, pg 657, 2015).* *Environmental*
51 *Science & Technology*, 2015. **49**(3): p. 1986-1986.
52
53
54
55
56
57
58
59
60

- 1
2
3 37. Nebel, H., et al., *On the structure of amorphous calcium carbonate - A detailed study by*
4 *solid-state NMR spectroscopy*. Inorganic Chemistry, 2008. **47**(17): p. 7874-7879.
5
6
7 38. Kohn, S.C., R.A. Brooker, and R. Dupree, *C-13 MAS NMR - A method for Studying CO₂*
8 *specitation in Glasses*. Geochimica Et Cosmochimica Acta, 1991. **55**(12): p. 3879-3884.
9
10
11 39. Brooker, R.A., et al., *Solubility, speciation and dissolution mechanisms for CO₂ in melts*
12 *on the NaAlO₂-SiO₂ join*. Geochimica Et Cosmochimica Acta, 1999. **63**(21): p. 3549-
13 3565.
14
15
16
17
18 40. Su, Z.W. and P. Coppens, *Relativistic X-ray elastic scattering factors for neutral atoms*
19 *Z=1-54 from multiconfiguration Dirac-Fock wavefunctions in the 0-12 angstrom(-1) sin*
20 *theta/lambda range, and six-Gaussian analytical expressions in the 0-6 angstrom(-1)*
21 *range (vol A53, pg 749, 1997)*. Acta Crystallographica Section A, 1998. **54**: p. 357-357.
22
23
24
25
26
27 41. Hesse, K.F. and B. Simons, *Crystal Structure of Synthetic K₂Mg(CO₃)₂*. Zeitschrift Fur
28 *Kristallographie*, 1982. **161**(3-4): p. 289-292.
29
30
31
32 42. Ihinger, P.D., *An Experimental Study of the Interaction of Water with Granitic Melt*. 1991,
33 *California Institute of Technology*.
34
35
36
37 43. Navrotsky, A., *High temperature reaction calorimetry applied to metastable and*
38 *nanophase materials*. Journal of Thermal Analysis and Calorimetry, 1999. **57**(3): p. 653-
39 658.
40
41
42
43 44. Navrotsky, A., *High-temperature oxide melt calorimetry of oxides and nitrides*. Journal of
44 *Chemical Thermodynamics*, 2001. **33**(8): p. 859-871.
45
46
47
48 45. Herzfeld, J. and A.E. Berger, *Sideband Intensities in NMR-Spectra of Samples Spinning at*
49 *the Magic Angle*. Journal of Chemical Physics, 1980. **73**(12): p. 6021-6030.
50
51
52
53 46. Eichele, K., *HBA*. 2015, Universitaet Tuebingen.
54
55
56
57
58
59
60

- 1
2
3 47. Tissen, J., G.J.M. Janssen, and J.P. Vandereerden, *Molecular Dynamics Simulation fo*
4 *Binary Mixtures of Molten Alkali Carboantes*. Molecular Physics, 1994. **82**(1): p. 101-111.
5
6
7
8 48. Costa, M.F. and M.C.C. Ribeiro, *Molecular dynamics of molten Li_2CO_3 - K_2CO_3 (vol 138,*
9 *pg 61, 2008)*. Journal of Molecular Liquids, 2008. **142**(1-3): p. 161-161.
10
11
12 49. Ribeiro, M.C.C., *First sharp diffraction peak in the fragile liquid $Ca_{0.4}K_{0.6}(NO_3)_{1.4}$* .
13 *Physical Review B*, 2000. **61**(5): p. 3297-3302.
14
15
16
17 50. Ribeiro, M.C.C., *Ionic dynamics in the glass-forming liquid $Ca_{0.4}K_{0.6}(NO_3)_{1.4}$: A*
18 *molecular dynamics study with a polarizable model*. *Physical Review B*, 2001. **63**(9).
19
20
21 51. Ribeiro, M.C.C., *Molecular dynamics study on the glass transition in*
22 *$Ca_{0.4}K_{0.6}(NO_3)_{1.4}$* . *Journal of Physical Chemistry B*, 2003. **107**(35): p. 9520-9527.
23
24
25
26 52. Cromer, D.T. and J.B. Mann, *X-ray Scattering Functions Computed from Numerical*
27 *Hartree-Fock Functions*. *Acta Crystallographica Section a-Crystal Physics Diffraction*
28 *Theoretical and General Crystallography*, 1968. **A 24**: p. 321-&.
29
30
31
32
33 53. Shen, G.Y., et al., *Structural investigation of amorphous materials at high pressures using*
34 *the diamond anvil cell*. *Review of Scientific Instruments*, 2003. **74**(6): p. 3021-3026.
35
36
37
38 54. Kono, Y., et al., *Ultralow viscosity of carbonate melts at high pressures*. *Nature*
39 *Communications*, 2014. **5**.
40
41
42
43
44
45
46
47
48
49
50
51
52
53
54
55
56
57
58
59
60

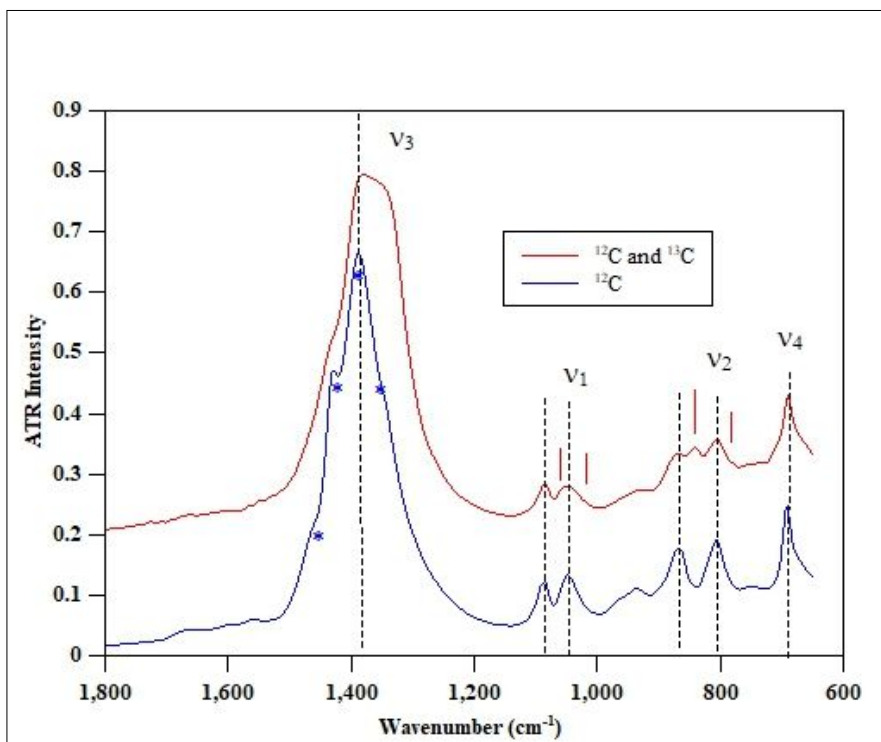


Figure 1a. FTIR absorbance spectra taken using micro-ATR. The ¹²C sample has two peaks assigned to ν_1 symmetric stretching at 1049 and 1088 cm^{-1} and two peaks assigned to ν_2 out-of-plane bending at 806 and 870 cm^{-1} . Only one ν_4 in-plane bend peak is seen at 691 cm^{-1} , but the detector response may have cut off a second peak at lower wavenumber. The ν_3 asymmetric stretch is more complex, but can be fitted with 4 peaks representing two doublets. ν_3 are approximately at 1340, 1377, 1395 and 1431 cm^{-1} . In the upper spectra, the approximate magnitude of the isotopic shift related to ¹³C is indicated by vertical ticks. The ¹³C peaks are marked with an asterisk.

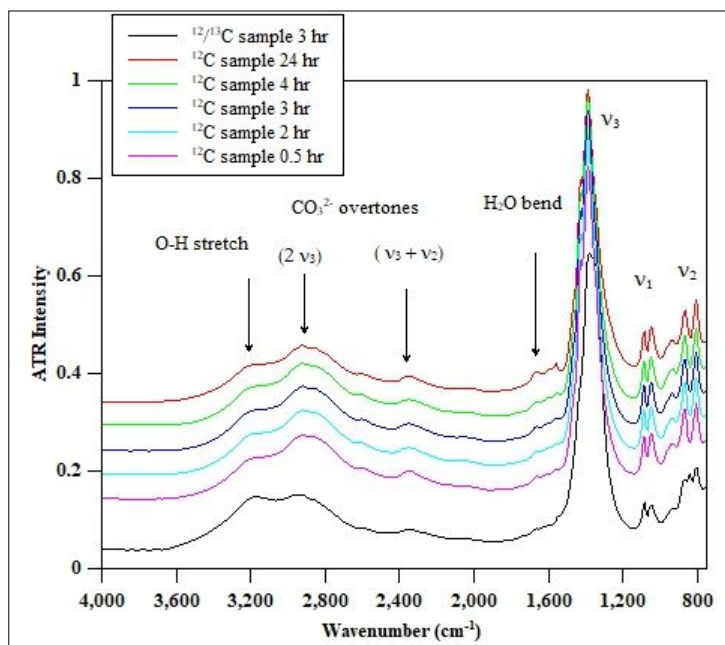


Fig 1b shows the glasses do not change their water content in the first 24 hrs. However it should be noted that they eventually turn to a white powder within 3-4 weeks. The peak at 3200 cm^{-1} is assumed to represent O-H stretching, but is a lower frequency than observed in silicate glasses.

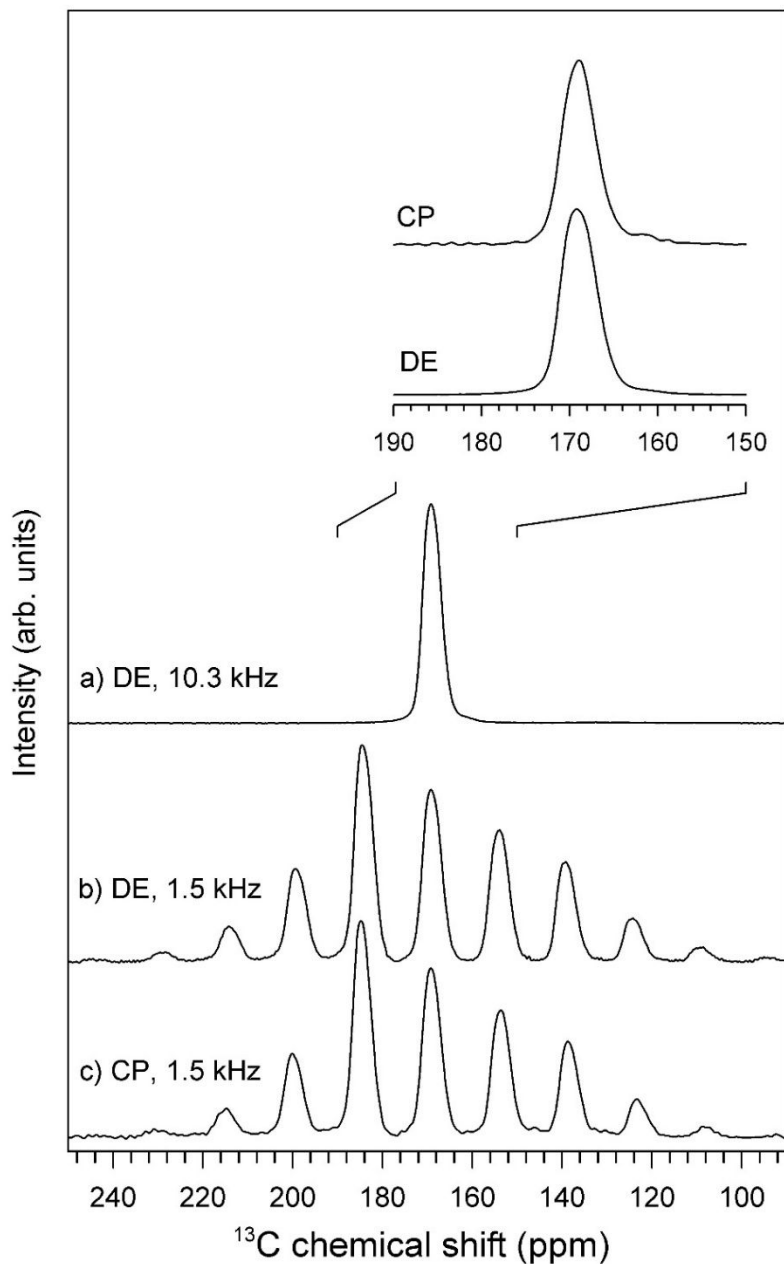


Figure 2. ^{13}C MAS-NMR spectra of ^{13}C -labelled $0.55\text{K}_2\text{CO}_3 \cdot 0.45\text{MgCO}_3$ glass acquired at 100.56 MHz (9.4 T) and spinning rates of (a) 10.3 kHz and (b-c) 1.5 kHz. Spectra in (a-b) were taken by direct ^{13}C excitation (DE) with $4.5 \mu\text{s}$ pulses separated by a 30 s relaxation delay for (a) 800 and (b) 280 acquisitions, and in (c) by standard $^1\text{H} \rightarrow ^{13}\text{C}$ cross-polarization (CP) with a 2 ms contact time, 2 s relaxation delay, for 800 scans. Inset shows center bands at expanded scale.

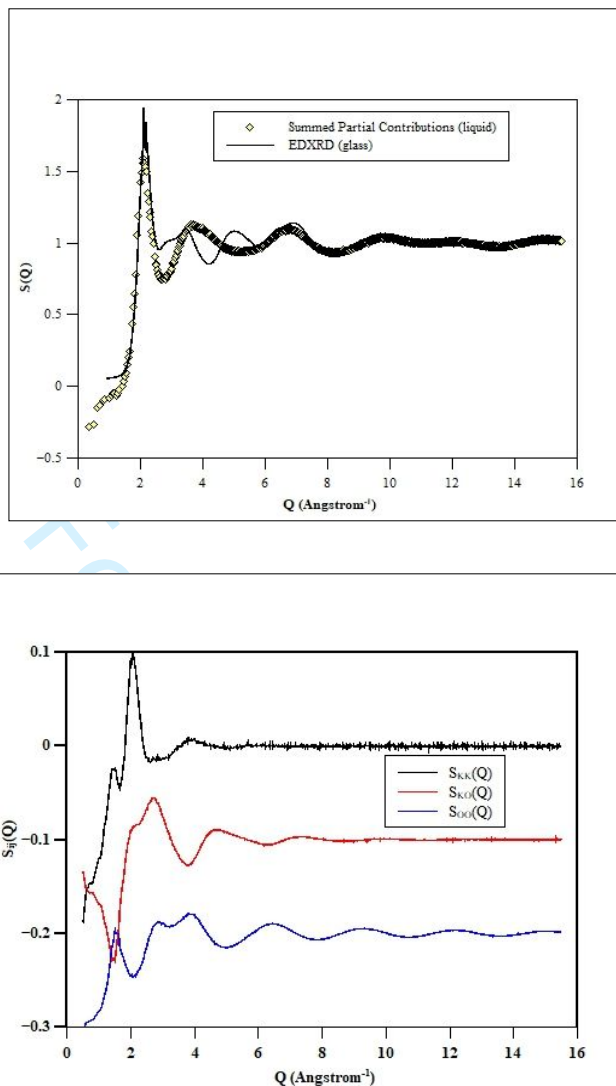


Figure 3. Energy dispersive (collected at sector 16 APS) for 55% K_2CO_3 -45% $MgCO_3$ glass compared with the summed partial contributions for the simulated liquids of the same composition (top) the lower panel shows the individual partial contributions with X-ray weighting (Ashcroft-Langreth) for K-K, K-O and O-O which dominate the X-ray scattering pattern. There is considerable mismatch between the experiment and simulation. This could result from difference between the fully relaxed liquid and the vitreous form of this carbonate.

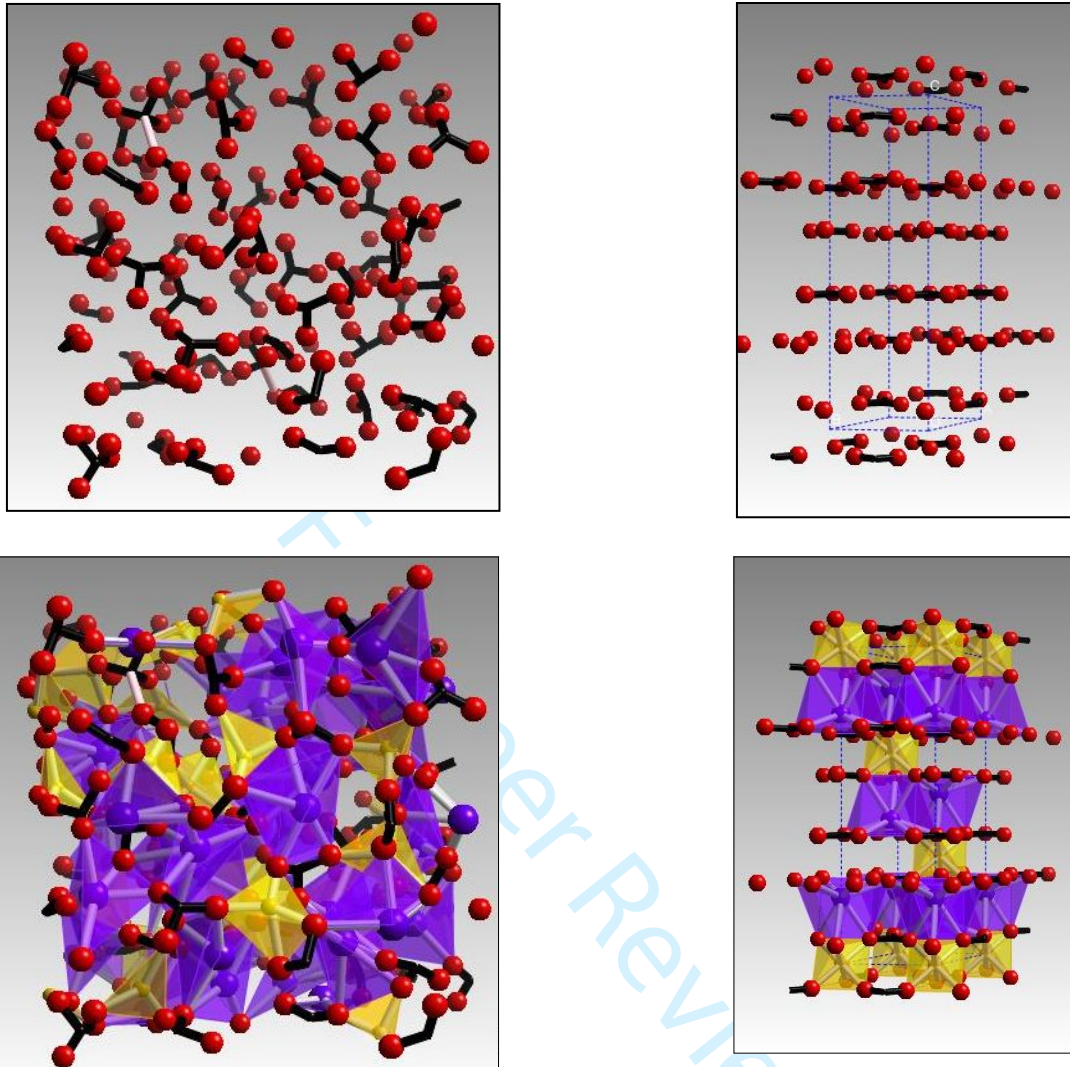


Figure 4: Molecular dynamics snapshots of the 55% K_2CO_3 -45% $MgCO_3$ liquid at 1800K showing the distribution of the carbonate anions. C-O bonds are shown in black (a) with some longer C-O bond lengths (shown in grey) and formation of the CO_{3+1} configuration apparent even at ambient pressure. This is compared with the rhombahedral crystal structure of $K_2Mg(CO_3)_2$ [41](b) with the unit cell illustrated, the rigid, triangular carbonate anions form planes perpendicular to the c-axis. In the lower figure potassium and magnesium atoms are also shown (c) the structure is dominated by the strong interaction between the large, blue potassium cations and the distorted

1
2
3
4
5
6
7
8
9
10
11
12
13
14
15
16
17
18
19
20
21
22
23
24
25
26
27
28
29
30
31
32
33
34
35
36
37
38
39
40
41
42
43
44
45
46
47
48
49
50
51
52
53
54
55
56
57
58
59
60

carbonate. The coordination polyhedral of potassium and magnesium are shown for the ambient pressure crystal structure.

For Peer Review

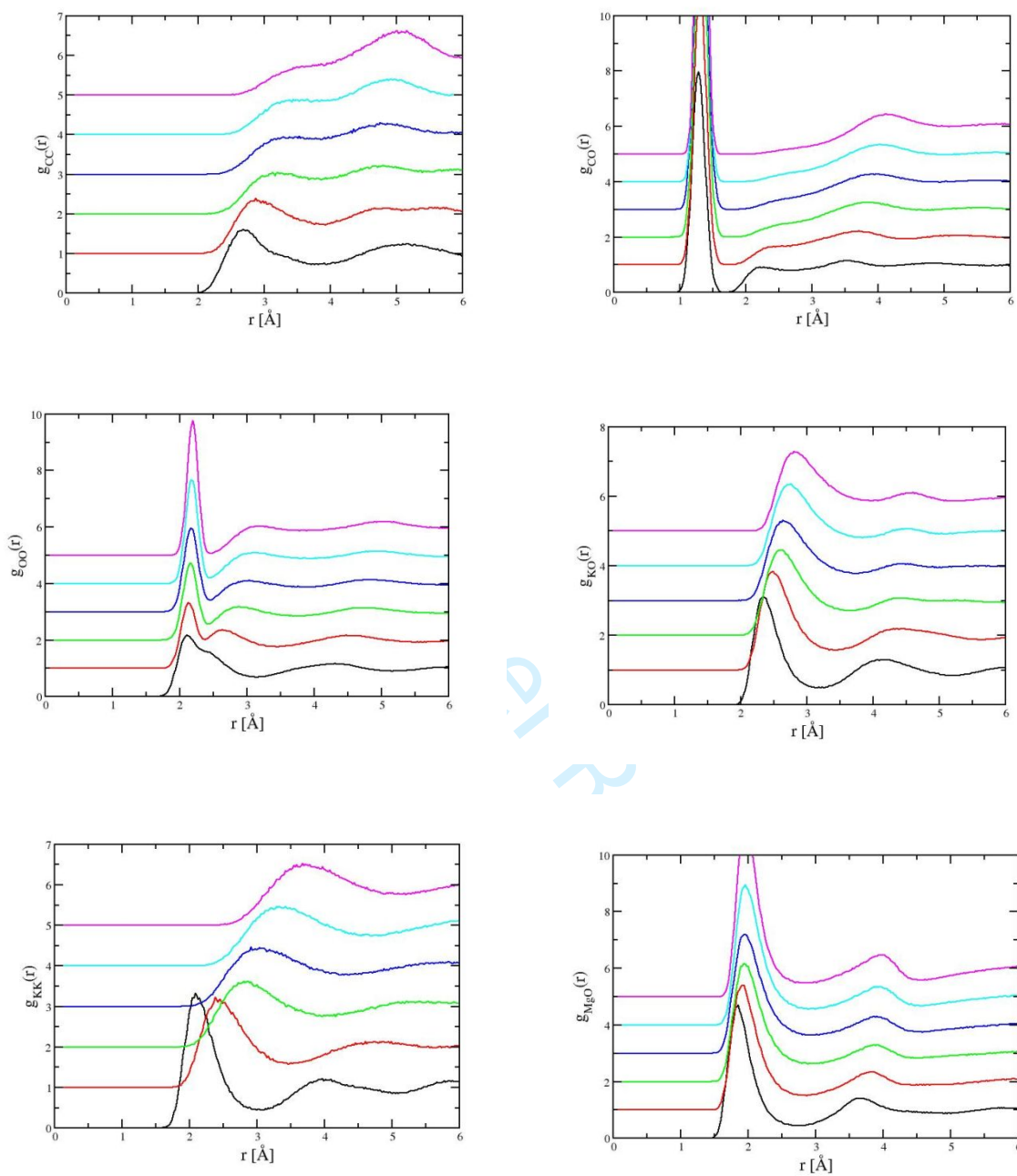


Figure 5. Six of the partial radial distribution functions to illustrate the response of the K_2CO_3 - MgCO_3 liquids to pressure. The curves are generated by the simulations at six different densities (pressures) with the lowest densities the topmost curves. The changes in O-O, K-K and K-O partial contribution represent the changes in the potassium sub-density and strong interaction between the

1
2
3 oxygen atoms in the carbonate anion and the potassium cations. This results in the emergence of
4
5 the second C-O length scale seen at high pressure in the C-O and C-C partial contributions. The
6
7 Mg-O partial contribution changes little with pressure.
8
9
10
11
12
13
14
15
16
17
18
19
20
21
22
23
24
25
26
27
28
29
30
31
32
33
34
35
36
37
38
39
40
41
42
43
44
45
46
47
48
49
50
51
52
53
54
55
56
57
58
59
60

For Peer Review

1
2
3
4
5
6
7
8
9
10
11
12
13
14
15
16
17
18
19
20
21
22
23
24
25
26
27
28
29
30
31
32
33
34
35
36
37
38
39
40
41
42
43
44
45
46
47
48
49
50
51
52
53
54
55
56
57
58
59
60

For Peer Review

SUPPORTING INFORMATION

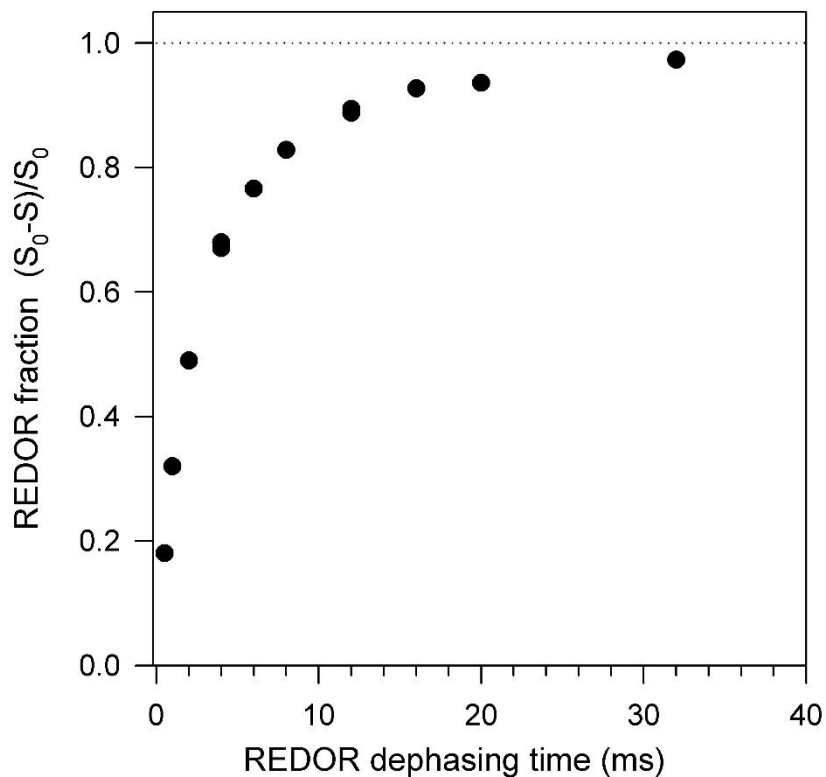
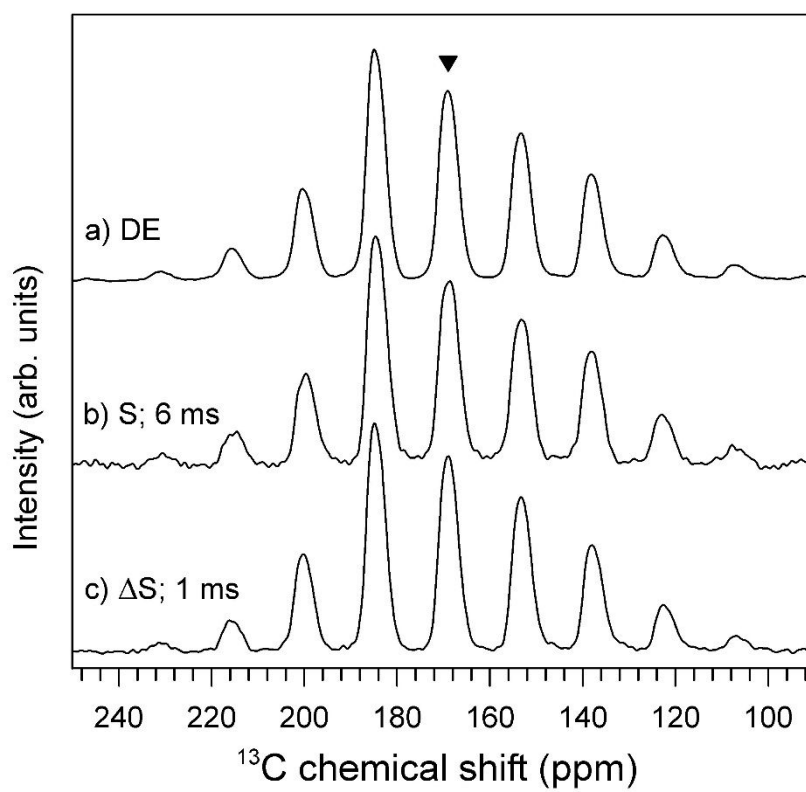


Figure S1. $^{13}\text{C}\{^1\text{H}\}$ rotational echo double resonance (REDOR) dephasing for the ^{13}C -labelled $0.55\text{K}_2\text{CO}_3\cdot 0.45\text{MgCO}_3$ glass obtained from the intensities of the spin echo (S_0) and dephased (S) spectra. The data were acquired at 125.68 MHz (11.7 T) and a spinning rate of 8.0 kHz. The ^{13}C spin echoes were obtained by direct excitation pulses of 4 and 8 μs ($90^\circ/180^\circ$). ^1H dephasing employed 10 μs 180° pulses every one-half rotor period.



1
2
3 Figure S2. Comparison of ^{13}C MAS-NMR and $^{13}\text{C}\{^1\text{H}\}$ rotational echo double resonance
4 (REDOR) spectra of ^{13}C -labelled $0.55\text{K}_2\text{CO}_3 \cdot 0.45\text{MgCO}_3$ glass acquired at 125.68 MHz (11.7 T)
5 and spinning rate of 1.95 kHz. (a) acquired by direct ^{13}C excitation (DE) with 4 μs pulses
6 separated by a 30 s relaxation delay; (b) REDOR dephased spectrum (S) at 77% dephasing (6 ms),
7 emphasizing ^{13}C weakly coupled to ^1H ; (c) REDOR difference spectrum ($\Delta\text{S} = \text{S}_0 - \text{S}$) at 30%
8 dephasing (1 ms), emphasizing ^{13}C more strongly coupled to ^1H . Center band is denoted by
9 triangle symbol; all other peaks are spinning sidebands. Analysis of these spinning sideband
10 intensities for all three spectra yields chemical shift tensor values that are within uncertainty.
11
12
13
14
15
16
17
18
19
20
21
22
23
24
25
26
27
28
29
30
31
32
33
34
35
36
37
38
39
40
41
42
43
44
45
46
47
48
49
50
51
52
53
54
55
56
57
58
59
60

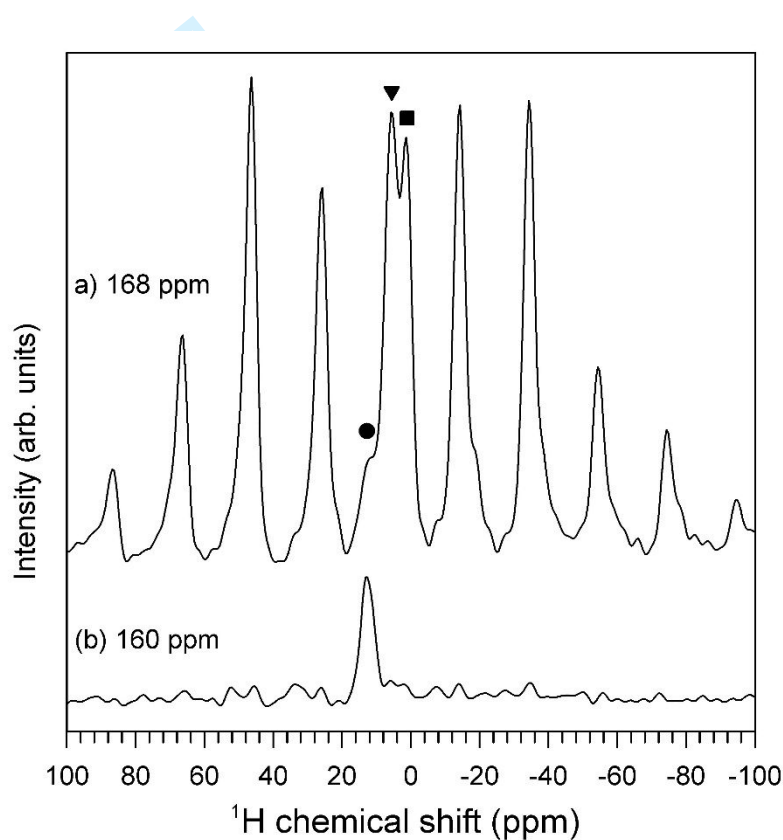


Figure S3. ^{13}C -detected ^1H MAS-NMR spectra of ^{13}C -labelled $0.55\text{K}_2\text{CO}_3 \cdot 0.45\text{MgCO}_3$ glass acquired at 399.97 MHz (9.4 T) and a spinning rate of 8.0 kHz. Spectra correspond to 1-dimensional cross-sections from 2-dimensional CP-heteronuclear correlation data, taken at ^{13}C chemical shifts corresponding to the main carbonate peak (a), and a minor hydrogen carbonate signal (b). The CP contact time was 2 ms. Center bands are denoted by symbols, including

1
2
3 hydrogen carbonate (●; 12.5 ppm), rigid structural water (▼; 5.5 ppm), and hydroxyl (■; 1.1 ppm).
4
5

6 All other peaks are spinning sidebands arising dominantly from the structural water.
7
8
9
10
11
12
13
14
15
16
17

18
19 [†] Currently at University of Manchester at Harwell, Diamond Light Source, Harwell Campus, Didcot, Oxfordshire,
20 OX11 0DE
21
22
23
24
25
26
27
28
29
30
31
32
33
34
35
36
37
38
39
40
41
42
43
44
45
46
47
48
49
50
51
52
53
54
55
56
57
58
59
60